

TECHNISCHE UNIVERSITÄT MÜNCHEN

Department Chemie

Lehrstuhl für Technische Chemie II

# **Selective Methane Oxidation on Zeolite Stabilized Copper Oxide Clusters**

Sebastian Grundner

Vollständiger Abdruck der von der Fakultät für Chemie der Technischen Universität

München zur Erlangung des akademischen Grades eines

**Doktors der Naturwissenschaften (Dr. rer. nat.)**

genehmigten Dissertation.

Vorsitzender: Univ.-Prof. Dr. K.-O. Hinrichsen

Prüfer der Dissertation:

1. Univ.-Prof. Dr. J. A. Lercher
2. Univ.-Prof. Dr. K. Köhler
3. Prof. M. Tromp, Ph.D. (Univ. Amsterdam,  
Niederlande)

Die Dissertation wurde am 21.12.2015 bei der Technischen Universität München eingereicht und durch die Fakultät für Chemie am 26.01.2016 angenommen.



*Dedicated to Lei*

*“The most exciting phrase to hear in science, the one that heralds new discoveries, is not 'Eureka!' but 'That's funny...’ “*

Isaac Asimov

# Statutory Declaration

I declare that I have authored this thesis independently, that I have not used other than the declared sources/resources, and that I have explicitly marked all material which has been quoted either literally or by content from the used sources. At the end of each chapter all collaborators are listed and their specific contribution is addressed. Published content of this thesis is clearly marked at the beginning of each chapter and reused according to the terms of the publisher. The content and structure of Chapter 2 and 3 vary significantly from the corresponding publications. Chapter 4 is not publication-based. Therefore, this thesis is not cumulative.

\_\_\_\_\_, \_\_\_\_\_

# Acknowledgements

After more than four years, I am finally submitting my thesis. With a feeling of relief I remember all the people who supported me in one way or another. It was a difficult time, but nevertheless interesting with a steep learning curve.

First, I want to thank my supervisor Prof. Johannes Lercher. The scientific discussions with you showed me the way. With your deep knowledge of science and your sharp intellect, you taught me how to do good science, revealed misleading hypotheses as such and brought me back on the right track. Thank you for your trust and your guidance!

I am very grateful to Dr. Maricruz Sanchez-Sanchez for supervising me. With your scientific knowledge, your excellent writing skills and your polite way of communication you have a major contribution to this thesis. Thank you for revising my thesis and manuscripts in such an accurate and efficient way.

Special thank goes to Monica Markovits for introducing me to the lab and teaching me all kind of experimental procedures in a very patient way. I want to thank my collaborators Dr. Guanna Li, Dr. Evgeny Pidko and Dr. Jiri Dedecek for fruitful discussions and successful cooperation in the EU NEXT-GTL project. I would further like to thank Prof. Moniek Tromp and Prof. Andreas Jentys for their input in XAS analysis. Xaver Hecht helped a lot with technical problems. Thank you also for your support to Bettina Federmann, Steffi Seibold, Uli Sanwald, Andreas Marx and Martin Neukamm.

All students who worked with me are acknowledged for their experimental contribution, especially Wanqiu Luo for her good work throughout her Master's Thesis. The big office was always a fun place with a lot of nice people and chats. I want to thank my office mates Edith Berger, Sebastian Eckstein, Andreas Ehrmaier, Christian Gärtner, Claudia Himmelsbach, Lou Yu, Liu Yuanshuai and Liu Yue for all their kindness and help. I want to thank my class mates who joined TC2, especially Sebastian Foraita, Elisabeth Hanrieder and Stanislav Kasakov for help and distraction at work. A special thanks to my friend Tobias Berto for discussions and support in all kind of situations. Thank

you to all current and former group members that are not listed above, I am grateful to all of you for a pleasant working atmosphere and your help.

Last but not least I want to thank my family. My parents supported me tremendously in every possible way during the last thirty years. Without you the way to get a PhD would have been much tougher. Danke Mama und Papa für alles, was ihr in den vergangenen dreißig Jahren für mich getan habt! Now is the time to thank the most special persons in my life. Lei, thank you for all your support, encouragement and love! Thank you Ferdi, for always succeeding in cheering me up! You two are the sunshine in my life.

Sebastian

December 2015

# Abbreviations

Å	Angstrom
AAS	Atomic absorption spectroscopy
BAS	Brønsted acid site
BET	Brunauer-Emmett-Teller
DFT	Density functional theory
EPR	Electron paramagnetic resonance
eV	Electronvolt
EXAFS	Extended X-ray absorption fine structure
g	Gram
h	Hour
IR	Infrared
K	Kelvin
kJ	Kilojoule
ml	Millilitre
min	Minute
MOR	Mordenite
X-MR	X-membered ring with X being the number of TO <sub>4</sub> in the ring
μmol	Micromole
TEM	Transmission electron microscopy
TOF	Turnover frequency
TPD	Temperature programmed desorption
UV-vis	Ultraviolet-visible
wt. %	Weight percent
XANES	X-ray absorption near edge structure
XAS	X-ray absorption spectroscopy
ZSM-5	Zeolite Socony Mobile-5

# Abstract

Copper oxide clusters stabilized in the micropores of zeolites have been found to selectively oxidize methane to methanol. The synthesis of a catalyst with homotopic trinuclear copper oxide clusters was achieved via ion exchange and oxidation. The steric and chemical environments of these clusters characterized by combinations of physicochemical measurement were critical to activate and convert methane. While the absence of water was critical for methane oxidation, the presence of water was required to realize its desorption. The presence of water reorganizes the  $\text{Cu}^{2+}$  cations requiring high temperatures to allow formation of the copper-oxide trimer clusters.

## Kurzzusammenfassung

Zeolithmikroporen stabilisieren Kupferoxidcluster, die selektiv Methan zu Methanol oxidieren. Die Synthese von homotopen trinuklearen Kupferoxidclustern erfolgte mittels Ionenaustausch und Oxidation. Die sterische und chemische Umgebung der Cluster, die durch eine Kombination physikochemischer Messungen charakterisiert wurde, ist entscheidend für die Aktivierung und Umsetzung von Methan. Während die Abwesenheit von Wasser wesentlich für die Oxidation von Methan ist, ist die Gegenwart von Wasser für die Desorption erforderlich. The Gegenwart von Wasser führt zur Reorganisation der  $\text{Cu}^{2+}$ -Kationen, was hohe Temperaturen für die Bildung des trinuklearen Kupferoxidclusters erfordert.

# Table of Contents

<b>1</b>	<b>General Introduction .....</b>	<b>1</b>
1.1	Methanol Economy .....	1
1.2	Commercial Route for the Conversion of Methane to Methanol .....	2
1.2.1	Reforming.....	2
1.2.2	Methanol Synthesis .....	2
1.3	Selective Partial Oxidation of Methane to Methanol .....	4
1.4	Zeolites .....	8
1.4.1	Structure of Zeolites .....	8
1.4.2	Nature of Acid Sites.....	11
1.4.3	Distribution and Siting of Framework Al .....	12
1.5	Catalysis on Copper Exchanged Zeolites .....	17
1.5.1	Catalytic Decomposition of Nitrogen Oxides .....	17
1.5.2	C-H Bond Activation .....	18
1.6	Scope of the Thesis .....	21
1.7	References .....	23
<b>2</b>	<b>Single-Site Trinuclear Copper Oxygen Clusters in Mordenite for Selective Conversion of Methane to Methanol .....</b>	<b>28</b>
2.1	Abstract.....	28
2.2	Introduction .....	29
2.3	Results and Discussion.....	30
2.3.1	Preparation of a Single-Site Copper Oxygen Cluster .....	30
2.3.2	Siting of Copper in Mordenite .....	31
2.3.3	Testing of Activity for Selective Oxidation of Methane.....	37
2.3.4	Spectroscopic Characterization.....	39
2.3.5	Copper Exchanged Mordenite as Biomimetic Model System .....	50
2.4	Conclusions .....	51
2.5	Experimental Section .....	52

2.6	Acknowledgements.....	61
2.7	Appendix.....	62
2.8	References .....	70
<b>3</b>	<b>Synthesis of Single-Site Copper Catalysts for Methane Partial Oxidation.....</b>	<b>73</b>
3.1	Abstract.....	73
3.2	Introduction .....	74
3.3	Results and Discussion.....	76
3.3.1	Effect of Co-Cations on Activity for Methane Partial Oxidation.....	76
3.3.2	Impact of pH on Activity for Methane Partial Oxidation .....	78
3.3.3	Siting of Sodium in Mordenite .....	83
3.3.4	Copper Exchange Stoichiometry .....	84
3.3.5	Impact of Sodium on Formation of Copper Oxo Clusters .....	85
3.3.6	<i>In Situ</i> UV-vis Spectroscopy .....	88
3.4	Conclusions .....	91
3.5	Experimental Section .....	92
3.6	Acknowledgements.....	94
3.7	Appendix.....	95
3.8	References .....	100
<b>4</b>	<b>Elementary Steps of the Selective Oxidation of Methane to Methanol over Copper Exchanged Mordenite .....</b>	<b>102</b>
4.1	Abstract.....	102
4.2	Introduction .....	103
4.3	Results and Discussion.....	105
4.3.1	Processes Involved in the Thermal Activation.....	105
4.3.2	Methane Oxidation .....	119
4.3.3	Effect of Steam Treatment in Methanol Production .....	124
4.4	Conclusions .....	125
4.5	Experimental Section .....	126

4.6	Acknowledgements.....	129
4.7	Appendix.....	130
4.8	References .....	134
<b>5</b>	<b>Summary and Conclusions .....</b>	<b>137</b>
<b>6</b>	<b>Zusammenfassung.....</b>	<b>139</b>
	Curriculum Vitae .....	141
	List of Publications .....	142

# 1 General Introduction

## 1.1 Methanol Economy

Natural gas is an abundant energy source with reserves exceeding the energy content of the world's reserves for oil.<sup>[1]</sup> The global demand for natural gas is increasing significantly faster than that for oil.<sup>[2]</sup> However, transportation of large amounts of natural gas from remote locations far away from consumer markets requires complex logistics. For intercontinental transport, natural gas is usually liquefied in an energy-intensive process. Several explosions point out the potential risk of LNG.<sup>[3]</sup> Therefore, novel chemistry is required to convert natural gas into easily condensable energy carriers that can be readily integrated into the existing chemical infrastructure.<sup>[4,5]</sup> These processes are referred to as gas-to-liquid (GTL) technology.

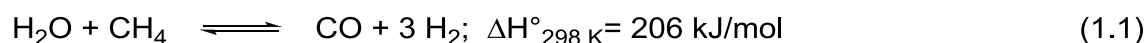
The primary component of natural gas is methane, accounting for 90% of the gas volume.<sup>[6]</sup> Consequently, natural gas exploitation is focused on methane conversion. The current dominant method is conversion of methane with  $\text{H}_2\text{O}$ ,  $\text{O}_2$  or  $\text{CO}_2$  to synthesis gas (syn-gas, a mixture of  $\text{CO}$  and  $\text{H}_2$ ), followed by synthesis of methanol and the subsequent conversion of methanol to hydrocarbons with zeolite catalysts<sup>[7]</sup> or via direct hydrocarbon synthesis via the Fischer-Tropsch process.<sup>[8]</sup> The syn-gas based methods suffer of high energy needs and relatively high production costs. In contrast, oxidative coupling of methane to ethane and ethylene,<sup>[9]</sup> dehydroaromatization,<sup>[10]</sup> and the direct partial oxidation of methane to methanol allow a direct conversion of natural gas and therefore permit potentially lower capital and operation cost.

The methanol economy proposed by George Olah emphasizes the high potential of methanol to substitute crude oil as fuel, energy carrier and industrial feedstock.<sup>[11]</sup> Methanol can be stored, transported and distributed using essentially existing infrastructure and can be used directly as fuel for combustion engines.<sup>[12]</sup> The volumetric energy density of methanol is more than five times higher than that of hydrogen.<sup>[13]</sup> In contrast to the proposed ethanol economy, methanol does not compete with edible food/oil production.

## 1.2 Commercial Route for the Conversion of Methane to Methanol

### 1.2.1 Reforming

To date, reforming is the key technology for conversion of methane to synthesis gas (syn-gas). Syn-gas is a mixture of CO and H<sub>2</sub> that can be transformed further into important industrial base chemicals like methanol or hydrocarbons. Steam reforming (equation 1.1) results in a high H<sub>2</sub>:CO ratio. In contrast, dry reforming (equation 1.2) produces CO rich syn-gas which is more feasible for the production of bulk chemicals.<sup>[14]</sup> However, the absence of water and the higher C:H ratio favor coke formation. Since reforming involves the conversion of stable molecules such as water and methane or CO<sub>2</sub> and methane respectively, the reaction is strongly endothermic and therefore favored by high temperatures. Furthermore, due to the increase in the number of moles by reforming, low pressures are required in order to achieve high conversions. The industrial process of steam reforming takes place in a plug flow reactor with an inlet temperature of 450-650 °C and an outlet temperature of 850-950 °C.



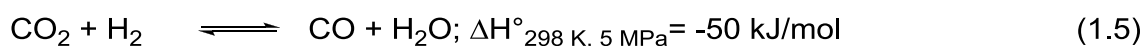
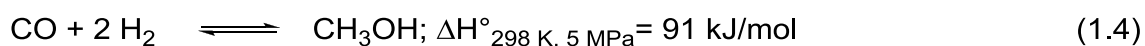
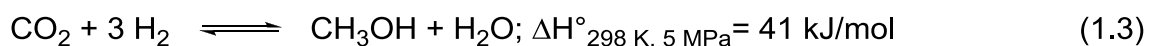
Ni is the preferred element for steam reforming. For dry reforming Rh shows a good activity and stability, while Ni catalyst show a high rate of coke formation.<sup>[14]</sup>

### 1.2.2 Methanol Synthesis

On an industrial scale, methanol is produced by conversion of syn-gas. Methanol synthesis is exothermic and involves a decrease of the number of moles. Therefore, according to Le Chatelier's principle, high conversions are achieved at high pressures and low temperatures. The first process

commercialized by BASF in 1923 was based on ZnO/Cr<sub>2</sub>O<sub>3</sub> catalysts in a high pressure loop at 240-300 bar and 350-400 °C. In 1960, the production of sulphur-free synthesis gas enabled the use of more active Cu/ZnO catalysts. Nowadays Cu/ZnO/Al<sub>2</sub>O<sub>3</sub> catalysts are almost exclusively applied. These catalysts are operated within a temperature range of 250-280 °C and pressures in the range of 60-80 bar.<sup>[15]</sup>

The following equations describe the thermodynamics of the system. Methanol is mainly formed by transformation of CO<sub>2</sub> (equation 1.3). CO<sub>2</sub> is formed from syn-gas due to the water gas shift reaction (equation 1.5). Direct hydrogenation of CO (equation 1.4) does not play a role in methanol synthesis.<sup>[16]</sup>



## 1.3 Selective Partial Oxidation of Methane to Methanol

The high thermodynamic stability of methane with its high symmetry and highest C-H bond energy amongst organic substrates ( $435 \text{ kJ mol}^{-1}$ ) makes the activation and functionalization of methane challenging.<sup>[17,18]</sup> The partial oxidation of methane to methanol is a promising route for natural gas valorization. In contrast to the energy intensive two step commercial route of methanol synthesis, partial oxidation of methane allows a direct conversion of natural gas to methanol at low temperatures. Since C-H activation is dominated by radical pathways involving H atom removal, the selectivity of such reactions is limited.<sup>[19]</sup> Methane is prone to over-oxidation due to the gradually more facile second, third and fourth C-H bond activation leading to the cleavage of all C-H bonds and the formation of  $\text{CO}_2$ . To prevent over-oxidation, selective oxidation requires a rather mild oxidant and a catalyst stabilizing the intermediate after the first C-H bond cleavage.<sup>[17]</sup>

Homogeneous as well as heterogeneous catalysts have been explored for selective partial oxidation of methane to methanol resulting in great leads, but limited success to achieve economically sensible conversion. Shilov developed the first system able to activate terminal C-H bonds in a catalytic cycle using  $\text{K}_2\text{PtCl}_4$  as catalyst and stoichiometric amounts of  $\text{K}_2\text{PtCl}_6$ . The complexes tolerate oxidizing conditions, including dioxygen itself, and directly produce oxygenated products. However one equivalent of Pt(IV) is consumed per equivalent of alkane oxidized, while Pt(II) acts as catalyst.<sup>[20]</sup>

The most successful approach in homogeneous catalysis has been based on Periana chemistry<sup>[21,22]</sup> using a noble metal center (Figure 1.1 a) to cleave the C-H bond and a strong oxidant such as  $\text{SO}_3$  (in concentrated sulfuric acid) to oxidize the  $\text{CH}_3$  radical to  $\text{CH}_3^+$ , with the anion ( $\text{SO}_4^{2-}$ ) acting as protecting group against further oxidation. This protecting group has to be hydrolyzed to yield methanol. Despite significant progress over the last decade by Periana *et al.* showing that noble metals are able to catalyze the Shilov reaction with high selectivity and yield, use of highly corrosive media and problems in recycling

the catalysts makes difficult an application at large scale. A recent elegant immobilization of the noble metal catalyst into a nitrogen containing carbon (Figure 1.1 b) appears to solve the problem of catalyst recycle but without solving the problems associated with  $\text{H}_2\text{SO}_4/\text{SO}_3$  corrosivity.<sup>[17,23]</sup>

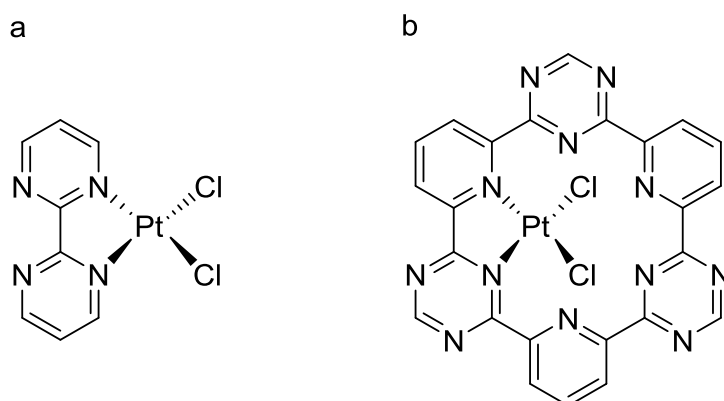


**Figure 1.1:** a) Structure of the Periana catalyst 2,2'-bipyrimidine platinum chloride for selective partial oxidation of methane in fuming sulfuric acid and b) its immobilization as platinum chloride in triazine based frameworks.

Another approach for the selective conversion of methane to methanol in a single step is the biocatalytic transformation. Methanotrophic bacteria convert methane into methanol under aerobic conditions and at ambient temperature using metalloenzymes, i.e., methane monooxygenases (MMOs). Two forms of MMOs at different cellular locations are known, a cytoplasmic MMO (soluble, sMMO) and a membrane bound MMO (particulate, pMMO). In the sMMO, the active site of the hydroxylase contains a bis( $\mu$ -oxo)diiron core.<sup>[24]</sup> For the configuration of the active site in pMMO, the consensus view is that a Cu cluster is responsible for the insertion of oxygen in methane at ambient temperature with very high efficiency ( $\text{TOF} = 1\text{s}^{-1}$ ).<sup>[25]</sup> On the other hand, the difficulties associated with handling and purification of pMMO as well as the complexity of its structure make its industrial application challenging.<sup>[26]</sup> Furthermore, it is also difficult to achieve an unambiguous structural characterization of the enzyme, in particular under the catalytic conditions. Thus, there is still debate on the nuclearity of the active Cu core in pMMO.

While some authors have assigned the activity to a Cu dimer,<sup>[27]</sup> recent publications by Chan *et al.* pointed to three Cu atoms comprising the active site (Figure 1.2).<sup>[18,28-30]</sup>

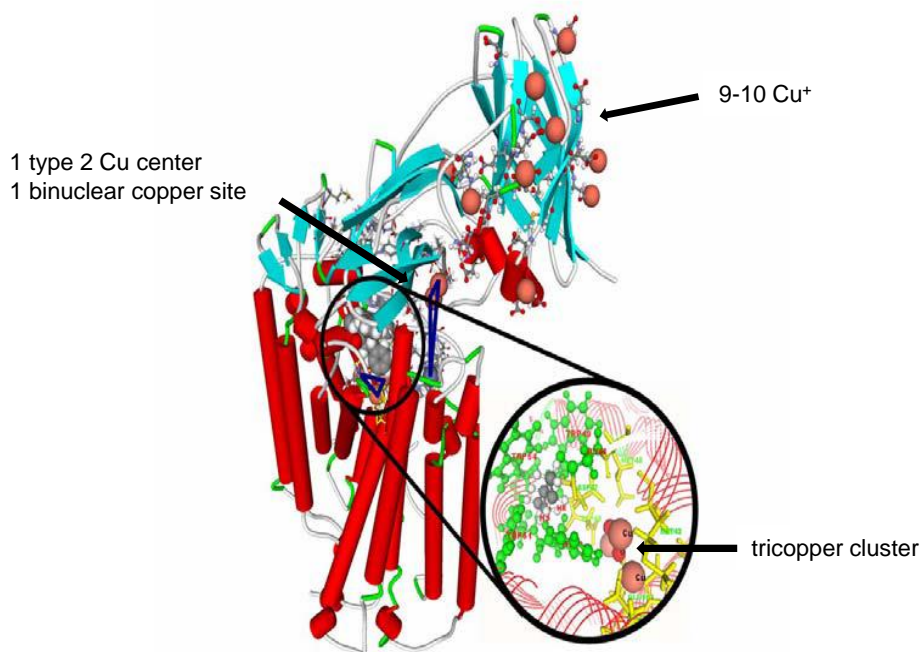


**Figure 1.2:** Structure of the integral membrane protein particulate methane monooxygenase (pMMO) according to the X-ray crystal structure of Lieberman and Rosenzweig<sup>[31]</sup> and the copper siting according to Chan (adapted from ref.<sup>[32]</sup>).

Inspired by the superb activity and selectivity of enzymes, a series of Cu and Fe exchanged zeolites have been explored and found active for the selective conversion of methane to methanol.<sup>[33-35]</sup> The main drawback of all these catalysts, however, is that either high temperature is needed to reactivate the catalyst after a successful catalytic cycle or that H<sub>2</sub>O<sub>2</sub> has to be used to work continuously.<sup>[36]</sup> The use of H<sub>2</sub>O<sub>2</sub> is expensive, but costs can be reduced by low temperature *in situ* generation of H<sub>2</sub>O<sub>2</sub>.<sup>[37]</sup> Furthermore, the required H<sub>2</sub> for the H<sub>2</sub>O<sub>2</sub> generation originates from steam reforming, and therefore this approach does not fully constitute an alternative route of methane valorization. The

combination of the difficult chemical route with separate catalyst activation and methane reaction steps and the low concentration of active sites make the use of metal exchanged zeolites for methane oxidation currently economically not feasible. However, due to the low production costs and high stability of transition metal exchanged zeolites, this class of catalysts is very promising for a large scale industrial process.

## 1.4 Zeolites

### 1.4.1 Structure of Zeolites

Zeolites are crystalline aluminosilicates with pores and cavities of molecular dimensions. The primary building unit is the  $\text{TO}_4$  tetrahedron with T being mostly Si and Al. The three-dimensional structure is formed by corner-sharing of  $\text{TO}_4$  tetrahedra that are interlinked with four neighbors through common O atoms. By different arrangement of the primary building blocks, up to 20 secondary building units can be formed (Figure 1.3). These topological subunits can be combined to a big variety of three-dimensional structures. 180 distinct zeolite topologies are known and classified by a framework type code denoted by three capital letters.

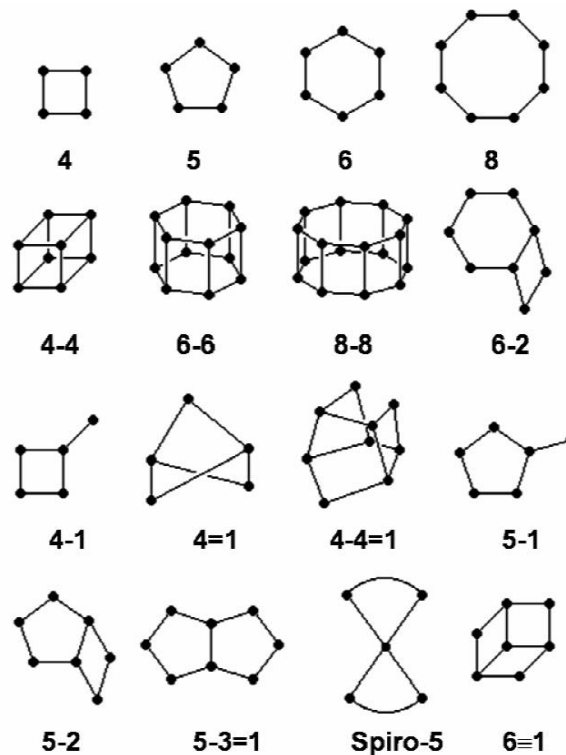


**Figure 1.3:** Selection of most common secondary building units of zeolite structures. The spots indicate the T-atoms (Si or Al). The oxygen bridges are represented by lines.

Zeolites are classified according to their pore size in small-pore, medium-pore and large-pore zeolites. The size of channels, channel intersections and cavities depends on the number of T-atoms that form the pores. Typically, zeolite pores consist of 6 to 14 T-atoms, so called 6 to 14 membered rings (MR). Zeolite A (LTA) consisting of 8-MR is a typical small-pore zeolite with a pore diameter of 4 Å, whereas zeolite Y (FAU) is a typical large pore zeolite with 12-MR and a pore size of 7 Å. ZSM-5 (MFI) is the most popular medium-pore zeolite with a pore diameter of 5 Å. The most commonly used zeolite topologies are compiled in Table 1.1.<sup>[38]</sup>

**Table 1.1:** Industrially important zeolite topologies

Topology	Pore geometry	Pore size [Å]	Channel system	Classification
LTA	8-ring	4.1 x 4.1	3-dimensional	small-pore
FER	8-ring	3.5 x 4.8	2-dimensional	medium-pore
	10-ring	4.2 x 5.4		
MFI	10-ring	5.1 x 5.5	2-dimensional	medium-pore
	10-ring	5.3 x 5.6		
MOR	8-ring	2.6 x 5.7	1-dimensional	large-pore
	12-ring	6.5 x 7.0		
BEA	12-ring	6.6 x 6.7	3-dimensional	large-pore
	12-ring	5.6 x 5.6		
FAU	12-ring	7.4 x 7.4	3-dimensional	large-pore

Due to their relevance in this thesis, ZSM-5, MOR and CHA topologies are described in more detail below.

ZSM-5 is a three dimensional pentasil zeolite that consists of two intersecting elliptical 10-MR channels (Figure 1.4 a). The straight channels ( $5.3 \times 5.6 \text{ \AA}$ ) are orthogonal to the sinusoidal channels ( $5.1 \times 5.5 \text{ \AA}$ ) resulting in spacious intersections. ZSM-5 is of high industrial relevance as catalyst for shape selective cracking and isomerization reactions.<sup>[39,40]</sup>

The mordenite (MOR) topology consists of a main channel composed of 12-MR rings with perpendicular 8-MR side pockets (Figure 1.4 b). The side pockets are separated by a restriction of  $2.6 \times 5.7 \text{ \AA}$ , and their entrance (pore mouth) has an aperture of  $3.9 \times 5.7 \text{ \AA}$ . This diameter is substantially smaller than the aperture of the straight channels ( $6.5 \times 7.0 \text{ \AA}$ ). MOR is an efficient catalyst for alkane cracking, ammonia alkylation and dimethyl ether carbonylation.<sup>[41-43]</sup>

Chabazite (CHA) is a highly symmetric three dimensional framework of interconnected cages (Figure 1.4 c). The cages consist of twelve 4-MR, two 6-MR and six 8-MR. The 8-MR restrict the access to the cavities to molecules with a kinetic diameter of  $3.7 \text{ \AA}$ . H-SAPO-34 (i.e. a silicoaluminophosphate material with CHA structure) has been applied as a commercial methanol-to-olefin catalyst.<sup>[44]</sup> CHA based materials such as Cu-SSZ-13 and Cu-SAPO-34 are commercialized catalysts for the selective catalytic reduction of  $\text{NO}_x$  for diesel engine exhaust after-treatment.<sup>[45-47]</sup>

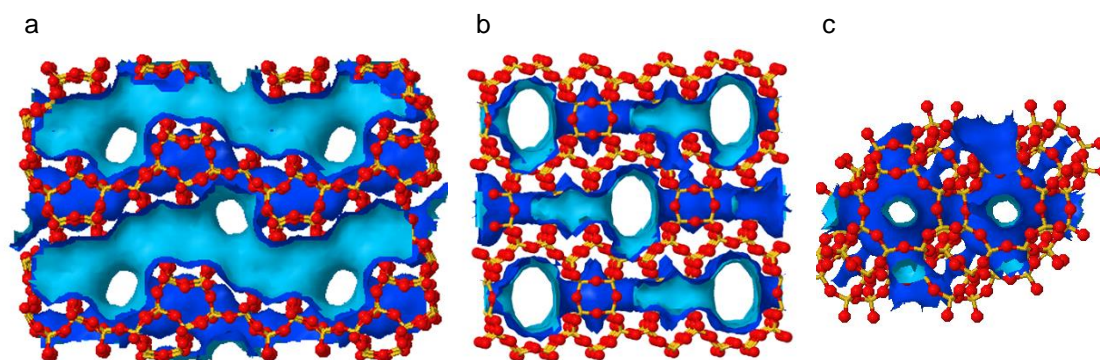


**Figure 1.4:** Framework structures of a) ZSM-5 viewed along  $[010]$ , b) MOR viewed along  $[001]$  and c) CHA viewed along  $[001]$  highlighting the surface of the channels. Colors: Si (yellow), O (red), channels (blue). (<http://www.iza-structure.org/databases/>).

The high crystallinity, thermal stability, large pore volume and internal surface area make zeolites suitable materials for heterogeneous catalysis. Two important properties of zeolites are of relevance for catalysis: (i) The acidity introduced by framework Al atoms and (ii) the well-defined pores and cavities with characteristic shapes and sizes. In this context, the distribution of framework Al sites is of high importance.

### 1.4.2 Nature of Acid Sites

Brønsted acid sites (BAS) in zeolites catalyze a broad range of industrial relevant reactions such as catalytic cracking, isomerization and alkylation of hydrocarbons.<sup>[48,49]</sup> Isomorphous substitution of  $\text{Si}^{4+}$  by the trivalent  $\text{Al}^{3+}$  introduces a negative charge into the zeolite framework. This negative charge is either balanced by a metal cation or a proton. In the latter case, a BAS is formed. The chemical structure of the bridged hydroxyl group in zeolites was first proposed by Uytterhoeven *et al.* as a Si-OH group strongly influenced by a neighboring tricoordinated  $\text{Al}^{3+}$  site.<sup>[50]</sup> Later, the structure of the BAS was elucidated as a bridging hydroxyl group with the oxygen covalently bond to a  $\text{Si}^{4+}$  as well as a  $\text{Al}^{3+}$  site (Figure 1.5).<sup>[51]</sup> Isomorphous substitution obeys Loewenstein's rule meaning that two Al tetrahedra cannot share one common connecting O atom. This implies Al-O-(Si-O)<sub>n</sub>-Al sequences with  $n \geq 1$  and therefore a minimum Si/Al ratio of 1.<sup>[48]</sup> During thermal activation, dealumination occurs to a certain extent generating extra framework Al species.

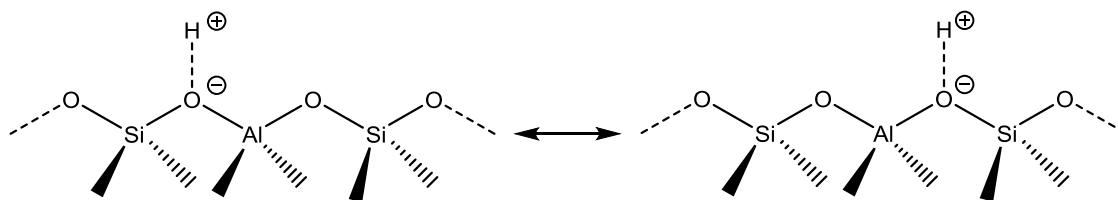


**Figure 1.5:** Brønsted acid site in a zeolite generated by isomorphous substitution of Al for Si. The negative charged induced by the Al is delocalized.

The term acidity may describe an extensive property, i.e. the density of acid sites. On the other hand, acidity can also describe an intensive property, i.e. the acid strength which is the ability to protonate bases of different strength.<sup>[48]</sup> The density of acid sites is related to the Si/Al ratio. The lower the Si/Al ratio, the higher the framework Al concentration and therefore the acid site density.<sup>[48]</sup> While the impact of the geometry on acid strength is still under debate,<sup>[52]</sup> the zeolite geometry has an enormous impact on catalytic activity due to shape selective effects. The Iglesia group pointed out the impact of spatial constraints in the side pockets of MOR on alkane activation.<sup>[41]</sup> It was shown that acid sites in the confined 8-MR of the side pockets are much more active for isobutene reactions than sites of similar acid strength within the 12-MR channels.<sup>[53]</sup> Consequently, the location of the framework Al sites is of high relevance for catalysis because it determines the spatial confinement of the acid site.

### 1.4.3 Distribution and Siting of Framework Al

For zeolites consisting of channels of different dimensions such as MOR (8-MR, 12-MR) and FER (8-MR, 10-MR), the distribution of the framework Al among this channels is of relevance for the catalytic activity and selectivity of those materials.<sup>[53]</sup> The shape and size of the molecular sieve pores determine the accessibility of the Brønsted acid sites - generated by the isomorphic substitution of  $\text{Si}^{4+}$  by  $\text{Al}^{3+}$  in the framework - to reactants with a certain kinetic diameter. Therefore adsorption of a probe molecule of a proper size allows infrared spectroscopic determination of the BAS distribution among channels and cavities of different dimensions. For example, in MOR only sites in the 12-MR main channels are accessible for n-hexane, while the 8-MR side pockets are inaccessible to n-hexane.<sup>[54]</sup> Selective perturbation of the O-H vibrations attributed to BAS in main channels by adsorption of n-hexane allowed accurate quantification of the O-H band attributed to BAS in the side pockets (Figure 1.6). Analogously, adsorption of 3-methylpentane allows determination of the acid site distribution among 8-MR and 10-MR of FER.<sup>[55]</sup>

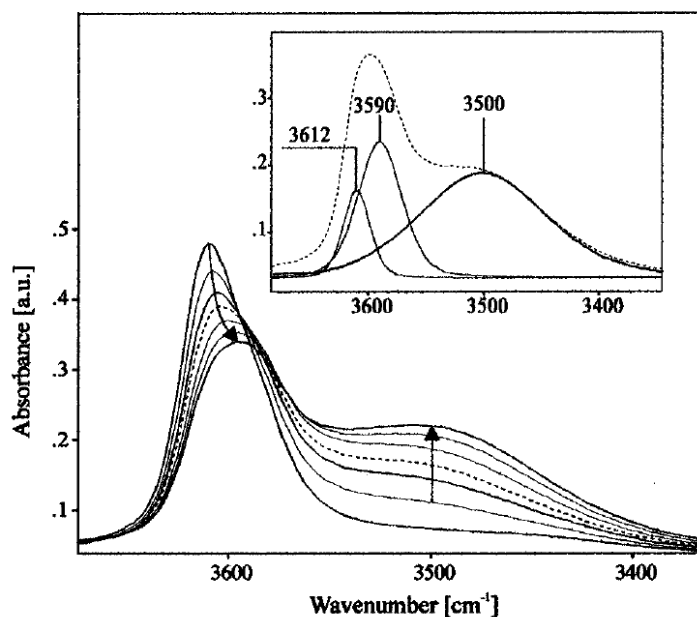


**Figure 1.6:** Infrared spectra of the O-H stretching vibrations of the Brønsted acid sites of H-MOR during adsorption of n-hexane at 303 K. The bands centered at  $3,612\text{ cm}^{-1}$  and  $3,590\text{ cm}^{-1}$  are attributed to BAS in the main channel and the side pockets respectively. The broad band at  $3,500\text{ cm}^{-1}$  is due to perturbed O-H vibrations. The lines correspond to increasing equilibrium pressure of n-hexane (from ref.<sup>[54]</sup>).

The bridging framework O between one Si and one isomorphously substituted Al site in the framework of a zeolite represents a negatively charged ligand able to coordinate transition metal cations with an open coordination sphere. Since the negative charge is delocalized over all framework oxygen atoms neighboring the framework Al, several coordinating oxygen ligands per Al site are available for a metal cation. Furthermore, the ion-exchange capacity of a zeolite depends on its framework Al content. In fully dehydrated zeolites, coordination of bare divalent cations requires two negatively charged framework Al sites in close proximity. Consequently, not only the concentration but also the siting and distribution of framework Al is relevant for the quantity and geometry of transition metal coordination.<sup>[52]</sup>

Dedecek *et al.* developed a method for quantification of Al sequences in zeolites by  $\text{Co}^{2+}$  exchange of sodium form (Figure 1.7). After dehydration, the bare divalent  $\text{Co}^{2+}$  is only exchanged to sites where a spatial proximity of two

framework Al sites is available. The following types of framework Al configurations were classified.<sup>[52,56,57]</sup>

- (i) Single Al atoms are defined as sequences with only one Al in one ring structure. Single Al sites do not coordinated  $\text{Co}^{2+}$ .
- (ii) Paired Al sites are two Al atoms with a  $\text{Al-O-(Si-O)}_n\text{-Al}$  sequence with  $n \leq 2$  in the ring of a cationic site. The close proximity of these two Al sites favors coordination of  $\text{Co}^{2+}$ .
- (iii) Unpaired Al sites are two Al atoms with a  $\text{Al-O-(Si-O)}_n\text{-Al}$  sequence with  $n > 2$  but at “visible” distance, meaning that a  $\text{Co}^{2+}$  cation can be coordinated by both framework Al sites at the same time.

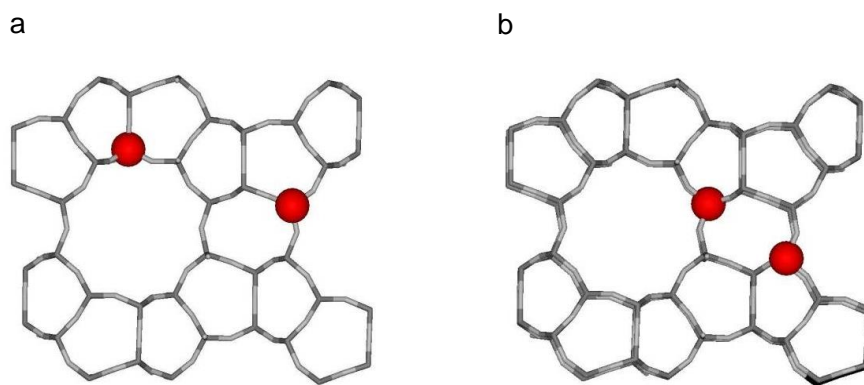


**Figure 1.7:** Schematic representation of a) isolated and b) paired framework Al sites in Si-rich zeolites. Isomorphously substitution Al is marked in red (adapted from ref.<sup>[52]</sup>).

The siting of framework Al in different primary building blocks and ring structures of the zeolite affects the coordination number and geometry of exchange sites. Three distinct types of exchange sites were found in industrial important pentasil zeolites such as MOR, FER, MFI and BEA (Figure 1.8). The characterization of these sites is based on the deconvolution of the UV-vis spectra of the  $\text{Co}^{2+}$ -exchanged zeolites after dehydration.<sup>[58]</sup>

- (i)  $\text{Co}^{2+}$  at the  $\alpha$ -site is coordinated by four framework O atoms which are arranged in a rectangle.
- (ii) At the  $\beta$ -site, a hexagonal coordination sphere is formed by a twisted six ring of framework O atoms.

- (iii) The  $\gamma$ -site is a boat-shaped site. The exact coordination of  $\text{Co}^{2+}$  at this site is not fully understood yet.

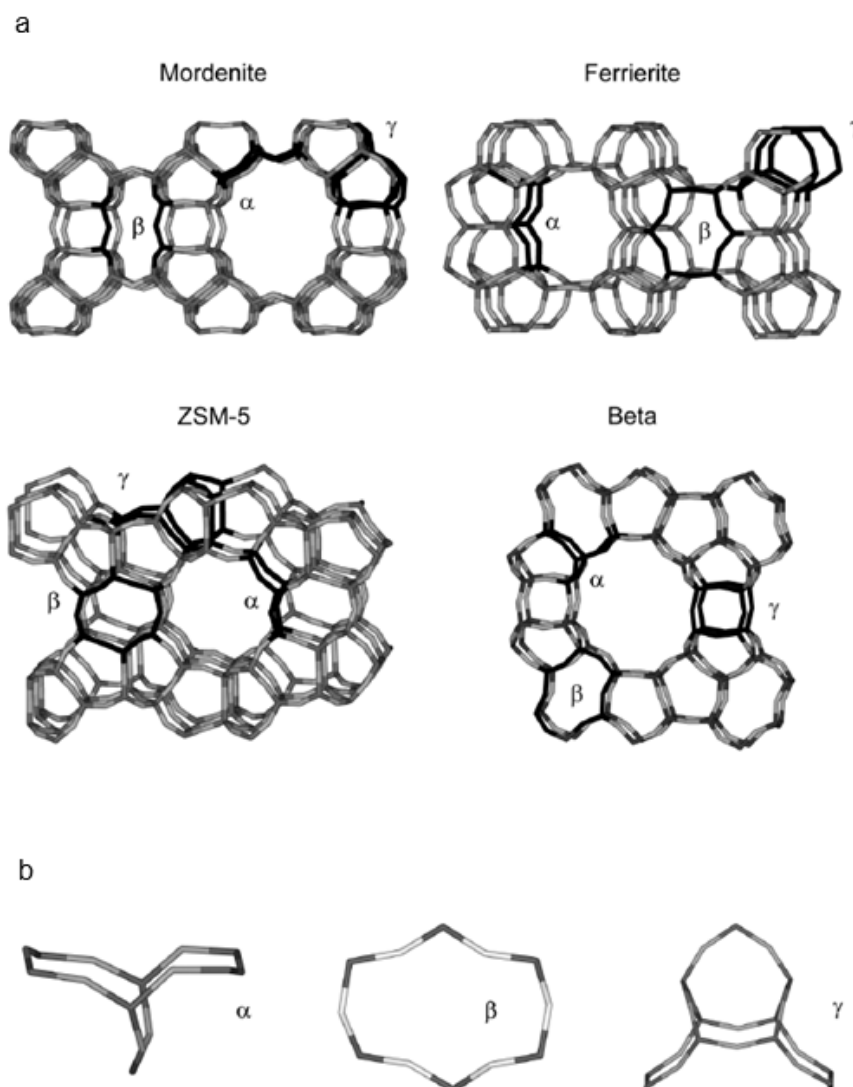


**Figure 1.8:** a) Location of the  $\alpha$ ,  $\beta$  and  $\gamma$ -sites in MOR, FER, ZSM-5 and BEA framework and b) local framework structures of the  $\alpha$ ,  $\beta$  and  $\gamma$ -site (from ref.<sup>[52]</sup>).

However, the siting of transition metal ions in MOR is still under debate. It was demonstrated that the siting of  $\text{Na}^+$  in the side pockets is thermodynamically favored over the main channel.<sup>[43]</sup> In accordance with this results, Dedecek *et al.* showed that the site in the twisted 8-MR is preferentially occupied by  $\text{Co}^{2+}$  in CoH-MOR.<sup>[59]</sup> In contrast, DFT studies suggest that the Cu oxo cluster is

located in the MOR main channel and that the 8-MR site is not occupied by  $\text{Cu}^{2+}$ .<sup>[60]</sup> Three sites were determined by analysis of room-temperature single-crystal X-ray data of partially dehydrated Cu-MOR.<sup>[61]</sup> One site was determined in the 12-MR, one in the 8-MR and a third site was found above the 8-MR adjacent to 12-MR. However, the siting of the Cu ions on dehydrated Cu-MOR cannot be inferred from this study.<sup>[62]</sup> Furthermore, Dedeck *et al.* pointed out that Al arrangement has a strong effect on the coordination and local charges of Cu ions in high silica zeolites.<sup>[63]</sup> This suggests that Cu siting varies within one zeolite topology in dependence of Al distribution.

## 1.5 Catalysis on Copper Exchanged Zeolites

### 1.5.1 Catalytic Decomposition of Nitrogen Oxides

Soon after preparation of synthetic zeolites A, X and Y succeeded, they were ion exchanged with transition metal ions (TMI) with the purpose of introducing new catalytic functionalities.<sup>[64-69]</sup> The potential of transition metal exchanged zeolites as oxidation catalysts was already studied in the early 1970s by Kubo.<sup>[70,71]</sup> Richardson studied systematically the oxidizing properties and catalytic activity of Cu exchanged Y zeolites (Cu-Y).<sup>[72-74]</sup> The low price of zeolites as well as the relatively low copper market prices compared to other transition metals makes Cu exchanged zeolites particularly promising catalysts for large scale industrial processes.

Since the discovery in the 1990s of the exceptionally high activity of Cu-ZSM-5 zeolites in the direct catalytic decomposition of  $\text{NO}_x$  (De $\text{NO}_x$ ) into  $\text{N}_2$  and  $\text{O}_2$ ,<sup>[75]</sup> Cu-zeolites have been studied extensively. De $\text{NO}_x$  activity was attributed to  $\text{Cu}^+$  sites which are generated by autoreduction of  $\text{Cu}^{2+}$  during thermal activation at 450 °C, under dry conditions.<sup>[76]</sup> The redox reaction of those  $\text{Cu}^+$  sites with  $\text{NO}_x$  to  $\text{N}_2$  and a  $\text{Cu}^{2+}$  oxo species is the key step of the De $\text{NO}_x$  reaction over Cu exchanged zeolites.<sup>[77]</sup>  $\text{Cu}^+$  sites are regenerated at high temperatures due to autoreduction via desorption and recombination of O at  $\text{Cu}^{2+}$  sites into molecular  $\text{O}_2$  and its subsequent desorption.<sup>[78-80]</sup>

In 2010, it was reported that Cu-SSZ-13 has excellent activity and  $\text{N}_2$  selectivity for the selective catalytic reduction (SCR) of  $\text{NO}_x$  with  $\text{NH}_3$ .<sup>[45]</sup> The superiority of Cu-SSZ-13 in comparison with other Cu zeolites tested in SCR like Cu-BEA and Cu-ZSM-5 is not understood yet. The structure of the Cu active sites in CHA zeolite has been recently widely studied.<sup>[47]</sup> Depending on the Si/Al ratio, Cu/Al ratio and the reaction temperature, Cu monomers and Cu dimers are formed in various extents. At temperatures below 250 °C transient Cu dimers are the active sites. In the range of 250-350 °C, dimers become less stable resulting in a decrease of SCR activity. Above 350 °C for low to intermediate Cu loadings monomers are forming the high temperature active sites.<sup>[81]</sup> The

increasing SCR rate with decreasing Si/Al ratio was attributed to the promoting effect of BAS due to a higher  $\text{NH}_3$  coverage.<sup>[82]</sup> The dynamics of Cu ion movement in the zeolite micropores of SSZ-13 were recently monitored by combined *in situ* spectroscopy. Hydrated  $\text{Cu}^{2+}$  ions are located in the cavities of the zeolite. The removal of water results in the movement of  $\text{Cu}^{2+}$  into their cationic positions where they strongly interact with the zeolite framework.<sup>[62]</sup> Hence, the reaction conditions in SCR, where variable concentrations of  $\text{H}_2\text{O}$  are present, strongly affect the position of the Cu ions.

## 1.5.2 C-H Bond Activation

### 1.5.2.1 Selective oxidation of benzene to phenol

Catalytic C-H activation over Cu exchanged zeolites was reported for the first time in 2002 for benzene hydroxylation.<sup>[83]</sup> Yields between 4% and 10% with high selectivities to phenol were achieved for the gas phase reaction with molecular oxygen.<sup>[84,85]</sup> Kubacka *et al.* showed a maximum phenol yield of 10% with a Cu–ZSM-5 with Si/Al of 48 and a Cu/Al ratio of 0.5. Selectivity to phenol on this system was above 95%.<sup>[85]</sup> A  $(\mu\text{-}\eta^2\text{:}\eta^2\text{-peroxo})\text{dicopper}$  complex was identified as active site based on the absorption band at  $30,300\text{ cm}^{-1}$  in the UV-vis spectrum which was assigned to a peroxo to copper ligand to metal charge transfer.<sup>[86]</sup>

### 1.5.2.2 Selective oxidation of methane to methanol

Groothaert *et al.* were the first to report on the selective oxidation of methane to methanol over Cu exchanged ZSM-5 and MOR in 2005.<sup>[33]</sup> After thermal treatment, the dehydrated material was activated in  $\text{O}_2$  or  $\text{N}_2\text{O}$ , at  $175\text{ }^\circ\text{C}$  and room temperature respectively. After contact with methane, typically at 100 to  $200\text{ }^\circ\text{C}$ , methanol was obtained by solvent extraction. Due to the significantly higher methanol yield of Cu exchanged MOR in comparison to Cu exchanged ZSM-5, most studies in the last five years have been focused on Cu-MOR materials.<sup>[87-90]</sup> Very recently, Cu exchanged in other 8-MR containing zeolites also showed significant activity in methane oxidation.<sup>[91]</sup>

After reaction with methane, the products are strongly adsorbed in the zeolite. Recent studies demonstrated that the conventional solvent extraction of Cu exchanged zeolites after activation and methane loading only extracted less than 50% of the formed methanol.<sup>[90-92]</sup> In contrast, steam treatment and HF extraction allowed an accurate quantification of the total product yield. A stepwise reaction procedure with (i) thermal activation in O<sub>2</sub> at 450 °C, (ii) reaction with methane at 200 °C and (iii) steam treatment at 135 °C for methanol release was first published by Alayon *et al.*<sup>[87]</sup> This opened the possibility to operate the process in a closed catalytic cycle. Steam treatment resulted in re-hydration of the material, requiring high temperature activation after each cycle.

EPR studies revealed that the majority of the sites found in calcined Cu-ZSM-5 are EPR silent due to antiferromagnetic coupling between close Cu centers.<sup>[93]</sup> This indicates the formation of a multinuclear Cu site. Based on their previous work on catalytic decomposition of NO<sub>x</sub>, Groothaert *et al.* ascribed the activity of Cu-ZSM-5 for selective oxidation of methane to methanol to a bis( $\mu$ -oxo)dicopper core (Figure 1.9 a) which was characterized by *in situ* UV-vis spectroscopy. A characteristic band at 22,200 cm<sup>-1</sup> appeared after activation in O<sub>2</sub> or N<sub>2</sub>O.<sup>[94]</sup> Upon reaction with methane at 175 °C, the band disappeared completely in less than 3 min.<sup>[33]</sup> However, the fact that this band is weak and broad in the most active material Cu-MOR, suggest that the active species in Cu-MOR is different from Cu-ZSM-5.<sup>[91,94]</sup> Later, by means of Raman spectroscopy and <sup>18</sup>O labeling experiments, a bis( $\mu$ -oxo) bridged dicopper core was ruled out as the active site. Instead, the activity for methane oxidation was assigned to a mono( $\mu$ -oxo) bridged dicopper core (Figure 1.9 b).<sup>[95]</sup> A recent study based on UV-vis and Raman spectroscopy postulates the presence of two distinct mono( $\mu$ -oxo) bridged dicopper species in MOR.<sup>[89]</sup>

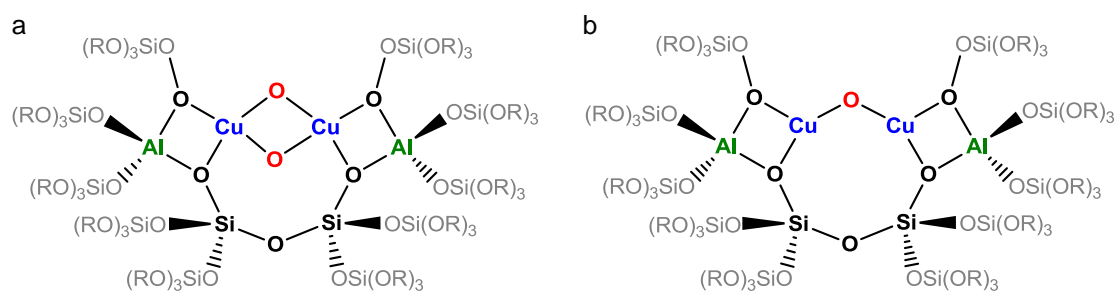


**Figure 1.9:** Structure of a) the bis( $\mu$ -oxo)dicopper core and b) the mono( $\mu$ -oxo)dicopper core anchored on a paired Al site in the 10-MR of ZSM-5.

Due to the outstanding activity of Cu-MOR in selective partial oxidation of methane to methanol, elucidation of the active site and its siting in the MOR structure is of high interest. However, the siting of transition metal ions in MOR is still under debate. As mentioned in section 1.4.3, the location and speciation of Cu in zeolites is affected by the Al arrangement. This suggests that Cu siting varies within one zeolite topology in dependence of the Al distribution. Therefore, the impact of the framework on the formation and location of Cu-oxo species with activity in methane oxidation to methanol needs to be addressed.

## 1.6 Scope of the Thesis

Selective partial oxidation of methane to methanol over Cu exchanged zeolites has been extensively investigated by means of spectroscopy on Cu-ZSM-5 and Cu-MOR systems. However, recent results raised questions and highlighted the necessity of a better understanding of Cu speciation in zeolites. There is evidence for the presence of spectator species in the most studied system Cu-ZSM-5 and Cu-MOR prepared from the Na-form of zeolite. Therefore, the assignation of characteristic spectroscopic features of these materials to the active site for methane oxidation needs to be revised taking into consideration the inactive Cu species within the zeolite framework.

In a first stage, this work aims at the preparation of a single-site copper oxygen cluster in MOR for the selective conversion of methane to methanol. X-ray absorption spectroscopy will be applied to identify the structure of the active copper oxygen cluster. Infrared spectroscopy of the residual BAS in activated Cu-MOR after adsorption of probe molecules such as n-hexane and pyridine will be used to determine the siting of the copper oxygen clusters within the MOR micropores. The concentration of these clusters will be quantified by the total yield of methane oxidation products after exposure to methane under conditions that assure that all active sites have performed one turnover.

As a next step, it is desirable to investigate the impact of catalyst preparation on the concentration and uniformity of the Cu sites. The ion exchange process with focus on the impact of pH and Cu precursor will be investigated. Since most studies of selective oxidation of methane to methanol over Cu exchanged zeolites use the Na-form as parent material, the impact of alkali and alkaline-earth co-cations on active site uniformity will be studied.

In the last part, the three step process of selective partial oxidation of methane to methanol will be investigated. The process of thermal activation is not understood in detail yet. It remains unclear which step during thermal activation requires the high activation temperature of 450 °C. Therefore, the role of dehydration and oxidation processes during heat treatment as well as the

dynamics of Cu ion movement on the activity of Cu-MOR will be investigated by means of *in situ* XAS spectroscopy. From the kinetic and spectroscopic studies, it will be possible to evaluate the impact of temperature, type of oxidant and oxidant partial pressure on Cu coordination, Cu oxidation state and activity of Cu species in selective partial oxidation of methane. Kinetics of the C-H activation on this Cu species will be derived. Finally, a possible reduction of the temperature gap within the three step process of methane conversion to methanol will be discussed.

## 1.7 References

- [1] Golisz, S.; Brent Gunnoe, T.; Goddard, W., III; Groves, J.; Periana, R. *Catal. Lett.* **2011**, *141*, 213.
- [2] Olah, G. A.; Goeppert, A.; Surya Prakash, G. K. *Beyond oil and gas- The methanol economy*, Wiley-VHC: Los Angeles, 2006.
- [3] Johnson, J. *Chem. Eng. News* **2005**, *83*, 19.
- [4] Kerr, R. A. *Science* **2010**, *328*, 1624.
- [5] Malakoff, D. *Science* **2014**, *344*, 1464.
- [6] Keller, G. E.; Bhasin, M. M. *J. Catal.* **1982**, *73*, 9.
- [7] Olsbye, U.; Svelle, S.; Bjorgen, M.; Beato, P.; Janssens, T. V. W.; Joensen, F.; Bordiga, S.; Lillerud, K. P. *Angew. Chem., Int. Ed.* **2012**, *51*, 5810.
- [8] Henrici-Olive, G.; Olive, S. *Angew. Chem., Int. Ed.* **1976**, *15*, 136.
- [9] Keil, F. J. *Nature Chem.* **2013**, *5*, 91.
- [10] Guo, X. G.; Fang, G. Z.; Li, G.; Ma, H.; Fan, H. J.; Yu, L.; Ma, C.; Wu, X.; Deng, D. H.; Wei, M. M.; Tan, D. L.; Si, R.; Zhang, S.; Li, J. Q.; Sun, L. T.; Tang, Z. C.; Pan, X. L.; Bao, X. H. *Science* **2014**, *344*, 616.
- [11] Olah, G. A. *Angew. Chem., Int. Ed.* **2005**, *44*, 2636.
- [12] Olah, G. A. *J. Am. Chem. Soc.* **2013**, *52*, 104.
- [13] Gurau, B.; Smotkin, E. S. *J. Power Sources* **2002**, *112*, 339.
- [14] Bitter, J. H.; Seshan, K.; Lercher, J. A. *J. Catal.* **1997**, *171*, 279.
- [15] Lange, J. P. *Catal. Today* **2001**, *64*, 3.
- [16] Nerlov, J.; Chorkendorff, I. *J. Catal.* **1999**, *181*, 271.
- [17] Palkovits, R.; Antonietti, M.; Kuhn, P.; Thomas, A.; Schuth, F. *Angew. Chem., Int. Ed.* **2009**, *48*, 6909.
- [18] Chan, S. I.; Lu, Y. J.; Nagababu, P.; Maji, S.; Hung, M. C.; Lee, M. M.; Hsu, I. J.; Minh, P. D.; Lai, J. C. H.; Ng, K. Y.; Ramalingam, S.; Yu, S. S. F.; Chan, M. K. *Angew. Chem., Int. Ed.* **2013**, *52*, 3731.
- [19] Limberg, C. *Angewandte Chemie International Edition* **2003**, *42*, 5932.
- [20] Labinger, J. A.; Bercaw, J. E. *Nature* **2002**, *417*, 507.
- [21] Periana, R. A.; Taube, D. J.; Evitt, E. R.; Loffler, D. G.; Wentrock, P. R.; Voss, G.; Masuda, T. *Science* **1993**, *259*, 340.
- [22] Periana, R. A.; Taube, D. J.; Gamble, S.; Taube, H.; Satoh, T.; Fujii, H. *Science* **1998**, *280*, 560.
- [23] Soorholtz, M.; White, R. J.; Zimmermann, T.; Titirici, M. M.; Antonietti, M.; Palkovits, R.; Schuth, F. *Chem. Commun.* **2013**, *49*, 240.

- [24] Rosenzweig, A. C.; Frederick, C. A.; Lippard, S. J.; Nordlund, P. *Nature* **1993**, 366, 537.
- [25] Bordeaux, M.; Galarneau, A.; Drone, J. *Angew. Chem., Int. Ed.* **2012**, 51, 10712.
- [26] Nguyen, H. H. T.; Elliott, S. J.; Yip, J. H. K.; Chan, S. I. *J. Biol. Chem.* **1998**, 273, 7957.
- [27] Himes, R. A.; Barnese, K.; Karlin, K. D. *Angew. Chem., Int. Ed.* **2010**, 49, 6714.
- [28] Chan, S. I.; Chen, K. H. C.; Yu, S. S. F.; Chen, C. L.; Kuo, S. S. J. *Biochemistry* **2004**, 43, 4421.
- [29] Ng, K. Y.; Tu, L. C.; Wang, Y. S.; Chan, S. I.; Yu, S. S. F. *ChemBioChem* **2008**, 9, 1116.
- [30] Chan, S. I.; Wang, V. C. C.; Lai, J. C. H.; Yu, S. S. F.; Chen, P. P. Y.; Chen, K. H. C.; Chen, C. L.; Chan, M. K. *Angew. Chem., Int. Ed.* **2007**, 46, 1992.
- [31] Lieberman, R. L.; Rosenzweig, A. C. *Nature* **2005**, 434, 177.
- [32] Chan, S. I.; Yu, S. S. F. *Acc. Chem. Res.* **2008**, 41, 969.
- [33] Groothaert, M. H.; Smeets, P. J.; Sels, B. F.; Jacobs, P. A.; Schoonheydt, R. A. *J. Am. Chem. Soc.* **2005**, 127, 1394.
- [34] Starokon, E. V.; Parfenov, M. V.; Pirutko, L. V.; Abornev, S. I.; Panov, G. I. *J. Phys. Chem. C* **2011**, 115, 2155.
- [35] Hammond, C.; Forde, M. M.; Ab Rahim, M. H.; Thetford, A.; He, Q.; Jenkins, R. L.; Dimitratos, N.; Lopez-Sanchez, J. A.; Dummer, N. F.; Murphy, D. M.; Carley, A. F.; Taylor, S. H.; Willock, D. J.; Stangland, E. E.; Kang, J.; Hagen, H.; Kiely, C. J.; Hutchings, G. J. *Angew. Chem., Int. Ed.* **2012**, 51, 5129.
- [36] Hammond, C.; Dimitratos, N.; Jenkins, R. L.; Lopez-Sanchez, J. A.; Kondrat, S. A.; ab Rahim, M. H.; Forde, M. M.; Thetford, A.; Taylor, S. H.; Hagen, H.; Stangland, E. E.; Kang, J. H.; Moulijn, J. M.; Willock, D. J.; Hutchings, G. J. *ACS Catal.* **2013**, 3, 689.
- [37] Edwards, J. K.; Solsona, B.; N, E. N.; Carley, A. F.; Herzing, A. A.; Kiely, C. J.; Hutchings, G. J. *Science* **2009**, 323, 1037.
- [38] Smeets, P. J.; Woertink, J. S.; Sels, B. F.; Solomon, E. I.; Schoonheydt, R. A. *Inorg. Chem.* **2010**, 49, 3573.
- [39] Ahn, J. H.; Kolvenbach, R.; Al-Khattaf, S. S.; Jentys, A.; Lercher, J. A. *ACS Catalysis* **2013**, 3, 817.
- [40] Schallmoser, S.; Ikuno, T.; Wagenhofer, M. F.; Kolvenbach, R.; Haller, G. L.; Sanchez-Sanchez, M.; Lercher, J. A. *J. Catal.* **2014**, 316, 93.
- [41] Gounder, R.; Iglesia, E. *J. Am. Chem. Soc.* **2009**, 131, 1958.

- [42] Boronat, M.; Martinez, C.; Corma, A. *Phys. Chem. Chem. Phys.* **2011**, *13*, 2603.
- [43] Veefkind, V. A.; Smidt, M. L.; Lercher, J. A. *Appl. Catal., A* **2000**, *194*, 319.
- [44] Haw, J. F.; Song, W.; Marcus, D. M.; Nicholas, J. B. *Acc. Chem. Res.* **2003**, *36*, 317.
- [45] Kwak, J. H.; Tonkyn, R. G.; Kim, D. H.; Szanyi, J.; Peden, C. H. F. *J. Catal.* **2010**, *275*, 187.
- [46] Gao, F.; Walter, E. D.; Washton, N. M.; Szanyi, J.; Peden, C. H. F. *Appl. Catal., B* **2015**, *162*, 501.
- [47] Beale, A. M.; Gao, F.; Lezcano-Gonzalez, I.; Peden, C. H. F.; Szanyi, J. *Chem. Soc. Rev.* **2015**, *44*, 7371.
- [48] Corma, A. *Chem. Rev.* **1995**, *95*, 559.
- [49] Corma, A.; Martinez, A. *Adv. Mater.* **1995**, *7*, 137.
- [50] Uytterhoeve, J. B.; Christner, L. G.; Hall, W. K. *J. Phys. Chem.* **1965**, *69*, 2117.
- [51] Mortier, W. J.; Sauer, J.; Lercher, J. A.; Noller, H. *J. Phys. Chem.* **1984**, *88*, 905.
- [52] Dedeczek, J.; Sobalik, Z.; Wichterlova, B. *Cat. Rev. - Sci. Eng.* **2012**, *54*, 135.
- [53] Gounder, R.; Iglesia, E. *Angew. Chem., Int. Ed.* **2010**, *49*, 808.
- [54] Eder, F.; Stockenhuber, M.; Lercher, J. A. *J. Phys. Chem. B* **1997**, *101*, 5414.
- [55] Subbotina, I. R.; Shelimov, B. N.; Kazanskii, V. B. *Kinet. Catal.* **2002**, *43*, 412.
- [56] Dedeczek, J.; Kaucky, D.; Wichterlova, B.; Gonsiorova, O. *Phys. Chem. Chem. Phys.* **2002**, *4*, 5406.
- [57] Dedeczek, J.; Kaucky, D.; Wichterlova, B. *Chem. Commun.* **2001**, 970.
- [58] Dedeczek, J.; Wichterlova, B. *J. Phys. Chem. B* **1999**, *103*, 1462.
- [59] Dedeczek, J.; Wichterlova, B. *J. Phys. Chem. B* **1999**, *103*, 1462.
- [60] Delabie, A.; Pierloot, K.; Groothaert, M. H.; Weckhuysen, B. M.; Schoonheydt, R. A. *Phys. Chem. Chem. Phys.* **2002**, *4*, 134.
- [61] Attfield, M. P.; Weigel, S. J.; Cheetham, A. K. *J. Catal.* **1997**, *170*, 227.
- [62] Kwak, J. H.; Varga, T.; Peden, C. H. F.; Gao, F.; Hanson, J. C.; Szanyi, J. *J. Catal.* **2014**, *314*, 83.
- [63] Dedeczek, J.; Sobalik, Z.; Tvaruzkova, Z.; Kaucky, D.; Wichterlova, B. *J. Phys. Chem.* **1995**, *99*, 16327.
- [64] Nicula, A.; Stamires, D.; Turkevich, J. *J. Chem. Phys.* **1965**, *42*, 3684.
- [65] Venuto, P. B.; Hamilton, L. A.; Landis, P. S. *J. Catal.* **1966**, *5*, 484.
- [66] Rabo, J. A.; Angell, C. L.; Kasai, P. H.; Schomaker, V. *Discuss. Faraday Soc.* **1966**, *41*, 328.
- [67] Ward, J. W. *J. Phys. Chem.* **1968**, *72*, 4211.

- [68] Christner, L. G.; Liengme, B. V.; Hall, W. K. *Trans. Faraday Soc.* **1968**, *64*, 1679.
- [69] Morice, J. A.; Rees, L. V. C. *Trans. Faraday Soc.* **1968**, *64*, 1388.
- [70] Kubo, T.; Kunugi, T.; Kumada, F.; Tominaga, H. *Nippon Kagaku Kaishi* **1972**, *8*, 1621.
- [71] Kubo, T.; Tominaga, H.; Kunugi, T. *Bull. Chem. Soc. Jpn.* **1973**, *46*, 3549.
- [72] Richards.Jt *J. Catal.* **1967**, *9*, 178.
- [73] Richards.Jt *J. Catal.* **1967**, *9*, 172.
- [74] Richards.Jt *J. Catal.* **1967**, *9*, 182.
- [75] Iwamoto, M.; Yahiro, H.; Tanda, K.; Mizuno, N.; Mine, Y.; Kagawa, S. *J. Phys. Chem.* **1991**, *95*, 3727.
- [76] Larsen, S. C.; Aylor, A.; Bell, A. T.; Reimer, J. A. *J. Phy. Chem.* **1994**, *98*, 11533.
- [77] Beutel, T.; Sarkany, J.; Lei, G. D.; Yan, J. Y.; Sachtler, W. M. H. *J. Phys. Chem.* **1996**, *100*, 845.
- [78] Sarkany, J.; Ditre, J. L.; Sachtler, W. M. H. *Catal. Lett.* **1992**, *16*, 241.
- [79] Lei, G. D.; Adelman, B. J.; Sarkany, J.; Sachtler, W. M. H. *Appl. Catal., B* **1995**, *5*, 245.
- [80] Groothaert, M. H.; van Bokhoven, J. A.; Battiston, A. A.; Weckhuysen, B. M.; Schoonheydt, R. A. *J. Am. Chem. Soc.* **2003**, *125*, 7629.
- [81] Gao, F.; Walter, E. D.; Kollar, M.; Wang, Y.; Szanyi, J.; Peden, C. H. F. *J. Catal.* **2014**, *319*, 1.
- [82] Gao, F.; Washton, N. M.; Wang, Y.; Kollár, M.; Szanyi, J.; Peden, C. H. F. *J. Catal.* **2015**, *331*, 25.
- [83] Yamanaka, H.; Hamada, R.; Nibuta, H.; Nishiyama, S.; Tsuruya, S. *J. Mol. Catal. A: Chem.* **2002**, *178*, 89.
- [84] Hamada, R.; Shibata, Y.; Nishiyama, S.; Tsuruya, S. *Phys. Chem. Chem. Phys.* **2003**, *5*, 956.
- [85] Kubacka, A.; Wang, Z.; Sulikowski, B.; Cortés Corberán, V. *J. Catal.* **2007**, *250*, 184.
- [86] Vanelderen, P.; Vancauwenbergh, J.; Sels, B. F.; Schoonheydt, R. A. *Coord. Chem. Rev.* **2013**, *257*, 483.
- [87] Alayon, E. M.; Nachtegaal, M.; Ranocchiari, M.; van Bokhoven, J. A. *Chem. Commun.* **2012**, *48*, 404.
- [88] Alayon, E. M. C.; Nachtegaal, M.; Bodi, A.; van Bokhoven, J. A. *ACS Catal.* **2014**, *4*, 16.

- [89] Vanelderen, P.; Snyder, B. E. R.; Tsai, M.-L.; Hadt, R. G.; Vancauwenbergh, J.; Coussens, O.; Schoonheydt, R. A.; Sels, B. F.; Solomon, E. I. *J. Am. Chem. Soc.* **2015**, *137*, 6383.
- [90] Narsimhan, K.; Michaelis, V. K.; Mathies, G.; Gunther, W. R.; Griffin, R. G.; Roman-Leshkov, Y. *J. Am. Chem. Soc.* **2015**, *137*, 1825.
- [91] Wulfers, M. J.; Teketel, S.; Ipek, B.; Lobo, R. F. *Chem. Commun.* **2015**, *51*, 4447.
- [92] Sheppard, T.; Hamill, C. D.; Goguet, A.; Rooney, D. W.; Thompson, J. M. *Chem. Commun.* **2014**, *50*, 11053.
- [93] Groothaert, M. H.; Pierloot, K.; Delabie, A.; Schoonheydt, R. A. *Phys. Chem. Chem. Phys.* **2003**, *5*, 2135.
- [94] Smeets, P. J.; Groothaert, M. H.; Schoonheydt, R. A. *Catal. Today* **2005**, *110*, 303.
- [95] Woertink, J. S.; Smeets, P. J.; Groothaert, M. H.; Vance, M. A.; Sels, B. F.; Schoonheydt, R. A.; Solomon, E. I. *Proc. Natl. Acad. Sci. U. S. A.* **2009**, *106*, 18908.

## 2 Single-Site Trinuclear Copper Oxygen Clusters in Mordenite for Selective Conversion of Methane to Methanol

### 2.1 Abstract

Copper exchanged zeolites with mordenite structure mimic the nuclearity and reactivity of active sites in particulate methane monooxygenase, which are enzymes able to selectively oxidize methane to methanol. In this Chapter<sup>1,2</sup> it is shown that the mordenite micropores provide a perfect confined environment for the highly selective stabilization of trinuclear copper-oxo clusters that exhibit a high reactivity towards activation of C-H bonds in methane and its subsequent transformation to methanol. The similarity with the enzymatic systems is also implied from the similarity of the reversible rearrangements of the trinuclear clusters occurring during the selective transformations of methane along the reaction path towards methanol, in both the enzyme system and copper exchanged mordenite.

---

<sup>1</sup> This chapter is based on the article of the same title as appeared in Nature Communications: Grundner, S.; Markovits, M. A. C.; Li, G.; Tromp, M.; Pidko, E. A.; Hensen, E. J. M.; Jentys, A.; Sanchez-Sanchez, M.; Lercher, J. A. *Nat. Commun.* **2015**, 6, 7546.

<sup>2</sup> All results on DFT calculations were provided by Guanna Li and Evgeny Pidko at Eindhoven University of Technology.

## 2.2 Introduction

Nature has found a way to convert methane in a single step to methanol via a biocatalytic transformation under aerobic conditions with methane monooxygenase (MMO) as catalysts using Cu and Fe as potential active metals. Two forms of MMOs at different cellular locations are known, a cytoplasmic MMO (soluble, sMMO) and a membrane bound MMO (particulate, pMMO). In sMMO, the active site of the hydroxylase contains a bis( $\mu$ -oxo)diiron core,<sup>[1]</sup> while in pMMO the active site is represented by a Cu cluster that catalyzes the insertion of oxygen into the methane C-H bond with a very high rate (rate normalized to the concentration of active sites, i.e., the turnover frequency (TOF) of about  $1\text{ s}^{-1}$ ).<sup>[2]</sup>

Aerobic and anaerobic handling during purification led to drastically different concentrations of Cu in the enzyme without inducing marked changes in the enzyme structure, and in turn, differences in the conclusions about the nature of the active site.<sup>[3]</sup> The group of Rosenzweig has attributed the catalytic activity to a Cu dimer<sup>[4-6]</sup>, while the group of Chan suggested a cluster of three Cu atoms to form the active site.<sup>[3,7-9]</sup> Following these leads, homogeneous<sup>[10-12]</sup> and heterogeneous<sup>[13,14]</sup> Cu based catalysts have been explored. In particular, studies of the heterogeneous Cu catalysts led to limited and conflicting insights despite the excellent spectroscopic work, because in nearly all cases the active site has been concluded to represent only a minority of the Cu species in the catalyst. However, the potential of Cu exchanged zeolites as biomimetic inorganic model system of pMMO is promising.<sup>[15,16]</sup> In this chapter, a new approach to prepare uniform Cu-oxo species in zeolites able to activate and convert methane has been developed.

## 2.3 Results and Discussion

### 2.3.1 Preparation of a Single-Site Copper Oxygen Cluster

A new approach to prepare uniform Cu-oxo species in zeolites able to activate and convert methane was developed which enables a selective stabilization of single-site Cu-oxo clusters in mordenite micropores. Three parameters turned out to have a significant impact on the uniformity of the sites within the zeolite.

First of all, a suitable zeolite matrix able to stabilize the active Cu cluster was chosen. In accordance with literature, Cu-MOR was found to have the highest activity in selective partial oxidation of methane to methanol.<sup>[17]</sup> Figure 2.1 shows that for a series of Cu<sup>2+</sup> exchanged zeolites the methane converted and methanol yield correlate with pore size of the zeolite. Large pore zeolites, such as BEA consisting of 12-MR, showed poor activity. The activity of 10-MR structures such as ZSM-5 was lower than the activity of 8-MR containing zeolites such as FER and MOR. Therefore the high activity of Cu-MOR was attributed to the ability of the 8-MR side pockets to selectively stabilize active Cu-oxo clusters.

Secondly, comparison of Cu exchanged H-MOR with Na-MOR revealed a significantly higher activity of the Cu exchanged H-MOR materials.<sup>[18]</sup> Na<sup>+</sup> is known to preferentially exchange into the side pockets of the MOR structure.<sup>[19]</sup> Hence, it is speculated that alkali cations compete for the Cu<sup>2+</sup> exchange sites and therefore inhibit the formation of the active Cu-oxo cluster in the side pockets. Consequently, H-MOR was chosen as parent material.

Lastly, the impact of the Cu salt was examined. It was shown that Cu<sup>2+</sup> acetate is the most suitable precursor giving high Cu-loadings and high active site concentrations. Ion exchange with Cu<sup>2+</sup> nitrate or chloride led to significantly low methane conversion. Therefore, it is concluded that low active site concentrations are present in those materials. This phenomenon is explained in detail in Chapter 3.

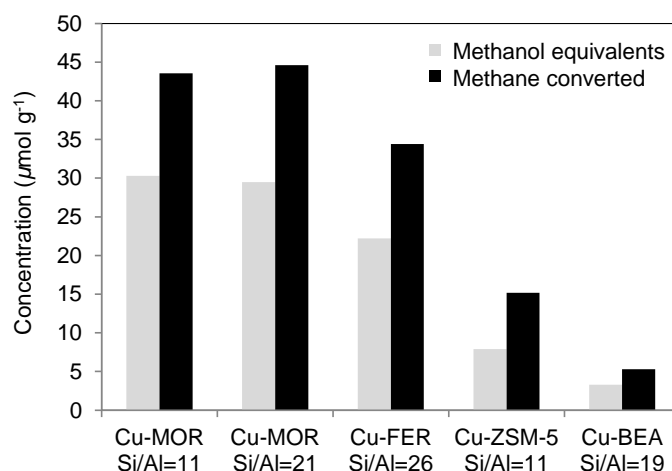


**Figure 2.1:** Methanol equivalents and methane converted for a series of Cu exchanged zeolites with a Cu loading of 1 wt% (150-160  $\mu\text{mol}$ ). Methanol equivalents take the concentration of formed methanol and the concentration of the secondary product dimethyl ether corresponding to two methanol molecules into account. Cu-zeolites were activated in oxygen at 450 °C for 1h and exposed to methane at 200 °C for 4h. The products were desorbed by steam treatment at 135 °C.

### 2.3.2 Siting of Copper in Mordenite

In order to get a fundamental understanding of the impact of the zeolite matrix on the high activity of Cu-MOR for selective partial oxidation of methane to methanol, the siting of Cu species in MOR was investigated in detail. Since the initial position of the Cu cations inside the framework must be related to the location of the exchangeable Brønsted acid sites (BAS) in MOR, the distribution and exchangeability of BAS in this material was investigated by means of infrared spectroscopy and Co exchange.

#### 1.1.1.1 Infrared spectroscopy – Adsorption of n-hexane

The MOR topology consists of a 12-MR main channel with perpendicular 8-MR side pockets. The entrance (pore mouth) of the side pocket (3.9 x 5.7 Å) is substantially smaller than the aperture of the large straight channel (6.5 x 7.0 Å). Distribution of acid sites of the parent H-MOR was determined by deconvolution of the band at 3,605  $\text{cm}^{-1}$  assigned to BAS in MOR (Figure 2.2 a). The O-H vibration corresponding to BAS comprises two bands, one corresponding to vibration into the large pores (3,612  $\text{cm}^{-1}$ ) and the other, at

lower frequency, vibrating into the side pockets ( $3,590\text{ cm}^{-1}$ ). Adsorption of n-hexane allows an accurate quantification of the BAS concentration in each position, as only BAS in the main channels are accessible to this probe molecule.<sup>[20]</sup> After n-hexane adsorption, the band attributed to BAS is shifted from  $3,600$  to  $3,590\text{ cm}^{-1}$ , indicating that the contribution of the main channel acid sites disappeared due to perturbation of those O-H groups with n-hexane (Figure 2.2 b). The perturbed acid sites are assigned to a broad band at  $3,500\text{ cm}^{-1}$  that is also emerging after n-hexane adsorption. Therefore the main features in the range of  $3,300$  to  $3,650\text{ cm}^{-1}$  can be fitted with the contributions of the BAS in the side pockets and the perturbed BAS. Consequently, the BAS in the main channel can be quantified, and a distribution of BAS in 8-MR and 12-MR is obtained (65 % and 35 % respectively). This method allows as well a verification of the deconvolution of the spectra of activated H-MOR before n-hexane adsorption. The BAS concentration and therefore the framework Al site concentration of the parent MOR was determined by quantification of Na concentration achieved after  $\text{Na}^+$  exchange.

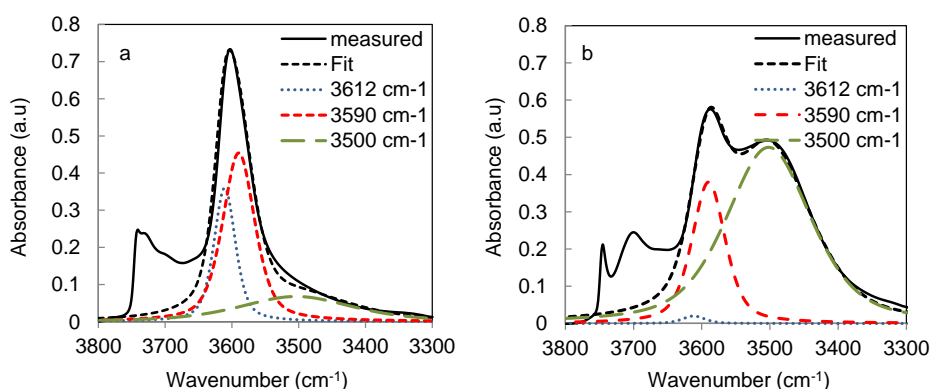


**Figure 2.2:** Infrared spectra of the O-H stretching vibrations of the Brønsted acid sites of H-MOR a) after activation at  $450\text{ °C}$  and b) during adsorption of n-hexane at  $30\text{ °C}$ . BAS are deconvoluted in bands attributed to main channel O-H ( $3,612\text{ cm}^{-1}$ ), side pocket O-H stretching vibrations ( $3,590\text{ cm}^{-1}$ ) and perturbed O-H ( $3,500\text{ cm}^{-1}$ ).

To obtain insight into the location of extra-framework Cu clusters, it was employed the same approach to investigate the distribution of residual BAS in Cu-MOR materials after their activation in  $\text{O}_2$ . The location of the Cu-oxo

clusters was inferred by direct comparison of the concentration of O-H groups associated with BAS in the activated Cu-MOR with the concentration of these groups in the parent H-MOR. Figure 2.3 shows the change of the O-H vibration bands attributed to main channel BAS (Figure 2.3 a,c ) and side pocket BAS (Figure 2.3 b,d) for two series of Cu-MOR with Si/Al 21 and 11 respectively. It should be emphasized that deconvolution of the band at  $3,605\text{ cm}^{-1}$  associated with BAS did not show any change of concentration of BAS in the main channel ( $3,612\text{ cm}^{-1}$ ) upon Cu exchange and subsequent thermal activation. Only the band associated to BAS in the side pockets ( $3,590\text{ cm}^{-1}$ ) was decreasing with increasing Cu concentration. Perturbation of BAS in the main channel with n-hexane confirmed these findings. In turn, this allows the conclusion that  $\text{Cu}^{2+}$  exchanges selectively those protons in the side pockets. It is hypothesized that the relatively high concentration of framework Al (65% of the total) in the side pockets is stabilizing the Cu-oxo ions. Therefore, the first conclusion is that the active Cu core is located in the side pockets and bound to framework Al sites.

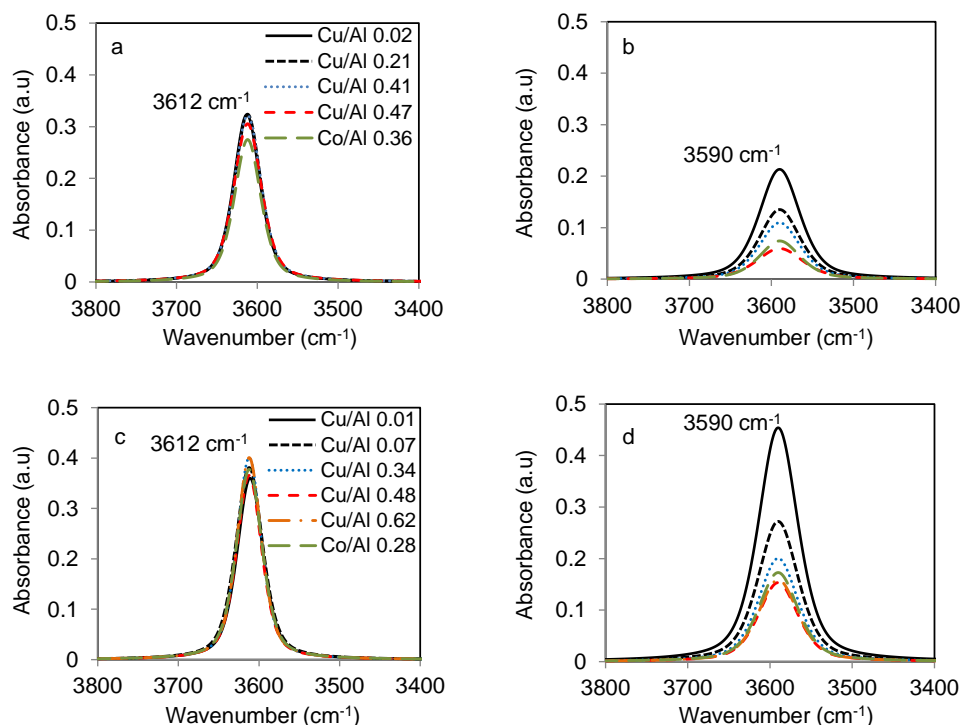


**Figure 2.3:** Deconvoluted bands of BAS in Cu exchanged MOR with a,b) Si/Al ratio 21 and c,d) Si/Al ratio 11. BAS vibration is deconvoluted in bands attributed to a), c) main channel OH at  $3,612\text{ cm}^{-1}$  and b),d) side pocket OH stretching vibrations at  $3,590\text{ cm}^{-1}$ .

BAS concentrations of Cu exchanged MOR were obtained by integration of the normalized, deconvoluted O-H vibration bands assigned to BAS in the main channel and side pockets. Those values were normalized to the total concentration of BAS in the parent H-MOR. Figure 2.4 shows the consumption of BAS versus Cu concentration for two series of Cu-MOR with Si/Al 21 and 11 respectively. A linear dependence of acid site consumption with increasing Cu loading up to a Cu/Al ratio of 0.4 was observed. Over-exchanged materials were obtained for higher Cu loading. The offset can be rationalized by dealumination during aqueous Cu exchange. A blank experiment with acetic acid showed the preparation procedure eliminates approximately 5 % of the total BAS, ca.  $70 \mu\text{mol g}^{-1}$ , by dealumination. The slopes of 0.71 and 0.69 in Figure 2.4 indicate that only two lattice aluminum ions were involved in binding of 3 Cu cations. This is the first evidence of an active site involving three Cu atoms anchored to two Al framework sites.

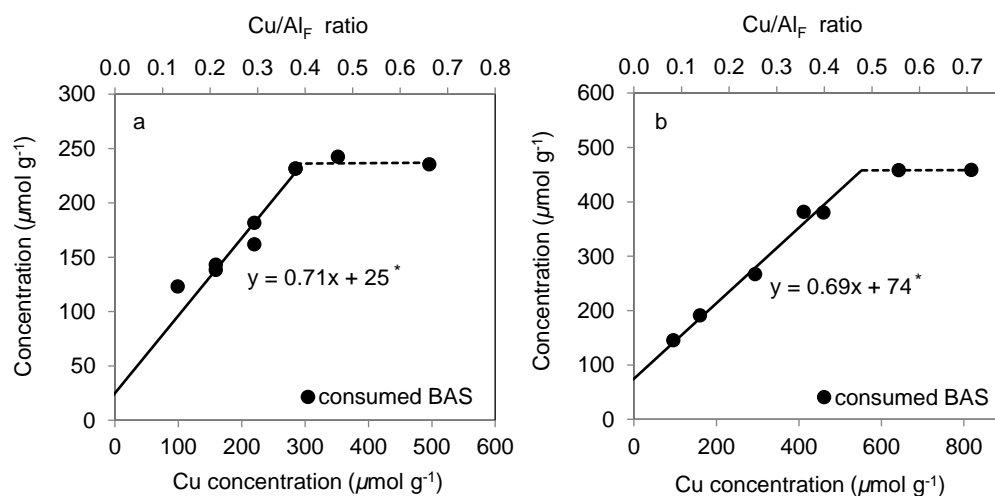


**Figure 2.4:** Framework aluminum coordination upon Cu loading. The concentration of tetrahedrally coordinated aluminum acting as ion exchange site for  $\text{Cu}^{2+}$  with total yield for Cu-MOR with a) Si/Al =21 and b) Si/Al =11. \* The slope of 0.71 and 0.69 respectively indicate an exchange stoichiometry of 2/3 meaning that 2  $\text{H}^+$  are substituted by 3  $\text{Cu}^{2+}$ . The offset of  $25 \mu\text{mol g}^{-1}$  and  $74 \mu\text{mol g}^{-1}$  respectively show slight dealumination of framework Al ( $\sim 5\%$ ) during Cu exchange.

### 1.1.1.2 Infrared spectroscopy - Adsorption of pyridine

More detailed infrared spectroscopic analysis of the acid site location and consumption upon Cu exchange can be achieved via pyridine adsorption.<sup>[21]</sup> Figure 2.5 shows a linear decrease of BAS concentration with increasing Cu loading. Quantification of acid sites by O-H stretching vibrations ( $3,605\text{ cm}^{-1}$ ) of the BAS of H-MOR after activation at  $450\text{ }^{\circ}\text{C}$  and quantified by vibrational band of the pyridinium ion after adsorption of pyridine ( $1,545\text{ cm}^{-1}$ ) resulted in a constant divergence of ca.  $300\text{ }\mu\text{mol/g}$  for various Cu loadings. Pyridine, due to its basicity and its spherical shape, can access those BAS in the main channel and in the pore mouth of the side pockets.<sup>[22]</sup> Therefore, the concentration of BAS located at the bottom of the side pockets can be calculated by the difference between BAS concentration determined by O-H stretching vibrations and BAS concentration quantified by pyridine adsorption. The constant value of  $300\text{ }\mu\text{mol/g}$  for various Cu concentrations indicates that the incorporated Cu is not interacting with framework Al sites at the bottom of the pockets.

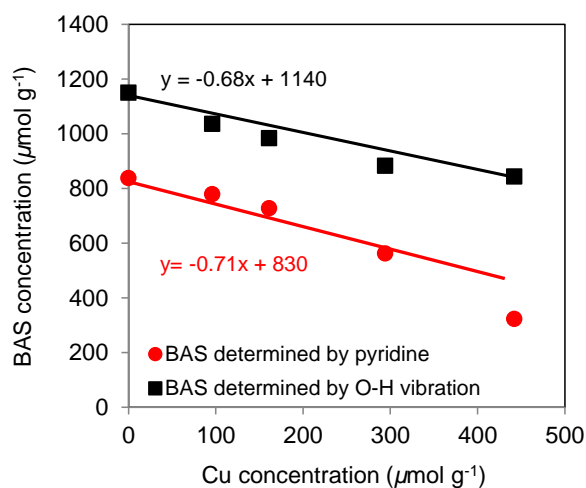


**Figure 2.5:** Infrared spectroscopic quantification of Brønsted acid sites in Cu-MOR. Plot of BAS concentration quantified by O-H stretching vibrations ( $3605\text{ cm}^{-1}$ ) of the BAS of H-MOR after activation at  $723\text{ K}$  and quantified by vibrational band of the pyridinium ion after adsorption of pyridine ( $1545\text{ cm}^{-1}$ ). The slopes of  $-0.68$  and  $-0.71$  respectively indicate that  $2\text{ H}^{+}$  are exchanged for  $3\text{ Cu}^{2+}$  in the pore mouth of the side pockets, which are accessible for pyridine.

In contrast, n-hexane has a strong preference for diffusion along the main channel (001) due to its elongated shape. Therefore, by comparison of pyridine adsorption with n-hexane adsorption data, the concentration of BAS at the pore mouth of the side pockets can be quantified (Table 2.1). Cu incorporation was found to exclusively affect those BAS located at the pore mouth of the side pockets, indicating that such position is where Cu active species are located. For Cu exchanged samples with Cu loading exceeding a Cu/Al ratio of 0.4, all the potential sites close to the entrance of the side pocket are occupied with Cu, and the Cu excess is believed to precipitate as inactive large Cu clusters on the outer surface of the zeolite.

**Table 2.1:** Acidity of Cu-MOR. Quantification of acid sites for a series of Cu-MOR<sup>a</sup> (Si/Al=11, Cu/Al ≤0.4).

Cu conc. ( $\mu\text{mol g}^{-1}$ )	BAS <sub>main channel</sub> <sup>b</sup> ( $\mu\text{mol g}^{-1}$ )	BAS <sub>SP bottom</sub> <sup>c</sup> ( $\mu\text{mol g}^{-1}$ )	BAS <sub>SP pore mouth</sub> <sup>d</sup> ( $\mu\text{mol g}^{-1}$ )	Total BAS ( $\mu\text{mol g}^{-1}$ )
0	400	310	380	1,090
100	430	270	330	1030
160	420	270	290	980
290	410	320	160	890
440	440	370	20	830

- a) Total concentration of BAS in H-MOR (Si/Al=11) was determined by Na exchange. For Cu exchanged MOR the normalized integral of the O-H vibration of BAS was used for deconvolution and quantification.
- b) Obtained by quantification of the band at  $3,612\text{ cm}^{-1}$  (after deconvolution of the band at  $3,605\text{ cm}^{-1}$  into  $3,612$ ,  $3,590$  and  $3,500\text{ cm}^{-1}$ ).
- c) Calculated by the difference of BAS concentration determined by a) and BAS concentration determined by pyridine.
- d) Calculated by the difference between BAS concentration quantified after n-hexane adsorption (band at  $3,590\text{ cm}^{-1}$ ) and BAS concentration in the SP bottom (c); an offset of  $70\text{ }\mu\text{mol g}^{-1}$  due to dealumination during Cu exchange was subtracted for H-MOR.

### 1.1.1.3 Determination of Al pairs by Co exchange

When Co exchange is performed under certain conditions,  $\text{Co}^{2+}$  ions exchange as monomers balancing two framework  $\text{AlO}_4^-$  tetrahedral.<sup>[23]</sup> In this way, the concentration of Co exchanged gives the concentration of framework Al sites which are paired. Paired Al sites are defined as  $\text{Al-O-(Si-O)}_n\text{-Al}$  sequences in one ring with  $n \leq 2$ , and in case of 8-MR in MOR,  $n \leq 3$ .<sup>[24]</sup> For the standard parent material used in this study, namely H-MOR with Si/Al 11, a pairing degree of 66% was determined by  $\text{Co}^{2+}$  exchange with Co-nitrate. Analogously, for H-MOR with Si/Al 21 a pairing degree of 60% was determined.

Deconvolution of the UV-vis spectra of those Co exchanged samples allows analysis of the distribution of the paired Al sites in the zeolite.<sup>[23]</sup> Dedecq *et al.* reported two dominant sites for  $\text{Co}^{2+}$  in dehydrated MOR: Site A is created by the 8-MR side pocket ( $\beta$ -type Co). Site E is located at the wall of the 12-MR main channel ( $\alpha$ -type Co). The occupancy of Site C is negligible (less than 5 % of the Co population in MOR).<sup>[25]</sup> The decomposition of the UV-vis spectra<sup>3</sup> of the Co exchanged standard parent material H-MOR with Si/Al 11 revealed that site A hosted 65% of all  $\text{Co}^{2+}$  ions ( $\beta$ -type  $\text{Co}^{2+}$ ), indicating that the majority of the paired Al sequences are located in the side pockets (see Appendix Table A 2.1). 26% of  $\text{Co}^{2+}$  was found as  $\alpha$ -type  $\text{Co}^{2+}$  at the E site in the main channel wall. The remaining  $\text{Co}^{2+}$  (9%) occurred as  $\gamma$ -type  $\text{Co}^{2+}$  at the C site. Consequently, ca. 43% (65% of 66% Al sites which are paired) of the total Al site concentration is attributed to paired sites in the side pockets. This value is in good agreement with the maximum ion exchanged Cu loading in the side pockets achieved for Cu/Al ratio 0.4.

### 2.3.3 Testing of Activity for Selective Oxidation of Methane

Using the approach discussed in the previous sections, a series of Cu-MOR with varying Cu concentrations was prepared. Subsequent calcination in flowing  $\text{O}_2$  at 450 °C converted these precursors to the active materials. The

---

<sup>3</sup> Measurement and analysis of UV-vis spectra of Cobalt exchanged mordenite was performed by Jiri Dědeček and Viktor Kreibich at the J. Heyrovský Institute of Physical Chemistry in Prague.

high temperature activation is necessary for the dehydration of the materials and the induced migration of the exchanged Cu ions towards formation of the oxide clusters. The activity of these clusters was evaluated by exposing the activated catalyst to methane at 200 °C followed by purging the zeolite with water in order to release the formed products. Methane loading in a flow of 16 ml min<sup>-1</sup> with a methane partial pressure of 900 mbar for 4 h resulted in maximum methane conversion. Further increase of the methane contact time did not affect the total conversion of methane achieved. Therefore, it is concluded that all active sites are titrated with methane after 4 h contact time. Hence, the total yield of products determined by steam assisted desorption corresponds to the active site concentration in the sample. Approximately 80 % of the methane converted by the materials was desorbed as methanol or dimethyl ether in the purge step. Furthermore, CO<sub>2</sub> corresponding to 20% of the methane conversion was detected during steam assisted desorption.

In Figure 2.6, the total yield of products (methane converted) is plotted against Cu loading for a series of Cu-MOR prepared from H-MOR as described in section 1.3.1. The total yield of methane oxidation products per g of zeolite catalyst was an order of magnitude higher than the maximum methanol yields reported in the recent literature for Cu-MOR (13  $\mu\text{mol g}^{-1}$ ).<sup>[17,26]</sup> The productivity of the active materials increased linearly with the Cu concentration pointing to a stoichiometry of three Cu cations needed to convert one methane molecule. The linear dependence of the activity on the Cu<sup>2+</sup> concentration strongly suggests that only one type of active site has been formed on a large series of samples with different Cu loading (Figure 2.6). The stoichiometry of methane activated per Cu valid for different Si/Al ratios is a further evidence of an active site involving three Cu atoms.

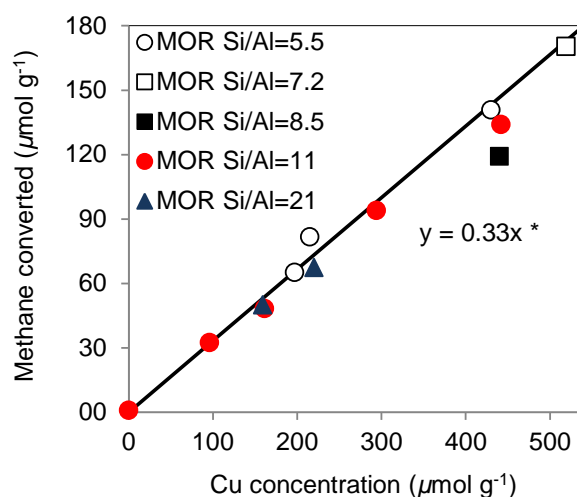


**Figure 2.6:** Methane converted as a function of Cu concentration in Cu-MOR for various Si/Al ratios \*The slope of 0.33 respectively indicates that 3 Cu centers are involved in the oxidation of one methane molecule.

## 2.3.4 Spectroscopic Characterization

In order to investigate the nature of the Cu species, X-ray adsorption spectroscopy (XAS) and ultraviolet-visible (UV-vis) spectroscopy of activated Cu-MOR samples were performed. Fitting of the obtained Cu K-edge extended X-ray adsorption fine structure (EXAFS) spectra with various copper oxo clusters predicted by density functional theory (DFT) calculations allowed evaluation of the nuclearity and the structure of the Cu cluster.

### 1.1.1.4 DFT modeling

The information obtained about the nuclearity and location of the Cu-oxo active sites by infrared spectroscopy and activity tests was used to propose several model structures for trinuclear Cu clusters in MOR to be studied by DFT calculations.<sup>4</sup> Their stability was evaluated and compared to dicopper clusters, as those typically described to be the active species for Cu-ZSM-5 in the literature.<sup>[27]</sup> Calculated reaction energies for interconversion of different Cu species indicated a high intrinsic stability of binuclear complexes at 0 K.

<sup>4</sup> All results on DFT calculations were provided by Guanna Li and Evgeny Pidko at Eindhoven University of Technology.

However, ab initio thermodynamic analysis in term of reaction Gibbs free energy depending on system temperature and pressure showed that a  $[\text{Cu}_3(\mu\text{-O})_3]^{2+}$  complex is the most stable species at 700 K in  $\text{O}_2$  atmosphere and under dry conditions (Figure 2.7). The proposed stoichiometry suggests a formal mixed Cu(II)/Cu(III) composition of the cluster. However, analysis of the electronic properties of the computed structures indicates that because of the substantial anion-radical nature of the oxygen ligands (Bader charge -0.76 e and -0.63 e compared to the Bader charge of -1.09e on oxygens in bulk CuO), all Cu site in the trinuclear cluster are more adequately described as being Cu(II) because their charges are very close to those computed for Cu centers in bulk CuO (+1.09 e). The results of Bader charge and spin polarized charge density analysis are summarized in the Appendix in Figure A 2.1.

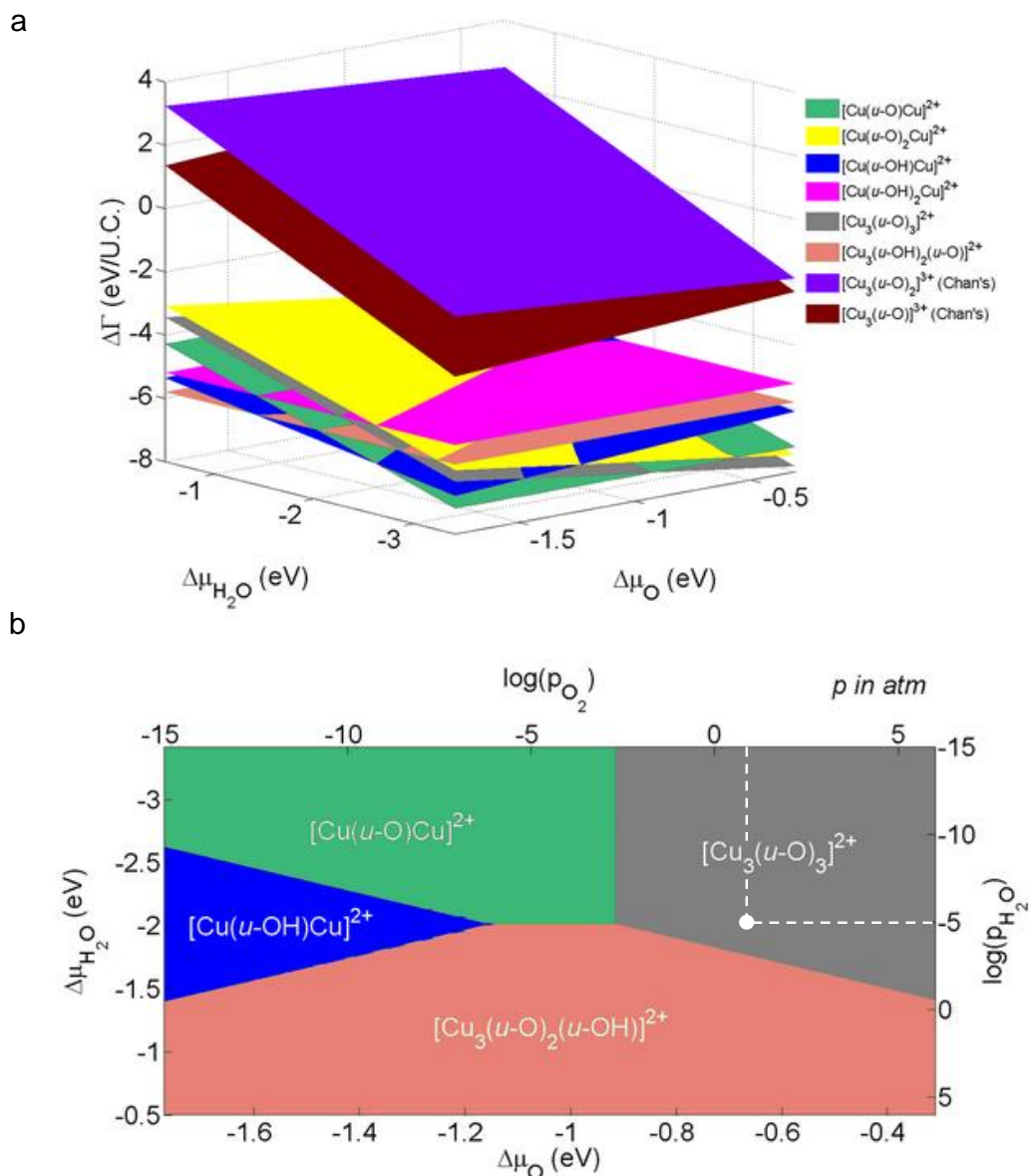


**Figure 2.7:** Ab initio thermodynamic analysis. a) Reaction free energy as a function of water and oxygen chemical potential and b) 2D projection of the lowest free energy  $\text{Cu}_x\text{O}_m\text{H}_n$  species in MOR supercell ( $\Delta\Gamma$  (eV/U.C.), cf. equation. (1)) as a function of oxygen chemical potential ( $\Delta\mu_{\text{O}}$ ) and water chemical potential ( $\Delta\mu_{\text{H}_2\text{O}}$ ).  $\Delta\mu_{\text{O}}$  and  $\Delta\mu_{\text{H}_2\text{O}}$  are translated into pressure scales at  $T = 700$  K; The conditions of our experiments (1 atm  $\text{O}_2$ , 10 ppm  $\text{H}_2\text{O}$ ) and consequently the location of the activated Cu-MOR are marked with a white dot.

The findings from infrared spectroscopy combined with  $\text{Co}^{2+}$  exchange indicate an Al arrangement of two Al in the 8-MR mouth pore of the side pocket. Consequently an Al arrangement of more than one framework Al site per side pocket was incorporated in the DFT model. DFT calculations are based on a unit cell containing paired (type I) and isolated (type II) Al sites located at the pore mouth of the side pockets (Figure 2.8).

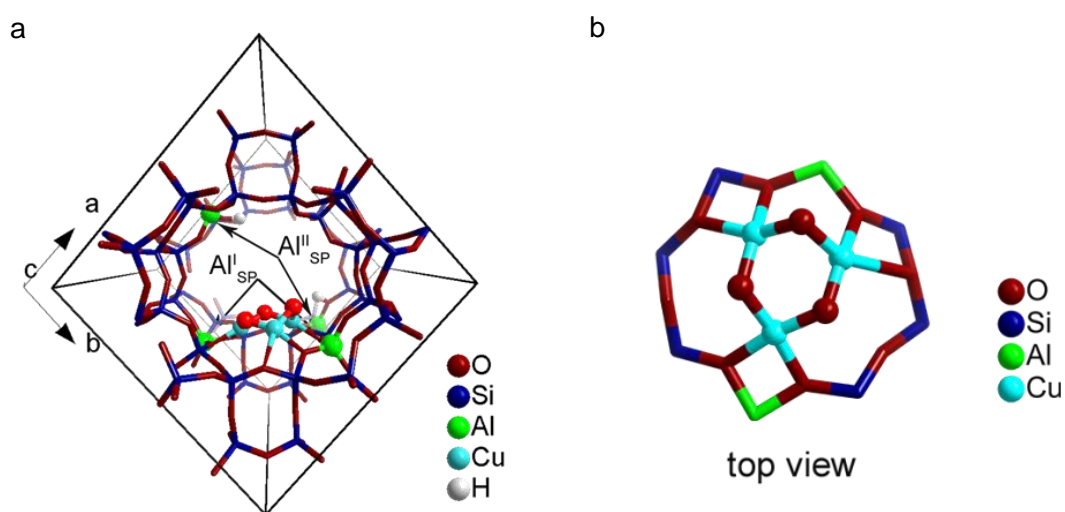


**Figure 2.8:** a) Location and b) structure of  $[\text{Cu}_3(\mu\text{-O})_3]^{2+}$  cluster in MOR zeolite model predicted by periodic DFT calculations (Si/Al=11). The zeolite model contained paired (type I) and isolated (type II) Al atoms located at the pore mouth of the side pocket. The cluster is stabilized by two anionic centers due to  $\text{Al}^{\text{I}}_{\text{SP}}$  lattice sites at the entrance of the MOR side-pocket so that the extraframework oxygens responsible for the initial C-H activation are pointing towards the main channel of MOR. The charge due to the remaining  $\text{Al}^{\text{II}}_{\text{SP}}$  is compensated by acidic protons resulting in BAS formation.

The DFT optimized geometric parameters of the proposed trinuclear Cu cluster show a low symmetry of this species (Figure 2.8). Therefore, Cu atoms in the cluster are not equivalent and two different shells need to be included. Coordination numbers are averaged for the 3 Cu scatterers (Table 2.2). The average coordination numbers derived from the DFT optimized geometric parameters of the most stable trinuclear cluster were applied for the EXAFS fit in order to take all Cu-O and Cu-Cu contributions into account.

**Table 2.2:** Determination of average coordination numbers per copper atom for the DFT model of  $[\text{Cu}_3(\mu\text{-O})_3]^{2+}$  in Cu-MOR.

Path	Average Distance <sup>a</sup> $R^{\text{DFT}}$ [Å]	Number of paths (DFT) <sup>b</sup>	Coordination number $N^c$
Cu-O <sub>EF</sub>	1.80 (±0.03)	6	2
Cu-O <sub>F</sub>	2.01 (±0.05)	5	1.66
Cu-O <sub>F</sub>	2.63 (±0.01)	1	0.33
Cu-Cu	2.74 (±0.01)	2	0.66
Cu-Cu	3.04 (±0.01)	4	1.33
Cu-O <sub>EF</sub>	3.23 (±0.03)	2	0.66

<sup>a</sup>Cu-O and Cu-Cu paths averaged values derived from data in Table A 2.4 (values predicted by DFT calculations, averaged over 3 Cu scatterers, statistical errors in brackets); <sup>b</sup>Number of paths that were averaged; <sup>c</sup>Coordination numbers averaged over 3 copper atoms obtained by dividing the number of paths in b by the number of Cu of the cluster.

A  $[\text{Cu}(\mu\text{-O})_2\text{Cu}]^{2+}$  core as well as a  $[\text{Cu}(\mu\text{-O})\text{Cu}]^{2+}$  core were previously proposed as the active site for methane activation in Cu-ZSM-5.<sup>[17,27]</sup> The DFT-optimized geometric parameters of those structures in the MOR unit cell together with the corresponding EXAFS refined parameters are tabulated in the Appendix (see Table A 2.2 and Table A 2.3).

#### 1.1.1.5 EXAFS spectroscopy

Cu species of an activated Cu-MOR sample were analyzed by X-ray absorption spectroscopy (XAS). The reactivity data discussed above point to a uniform nature of the Cu sites in the Cu-MOR materials prepared by the optimized procedure presented here and, therefore, Cu K-edge spectra are expected to yield unambiguous information of the structure of the active clusters.

Multiple k-weighted analysis is crucial for a reliable analysis in order to recognize and properly analyze both light and heavy scatterers and, in addition,

to consider the anti-phase behavior of the different Cu-Cu and Cu-O shells, with constructive and destructive interferences in different parts of the EXAFS range.<sup>[28]</sup> Therefore, the full EXAFS data were analyzed in *k*- and *R*-space using a combined  $k^1$ - $k^2$ - $k^3$  fitting procedure. A fit of the fully refined cluster was only accepted if the fit was of high quality in all *k*-weightings.

Figure 2.9 a and b compares the  $k^2$ -weighted and Fourier transformed EXAFS data measured at the Cu K-edge with the simulated EXAFS using the DFT-optimized  $[\text{Cu}(\mu\text{-O})\text{Cu}]^{2+}$  cluster in MOR unit cell with a structure previously proposed as the active site for methane activation in Cu-ZSM-5.<sup>[29]</sup> The most prominent peak can be observed below 2 Å in *R*-space and is associated with backscattering from the oxygen atoms to which Cu is directly bonded. The complex line shape suggests at least two distinct types of O-donor ligands with significantly different Cu-O distances due to framework ( $\text{O}_\text{F}$ ) and extra framework oxygen ( $\text{O}_\text{EF}$ ). Features above 2.0 Å in *R*-space arise from Cu-Cu and second shell Cu-O single-scattering paths. The experimental data significantly deviates from the simulated spectrum of a binuclear  $[\text{Cu}(\mu\text{-O})\text{Cu}]^{2+}$  complex. A particularly strong deviation can be seen at large interatomic distances ( $R \sim 2.25$  Å - not phase corrected), corresponding to the second coordination shell of Cu. Multiple scattering paths must be visible for a dimeric structure with a O-Cu-O structure, similar to typical CuO spectra.<sup>[30]</sup> The absence of this feature in the experimental spectra suggests the existence of more than one Cu-Cu path and, therefore, the presence of a Cu cluster with a nuclearity higher than 2. In contrast to the divergences found for the fit to a binuclear cluster, a good fit in all *k*-weightings of the experimental EXAFS data is achieved by the simulated EXAFS based on the DFT-optimized structure of the  $[\text{Cu}_3(\mu\text{-O})_3]^{2+}$  / MOR cluster model (Figure 2.9 c,d and Figure A 2.2). The fits of the  $k^1$ ,  $k^2$  and  $k^3$  weighted EXAFS spectra are displayed in the Appendix (Figure A 2.2).

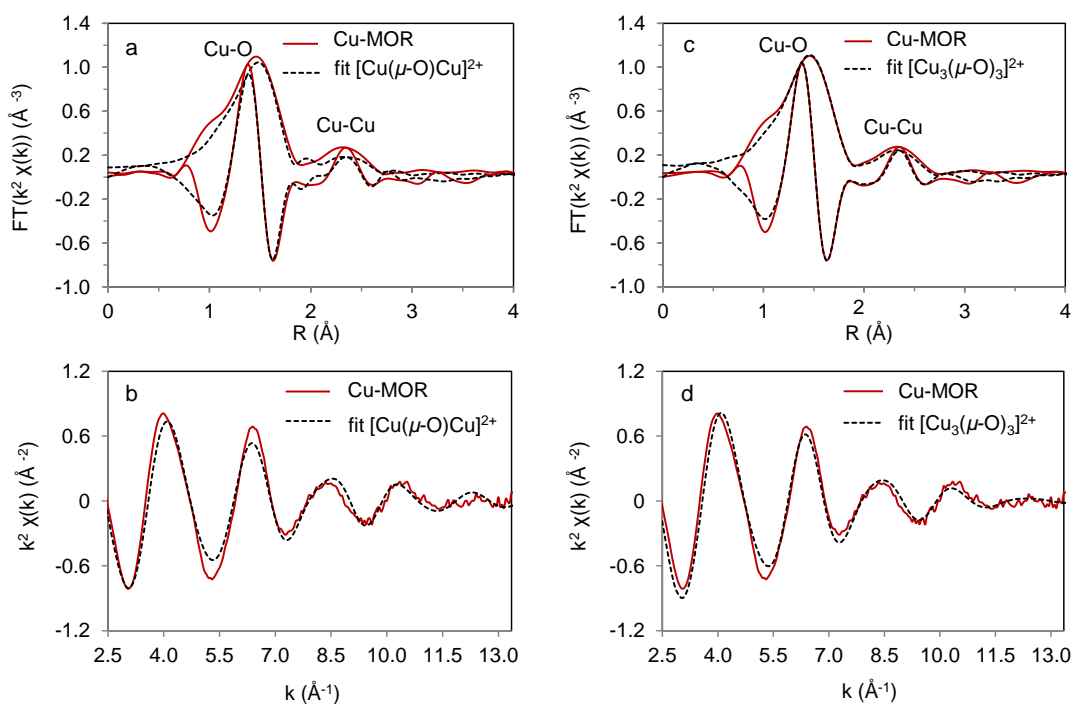


**Figure 2.9:** Comparison of the  $k^2$ -weighted Fourier transformed EXAFS at the Cu K-edge of the Cu-MOR zeolite activated in  $O_2$  at 723 K and EXAFS simulation of an intrazeolite a) binuclear  $[Cu(\mu-O)Cu]^{2+}$  and c) trinuclear  $[Cu_3(\mu-O)_3]^{2+}$  complex with b, d) the corresponding  $k^2$ -weighted experimental EXAFS oscillations and their simulation using the DFT computed model. Color key: measured spectra (red lines), simulated spectra (black lines).

Results of the fitting are summarized in Table 2.3. When the EXAFS fitting was started from an alternative trinuclear model, similar parameters were obtained. This indicates that the values shown in Table 2.3 are a true minimum. Different four-coordinate Cu clusters, e.g. cubane or ring type structures, were also tested as a starting model for the EXAFS analysis. A full refinement of experimental data with the  $Cu_4$  model results in exactly the same analysis as presented in the manuscript, which corresponds to the trimeric model rather than a  $Cu_4$  cubane type structure. This is another proof that the true minimum was refined.

**Table 2.3:** Copper EXAFS fitting results. Comparison of Cu K-edge EXAFS fit results<sup>a</sup> for O<sub>2</sub>-activated Cu-MOR zeolite with DFT optimized geometric parameters of [Cu<sub>3</sub>(μ-O)<sub>3</sub>]<sup>2+</sup> in Cu-MOR.

Backscatterer	Coordination numbers	Coordination numbers	Distance	Distance	Debye-Waller factor <sup>b</sup> Δσ <sup>2</sup>
	N <sup>DFT</sup>	N <sup>EXAFS</sup>	[Å]	[Å]	[Å <sup>2</sup> ]
Cu-O <sub>EF</sub>	2	2.2 (±0.8)	1.80	1.91 (±0.03)	0.003 (±0.003)
Cu-O <sub>F</sub>	1.66	1.6 (±0.5)	2.02	2.04 (±0.07)	0.004 (±0.005)
Cu-O <sub>F</sub>	0.33	0.4 (±0.5)	2.63	2.35 (±0.05)	0.003 (±0.010)
Cu-Cu	0.66	0.7 (±0.4)	2.74	2.86 (±0.04)	0.005 (±0.005)
Cu-Cu	1.33	1.5 (±0.7)	3.04	3.02 (±0.05)	0.010 (±0.006)
Cu-O <sub>EF</sub>	1	1.3 (±1.1)	3.23	3.50 (±0.09)	0.008 (±0.025)

<sup>a</sup>Combined k<sup>1</sup>, k<sup>2</sup> and k<sup>3</sup>-weighted fit, 2.4<k<12.0 Å<sup>-1</sup>, 1<R<3.6, E<sub>0</sub>=-1 (±3), R factor=0.003, S<sub>0</sub><sup>2</sup>(fixed)=0.9, statistical errors in brackets; <sup>b</sup>Debye-Waller factors were fixed (to the values obtained in the best fit with set coordination numbers) during EXAFS fit to reduce the number of fitting parameters. The values predicted by DFT calculations are averaged over 3 Cu scatterers. See also Table 2.2.

#### 1.1.1.6 *In situ* spectroscopy

Having shown that the single site in the present Cu-MOR catalysts is a [Cu<sub>3</sub>(μ-O)<sub>3</sub>]<sup>2+</sup> cluster, the next step was to monitor the formation of the cluster during activation under O<sub>2</sub> and its interaction with CH<sub>4</sub> under reaction conditions. For this purpose, an *in situ* study was performed by XAS and UV-vis spectroscopy. Figure 2.10 shows the XANES and EXAFS of Cu-MOR at different stages of the catalytic cycle. In agreement with the theoretical predictions, *in situ* XANES also suggests a predominant Cu<sup>2+</sup> character of activated Cu-MOR (Figure 2.10 a). The unchanged intensity of the weak pre-edge feature at 8977 eV and the pronounced new shoulder at 8987 eV (1s → 4p transition) show the Cu<sup>2+</sup> character of the active site after treatment in O<sub>2</sub> at 450 °C. Additionally, the decrease in white line intensity at 8997 eV upon activation is indicative for dehydration of the fresh sample leading to a change

from the octahedral coordination sphere  $\text{Cu}^{2+}$  in hexaquo-complexes to tetrahedral  $\text{Cu}^{2+}$  species.<sup>[31]</sup> These observations indicate that the active site is only formed upon heat-treatment in  $\text{O}_2$ , where a change in the coordination geometry of the active Cu site is observed, but no change in the oxidation state. The characteristic feature of monovalent Cu at 8983 eV is not present in the spectrum of the activated material.<sup>[32]</sup> Reference studies on Cu(II) and Cu(III) species show that it is very difficult to identify the contributions of divalent and trivalent Cu species.<sup>[33]</sup> Trivalent Cu does not have clearly pronounced features due to their low intensity at the rising edge. Thus, in the presence of divalent Cu, the features of trivalent Cu are hidden.

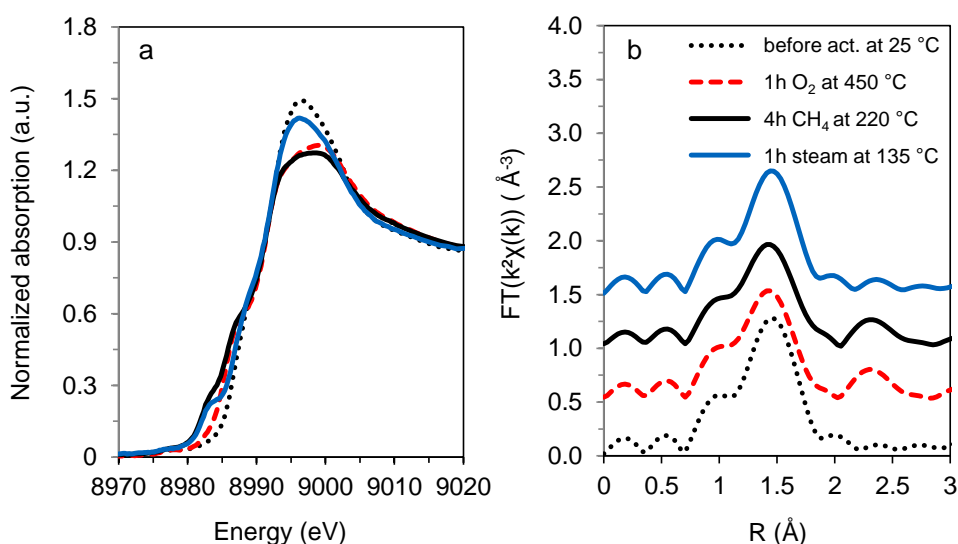


**Figure 2.10:** *In situ* XANES before activation and after activation in  $\text{O}_2$  at 450 °C for 1h.

At temperatures above 200 °C, the progressive formation of a feature at  $R > 2$  Å in EXAFS was observed (Figure 2.11), which can be attributed to new Cu-Cu path and therefore to the formation of Cu-oxo clusters with nuclearity  $\geq 2$ . *In situ* UV-vis spectroscopy of the activation of Cu-MOR in  $\text{O}_2$  showed the development of a very broad band centered at ca.  $31,000 \text{ cm}^{-1}$  (see Appendix Figure A 2.3), while a band at  $22,700 \text{ cm}^{-1}$ , assigned to extra-framework  $\text{O} \rightarrow \text{Cu}^{2+}$  charge transfer for the active species  $[\text{Cu}(\mu\text{-O})\text{Cu}]^{2+}$  in Cu-ZSM-5,<sup>[29]</sup> was not observed in any of the tested conditions. This fact further supports the

conclusion that the active Cu-oxo clusters reported here have a structure different from those described for conventionally prepared Cu-ZSM-5.

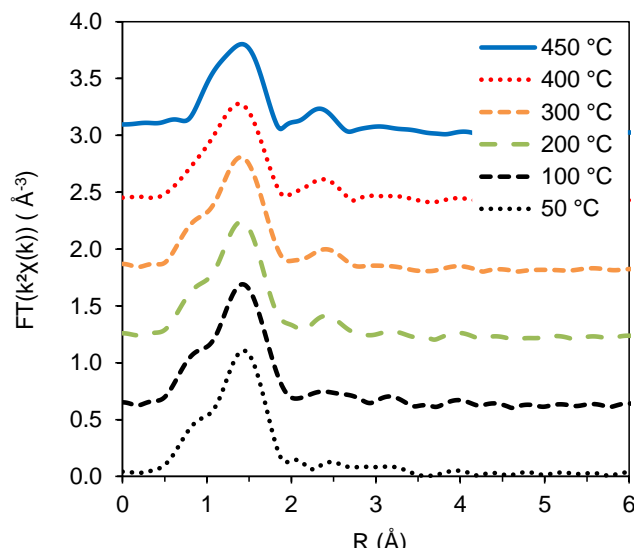


**Figure 2.11:** FT EXAFS of Cu-MOR during activation in pure O<sub>2</sub> flow with a heating rate of 10 °C min<sup>-1</sup>.

Upon reaction with CH<sub>4</sub>, the development of a new strong feature at 8,983 eV has been observed in XANES, which indicates a reduction of a fraction of intra-zeolite Cu<sup>2+</sup> to Cu<sup>+</sup> (Figure 2.10 a). This is in line with the thermal autoreduction reported in the literature,<sup>[30],[31]</sup> and also in good agreement with different mechanisms proposed for the donation of an oxygen atom from the metal oxide cluster to the methyl moiety.<sup>[16]</sup>

On the other hand, significant changes could not be noted in the EXAFS upon treatment with CH<sub>4</sub> (Figure 2.10b), indicating that the trinuclear structure of the active site is preserved at this step, presumably because the oxygenated products remained strongly attached to the cluster. In the UV-vis spectra, the broad band centered at 31,000 cm<sup>-1</sup>, which is stable at 200 °C under O<sub>2</sub> or N<sub>2</sub> disappears only after 20-30 min contact with CH<sub>4</sub> flow at 200 °C (Figure 2.12). The low rate of disappearance of this feature is in good agreement with the low rate of reaction predicted for the catalyst (at least 30 min in contact with CH<sub>4</sub> was necessary to measure significant amounts of methanol).

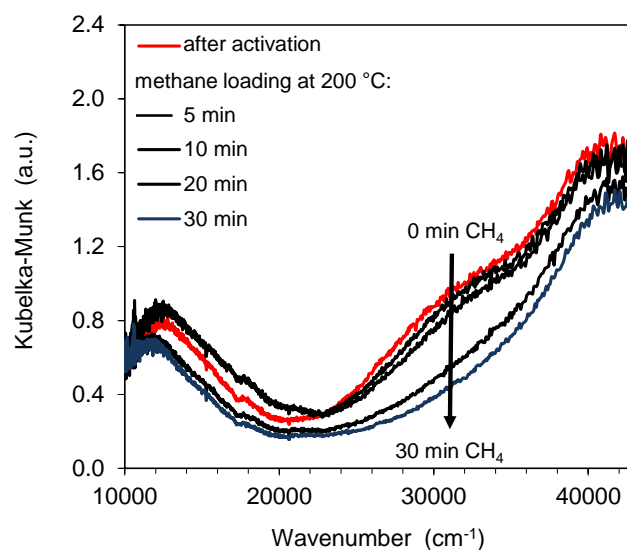


**Figure 2.12:** *In situ* UV-vis spectra of Cu-MOR after activation in O<sub>2</sub> at 450 °C and subsequent methane loading at 200 °C.

Desorption of methanol is only accomplished by steam treatment of the catalysts at 135 °C, which led to a substantial decrease of the Cu-Cu path in the EXAFS (Figure 2.10 b). The increased white line intensity upon steam treatment is indicative of formation of octahedral Cu<sup>2+</sup> which points to the complete hydrolysis of Cu species (Figure 2.10 a). It is concluded from these data that the trinuclear Cu cluster is hydrolyzed by contact with water. Interestingly, a re-activation of the material in O<sub>2</sub> at 500 °C completely restored the activity, even when the procedure was repeated up to 8 cycles (see Appendix Figure A 2.4). Identical XAS and UV-vis spectra were obtained for samples after a second activation, confirming that the [Cu<sub>3</sub>(μ-O)<sub>3</sub>]<sup>2+</sup> cluster is highly stable and re-forms by self-organization under dry oxidation conditions in MOR.

### 2.3.5 Copper Exchanged Mordenite as Biomimetic Model System

In literature, the potential of Cu exchanged zeolites as biomimetic model systems for methane oxidation in pMMO was emphasized.<sup>[15]</sup> The present results show conclusively that trimeric Cu oxo clusters are active and selective for partial methane oxidation. It should be noted in this context that Chan *et al.* recently proposed trinuclear Cu clusters to be active in pMMO and reported that it was possible to use tri-copper complexes for selective methane oxidation to methanol albeit with H<sub>2</sub>O<sub>2</sub> as oxidant.<sup>[9,34]</sup> The multiple Al framework atoms in the 8-MR side pockets of H-MOR provide the conditions to stabilize [Cu<sub>3</sub>(μ-O)<sub>3</sub>]<sup>2+</sup> clusters. It is hypothesized, in addition, that the 8-MR side pockets in MOR enhance the activity of the clusters by providing similar steric constraints as found for the hydrophobic cavity formed by the pmoA and pmoC subunits of pMMO.<sup>[5,7,8,20]</sup>

The material presented here is one of the few examples of catalysts with well-defined active sites evenly distributed in the zeolite framework, a truly single-site heterogeneous catalyst. This not only allows for much higher efficiencies in conversion of methane to methanol than previously reported, it also enables the unequivocal linking of the structure of the sites with their catalytic activity. Understanding why Cu clusters form reversibly, in varying reaction environments, while similar clusters remain stable in the enzyme, despite unfavorable conditions, is one of the big hurdles to achieve similar activities and selectivities in heterogeneous catalysts, as are usually found in enzymatic systems alone. The presented system is therefore a more than promising basis to tackle this challenge.

## 2.4 Conclusions

The choice of a MOR with high concentration of Al in the side pockets, together with an optimized synthetic approach for Cu exchange allowed preparation of Cu-MOR materials that exceed the activity in methane activation reported in the literature for analogous systems by one order of magnitude. In contrast to other metal exchanged zeolites where a mixture of Cu species with different structures and reactivities is detected,<sup>[35,36]</sup> the stoichiometry of converted methane to Cu for these Cu-MOR materials has demonstrated that it is possible to develop a Cu zeolite with only one type of active site.

*In situ* XAS spectroscopy demonstrated that the single-sites in activated Cu-MOR are trinuclear Cu-oxo cluster, namely  $[\text{Cu}_3(\mu\text{-O})_3]^{2+}$ , anchored to two framework Al atoms located at the pore mouth of the 8-MR side pockets. Therefore the EXAFS analysis is in excellent agreement with the results obtained by infrared spectroscopy. Furthermore, this active  $[\text{Cu}_3(\mu\text{-O})_3]^{2+}$  species has been found to be highly stable under dry conditions, in agreement with *ab initio* thermodynamic analysis based on DFT results. Even though steam treatment led to the hydrolysis of the cluster, it can be re-formed without loss of activity by re-activation in  $\text{O}_2$ . The present results show conclusively that trimeric Cu-oxo clusters are active and selective for partial methane oxidation.

## 2.5 Experimental Section

### Preparation of Cu and Co exchanged mordenite

H-MOR was obtained by calcination of commercial zeolite NH<sub>4</sub>-MOR (Clariant, Si/Al 11, 21) in synthetic air at 500 °C for 8 h. Cu-MOR with different Cu/Al ratios, was prepared by aqueous ion exchange of HMOR with Cu<sup>2+</sup>. The Cu<sup>2+</sup>-exchange was carried out at ambient temperature by contacting 5 g zeolite with 300 ml of an aqueous Cu(CH<sub>3</sub>COO)<sub>2</sub> (Sigma Aldrich, 99.99%) solution. The reaction time and the molarity of the solution was varied between 0.0025 and 0.01 M Cu(CH<sub>3</sub>COO)<sub>2</sub> in order to obtain Cu/Al ratios between 0.1 and 0.4. A series of several subsequent cycles of ion exchange with intermediate rinsing was performed in an attempt to increase the Cu/Al ratio (0.4-0.6). The pH of the solution was 5.5–6.0 during exchange. A typical exchange time was 20 h. After the last exchange step the samples were rinsed four times with doubly de-ionized water (50 ml per g MOR each time) with an intervening centrifugation step between each rinse. These rinse cycles were performed to ensure that the pores did not contain further non-exchanged Cu ions, which would form large CuO clusters during activation. Samples were then dried in static ambient air at 110 °C for 24 h. The Si, Al, Na and Cu contents were measured by atomic absorption spectroscopy (AAS) on a UNICAM 939 AA spectrometer after dissolution in boiling hydrofluoric acid. BET surface area was measured on a PMI automated Sorptomatic 1990 after activation at 350 °C. Co<sup>2+</sup>-exchange was prepared by aqueous ion-exchange of Na-MOR in 0.05 M Cu(NO<sub>3</sub>)<sub>2</sub> solution at room temperature following the procedure described by Dedecek *et al.*<sup>[23]</sup> Na-MOR was prepared by Na<sup>+</sup>-exchange of freshly calcined H-MOR with 0.5 M NaNO<sub>3</sub> solution for 24 h at 60 °C.

### Infrared spectroscopy

The samples for infrared spectroscopy were prepared as self-supporting wafers with a density of ca. 10 mg/cm<sup>2</sup>. Samples were first activated in vacuum (1.0 × 10<sup>-7</sup> mbar) at 450 °C for 1 h with a heating rate of 10 °C/min. Infrared spectra of adsorbed n-hexane were recorded on a Vertex 70 spectrometer from Bruker

Optics at a resolution of  $4\text{ cm}^{-1}$ . After pretreatment, the activated samples were cooled to  $30\text{ }^{\circ}\text{C}$ , *n*-hexane (0.5-5 mbar) was adsorbed and equilibrated for at least 30 min. All spectra were recorded at  $30\text{ }^{\circ}\text{C}$ . Infrared spectra of adsorbed pyridine were measured on Thermo Nicolet 5700 FT-IR spectrometer with a resolution of  $4\text{ cm}^{-1}$ . After activation, the total concentration of Brønsted acid sites (BAS) was determined at  $150\text{ }^{\circ}\text{C}$  after adsorption of 0.1 mbar pyridine and subsequent evacuation for 30 min at the same temperature. All spectra were recorded at  $150\text{ }^{\circ}\text{C}$ .

### Testing of activity for selective oxidation of methane to methanol

Cu-MOR samples were tested for their activity towards methane oxidation in an atmospheric pressure stainless steel plug flow reactor with 4 mm inner diameter. The reaction included three consecutive steps: (i) activation, (ii)  $\text{CH}_4$  loading and (iii) steam-assisted  $\text{CH}_3\text{OH}$  desorption. In a typical experiment, 0.1 g of Cu-MOR (250 - 400  $\mu\text{m}$ ) was calcined in an  $\text{O}_2$  flow (16 ml/min) at  $450\text{ }^{\circ}\text{C}$  for 1 h. The activated catalyst was cooled to  $200\text{ }^{\circ}\text{C}$  in  $\text{O}_2$  and flushed in He. In the subsequent  $\text{CH}_4$  loading step, 90%  $\text{CH}_4$  in He (16 ml/min) was passed over the sample for 4 h. The temperature was then decreased in He to  $135\text{ }^{\circ}\text{C}$ . A steam-assisted  $\text{CH}_3\text{OH}$  desorption step was carried out by passing an equimolar mixture of  $\text{H}_2\text{O}$  steam and He (20 ml/min) through the reactor bed for 30 min. The reaction products were identified and quantified by online mass spectroscopy by monitoring the time dependent evolution of signals at  $m/e$  28, 31, 44 and 46 characteristic for CO,  $\text{CH}_3\text{OH}$ ,  $\text{CO}_2$  and  $(\text{CH}_3)_2\text{O}$ , respectively. The He signal ( $m/e = 4$ ) was used as an internal standard. Productivity was calculated as the product of the effluent flow rate and the integral of the product concentrations as a function of time. The product  $(\text{CH}_3)_2\text{O}$  was assumed to be formed via condensation of two partially oxidized  $\text{CH}_4$  molecules corresponding to two  $\text{CH}_3\text{OH}$  equivalents. The sum of all detected products is referred to as total yield or methane converted.

## DFT calculation

All periodic DFT calculations<sup>5</sup> were performed using VASP software with generalized gradient approximated PBE exchange-correlation functional.<sup>[37,38]</sup> Projected augmented wave (PAW) method and plane wave basis set with a cutoff of 400 eV were employed. Brillouin zone-sampling was restricted to the  $\Gamma$  point.<sup>[39]</sup> A supercell of all-silica mordenite (MOR) constructed by a doubling monoclinic primitive cell along c axis with lattice parameters of  $a = b = 13.648$ ,  $c = 15.015$  Å, and  $\gamma = 97.2^\circ$  as optimized by DFT was used as an initial model.<sup>[40]</sup> To compensate for the positive charge of the extra-framework cationic Cu complexes, two framework  $\text{Si}^{4+}$  ions in MOR supercell were substituted by two  $\text{Al}^{3+}$  at the side pocket position of  $\text{Al}^{\text{I}}_{\text{SP}}$ . The other two  $[\text{AlO}_2]^-$  units at the side pocket position of  $\text{Al}^{\text{II}}_{\text{SP}}$  were charge compensated by two Brønsted acid sites.<sup>[41]</sup> The resulting MOR model had a Si/Al ratio of 11. Nudged-elastic band method (NEB)<sup>[42]</sup> was used to determine the minimum energy path and to locate the transition state structure for methane oxidation to methanol reaction. The maximum energy geometry along the reaction path obtained with the NEB method was further optimized using a quasi-Newton algorithm. In this step only the extra-framework atoms were relaxed. Spin polarized calculations were performed throughout this study. The calculated reaction paths following the spin PESs (potential energy surfaces) of ground electronic states with  $S = 1/2$  and  $S = 3/2$  were very close in energy both for intermediates and transition states of methane activation. Vibrational frequencies were calculated using the finite difference method as implemented in VASP. Small displacements (0.02 Å) were used to estimate the numerical Hessian matrix. The transition state was confirmed by the presence of a single imaginary frequency corresponding to the reaction path. Electron density analysis was carried out using VESTA.<sup>[43]</sup>

For molecular orbital analysis, single point calculations at the PBE/6-31+G(d,p) level of theory were carried out using the Gaussian 09 program<sup>[44]</sup> on a 8-membered ring cluster model directly cut from the periodic DFT-optimized

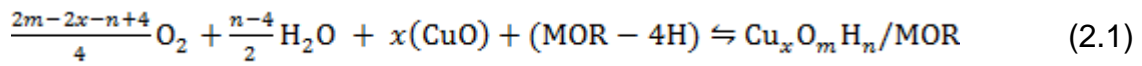
---

<sup>5</sup> All results on DFT calculations were provided by Guanna Li and Evgeny Pidko at Eindhoven University of Technology.

Cu<sub>3</sub>O<sub>3</sub>/MOR structure. The dangling Si-O bonds at the periphery of the cluster model were saturated by hydrogen atoms oriented in the direction of the next T-sites of the zeolite lattice. Both doublet and quartet ground spin states (S=1/2 and S=3/2) were considered.

### Ab initio thermodynamic analysis

To account for the effect of temperature as well as the presence of H<sub>2</sub>O and O<sub>2</sub> upon the catalysts activation on the stability of different extra-framework Cu complexes in Cu/MOR *ab initio* thermodynamic analysis was employed.<sup>6</sup> In this study, the thermodynamic analysis is performed with a reference to bulk copper oxide as the most plausible alternative to extraframework Cu species formed in the zeolite. The following reversible reactions were considered to compare equilibria among species with different chemical compositions:



The reaction Gibbs free energy  $\Delta G$  for equilibrium (2.1) is:

$$\Delta G(T, p) = G_{Cu_xO_mH_n/MOR}^s - G_{MOR-4H}^s - xG_{CuO}^s - \frac{2m-2x-n+4}{2}\mu_O^g - \frac{n-4}{2}\mu_{H_2O}^g \quad (2.2)$$

The vibrational and PV contributions of solids are neglected and the Gibbs free energies of zeolite and bulk copper oxide are approximated as their respective electronic energies directly computed by DFT. The chemical potentials of the gas phase O (O<sub>2</sub>) and H<sub>2</sub>O depend on  $T$  and  $p$ . It was assumed that the surrounding O<sub>2</sub> atmosphere forms an ideal-gas-like reservoir, and the reference state of  $\mu_{O_2}(T, p)$  was chosen to be the total electronic energy of an isolated O<sub>2</sub> molecule ( $E_{O_2}$ ). In other words, the chemical potential of oxygen at the reference state at 0 K is  $\mu_O(0K) = 1/2 E_{O_2}$  in which  $E_{O_2}$  is the DFT calculated total energy of O<sub>2</sub>. Then the chemical potential of oxygen at arbitrary  $T$  and  $p$  can be written as:

$$\mu_O(T, p) = \frac{1}{2}E_{O_2} + \Delta\mu_O(T, p) \quad (2.3)$$

where

---

<sup>6</sup> *Ab initio* thermodynamic analysis was performed by Guanna Li and Evgeny Pidko at Eindhoven University of Technology.

$$\Delta\mu_{\text{O}}(T, p) = \Delta\mu_{\text{O}}(T, p^0) + \frac{1}{2}RT \ln(p_{\text{O}_2}/p_{\text{O}_2}^0) = \frac{1}{2}[\Delta\mu_{\text{O}_2}(T, p^0) + RT \ln(p_{\text{O}_2}/p_{\text{O}_2}^0)] = \frac{1}{2}[H(T, p^0, \text{O}_2) - H(0\text{K}, p^0, \text{O}_2) - T(S(T, p^0, \text{O}_2) - S(0\text{K}, p^0, \text{O}_2)) + RT \ln(p_{\text{O}_2}/p_{\text{O}_2}^0)] \quad (2.4)$$

The chemical potential change ( $\Delta\mu_{\text{O}}(T, p)$ ) defined in such a manner includes all temperature and pressure dependent free energy contributions. The temperature and pressure-dependency of the chemical potential is obtained from the differences in the enthalpy and entropy of an  $\text{O}_2$  as well as  $\text{H}_2\text{O}$  molecules with respect to the reference state at the 0 K limit. For standard pressure (1 atm), the values tabulated in thermodynamic tables were employed.<sup>[45]</sup> This approach has been previously proven to provide rather accurate results for *ab initio* thermodynamic calculations.<sup>[46,47]</sup>

The chemical potential of  $\text{H}_2\text{O}$  as well as the chemical potential change were calculated exactly in the same way as described in the above:

$$\mu_{\text{H}_2\text{O}}(T, p) = E_{\text{H}_2\text{O}} + \Delta\mu_{\text{H}_2\text{O}}(T, p) \quad (2.5)$$

Bringing equations 2.3 and 2.5 into equation 2.2 and considering the Gibbs free energies of zeolite and bulk copper oxide are approximated as their respective DFT computed electronic energies, leading to:

$$\Delta G(T, p) = \Delta E - \frac{2m-2x-n+4}{2}\Delta\mu_{\text{O}} - \frac{n-4}{2}\Delta\mu_{\text{H}_2\text{O}} \quad (2.6)$$

where

$$\Delta E = E_{\text{Cu}_x\text{O}_m\text{H}_n/\text{MOR}} - \frac{2m-2x-n+4}{4}E_{\text{O}_2} - \frac{n-4}{2}E_{\text{H}_2\text{O}} - xE_{\text{CuO}} - E_{\text{MOR-4H}} \quad (2.7)$$

$E_{\text{Cu}_x\text{O}_m\text{H}_n/\text{MOR}}$  is the total electronic energy of a given Cu-containing MOR model,  $E_{\text{MOR-4H}}$  is the energy of the H-form of MOR with four  $\text{Al}^{3+}$  substituted at  $\text{Al}^{\text{I}}_{\text{SP}}$  and  $\text{Al}^{\text{II}}_{\text{SP}}$ ,  $E_{\text{CuO}}$ ,  $E_{\text{O}_2}$ , and  $E_{\text{H}_2\text{O}}$  correspond to the electronic energies of bulk CuO, gaseous  $\text{H}_2\text{O}$  and  $\text{O}_2$ , respectively. The factor  $x$  denotes the number of Cu atoms in the unit cell of  $\text{Cu}_x\text{O}_m\text{H}_n/\text{MOR}$ . Depending on the structure of the Cu complex,  $x$  can be 1, 2 or 3.

## X-ray absorption spectroscopy

X-ray absorption spectra were recorded at Diamond Light Source in Oxfordshire, UK on beamline B18. The electron energy was 3 GeV with a beam current of 300 mA. The beam size at the sample was  $200\ \mu\text{m} \times 250\ \mu\text{m}$ . Samples were prepared as self-supporting wafers (60-80 mg) and placed into an *in situ* XAS cell. The X-ray absorption spectra were collected *in situ* at the Cu K edge (8979 eV) during activation in oxygen at 450 °C, during exposure of the sample to CH<sub>4</sub> and after steam treatment. To avoid condensation, all lines of the setup were thermostated at 110 °C. The samples were activated in an O<sub>2</sub> flow of 30 ml/min at 450 °C for 1 h (heating ramp 10 °C/min) and afterwards cooled to 200 °C. After a short flush with He, CH<sub>4</sub> was loaded for 4 h at 220 °C (flow 30 ml/min). The temperature was then decreased under He flow to 135 °C and an equal molar mixture of water steam/He (50 ml/min) was passed for 2 h through the cell. The Cu K-edge XANES data processing and EXAFS analysis were performed using IFEFFIT version 1.2.11d with the Horae package (Athena and Artemis).<sup>[48,49]</sup> The amplitude reduction factor, i.e.  $S_0^2$ , was experimentally derived to be 0.9, from EXAFS analysis of Cu reference compounds with known structures, i.e. Cu(OAc)<sub>2</sub> and Cu(OH)<sub>2</sub>.<sup>[50,51]</sup> Fitting was done in k- and R-space and in multiple weightings of  $k^1$ ,  $k^2$  and  $k^3$ , simultaneously. A fit was only concluded to be good, if all fits in all weightings, as well in k- as in R-space were good and all included contributions were determined to be significant, tested by refinement of coordination numbers. Refinement of coordination numbers gave values with a deviation of less than 10% from the values predicted by the DFT model for all refined paths. Fits were performed using the optimized geometrical parameters for Cu-MOR obtained from the periodic DFT calculations as input model.

## EXAFS fitting and analysis

For the fitting of EXAFS spectra, the amplitude ( $S_0^2$ ), determined from reference materials, as well as the coordination numbers (CNs) derived from the DFT models were fixed in order to reduce the number of fitting parameters. In a second step Debye-Waller factors were fixed to the values obtained in the best fit with set coordination numbers and thus coordination numbers and bond

distances were refined. Only if the refined values of the distances and the corresponding coordination numbers were in good agreement with the DFT model a fit was considered as good. Although the R factor (0.009, see Appendix Table A 2.2 and Table A 2.3) is low, a significant deviation between the experimental data and the DFT model of a binuclear  $[\text{Cu}(\mu\text{-O})\text{Cu}]^{2+}$  complex can be observed and is particularly pronounced at larger interatomic distances (R), (Figure 2.9 a and b). The intensity of the fitted model and the imaginary part of the Fourier transform do not fit well in the Cu-Cu region. Moreover, large Debye Waller factors with large statistical errors are obtained for both the Cu-Cu and Cu-O<sub>F</sub> contributions (see Appendix Table A 2.2 and Table A 2.3). Possible multiple scattering paths, likely for a dimeric structure with fairly linear O-Cu-O structure motifs and for example clearly pronounced in CuO<sup>[30]</sup>, cannot be observed or analyzed. This suggests the presence of more than one Cu-Cu path and therefore the presence of a Cu species with nuclearity higher than 2. Comparison of various Cu trinuclear models proposed by DFT (Figure 2.7) showed that a good fit of the experimental EXAFS data is achieved by a trinuclear  $[\text{Cu}_3(\mu\text{-O})_3]^{2+}$  cluster (Figure 2.9 c and d), in good agreement with our calculations predicting this cluster to be the most stable under activation conditions. Results of the fitting are summarized in Table 2.3. It should be noted that the three Cu atoms in the trinuclear  $[\text{Cu}_3(\mu\text{-O})_3]^{2+}$  cluster have the same coordination numbers but slightly different bond lengths (see Appendix

Table A 2.4) and therefore EXAFS fitting requires averaging over three scatterers (Table 2.2). EXAFS fitting starting from alternative trinuclear models resulted in similar parameters, indicating that the values shown in Table 2.3 are a true minimum. Additionally, full refinement of all parameters including coordination numbers did not result in significant deviation of the parameters as obtained. A R-factor of 0.004 indicates a good fit. Naturally, the more complex structure of the trinuclear Cu cluster leads to more first and second shell scattering paths compared to the simpler binuclear structure. The quality of the data, in addition to fixing the coordination numbers and amplitudes, allows reliable refinement of all other parameters (number of independent data points is 16, with 13 parameters fitted). The Cu-Cu contributions are significant and realistic distances and low Debye Waller factors with low errors are obtained. The Cu-O<sub>EF</sub> contribution is shifted significantly compared to the model, with large errors, especially in Debye Waller factor. This is due to the small contribution of this shell at long distance and hence this shell cannot be determined with high accuracy. Different four-coordinate Cu-clusters, e.g. cubane or ring type structures, were also tested as a starting model for the EXAFS analysis. A full refinement of experimental data with the Cu<sub>4</sub> model results in exactly the same analysis as presented in the manuscript, which corresponds to the trimeric model rather than a Cu<sub>4</sub> cubane type structure.

## UV-vis spectroscopy

UV-vis measurements of the Cu-exchanged H-MOR samples were performed with an Avantes Avaspec 2048 spectrometer in the diffuse reflectance (DR) mode. The samples were measured as powders and placed in a quartz flow reactor (6 mm inner diameter) with square optical-grade quartz windows. The reactor was placed horizontally in a lab-made heating chamber with an 8-mm diameter hole on top, through which a high-temperature optical fiber (Avantes FCR- 7UV400–2ME-HTX UV-vis reflection probe) could be vertically directed to the reactor. The temperature was measured by a thermocouple located on the bottom of the quartz reactor. In a typical experiment, the UV/vis spectra were collected during treatment in oxygen, nitrogen or methane. The intensity of the DR UV/vis spectra is presented in the form of the Kubelka-Munk function,

defined as  $F(R) = (1-R)^2/(2 \cdot R)$  with  $R = R_s/R_r$ , with  $R_s$  -the reflectance of the sample and  $R_r$  -the reflectance of the H-MOR parent material used as a reference. The samples were first treated at 450 °C for 1 h in He (flow 16 ml/min), heating with a rate of 10°C/min. Subsequently, the sample was cooled to ambient temperature, He was replaced with O<sub>2</sub> and the sample was heated to 450 °C in O<sub>2</sub> flow (flow 16 ml/min). After cooling of the activated sample to 200 °C, the sample was contacted with a CH<sub>4</sub> (flow 16 ml/min).

## 2.6 Acknowledgements

The research was partly supported by the U.S. Department of Energy, Office of Basic Energy Sciences, Division of Chemical Sciences under Award DE-SC0012702. It was also supported by the EU NEXT-GTL (Innovative Catalytic Technologies & Materials for Next Gas to Liquid Processes) project. J. Heyrovský Institute of Physical Chemistry, Jiri Dědeček and Viktor Kreibich are acknowledged for measurement and analysis of UV-vis spectra of Cobalt exchanged mordenite. DFT calculations were performed by Guanna Li and Evgeny Pidko. SurfSARA and NWO are acknowledged for providing access to supercomputer resources. The XAS measurements were carried out with the support of the Diamond Light Source on Beamline B18 under Proposal SP8508. Gary L. Haller is acknowledged for fruitful discussions.

## 2.7 Appendix

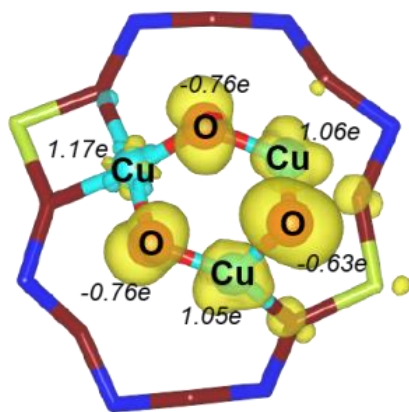


**Figure A 2.1:** Electronic properties of  $[\text{Cu}_3(\mu\text{-O})_3]^{2+}$  cluster in MOR zeolite model predicted by periodic DFT calculations (Si/Al=11). Illustration of spin-density and calculated atomic Bader charges for the extraframework Cu cluster.

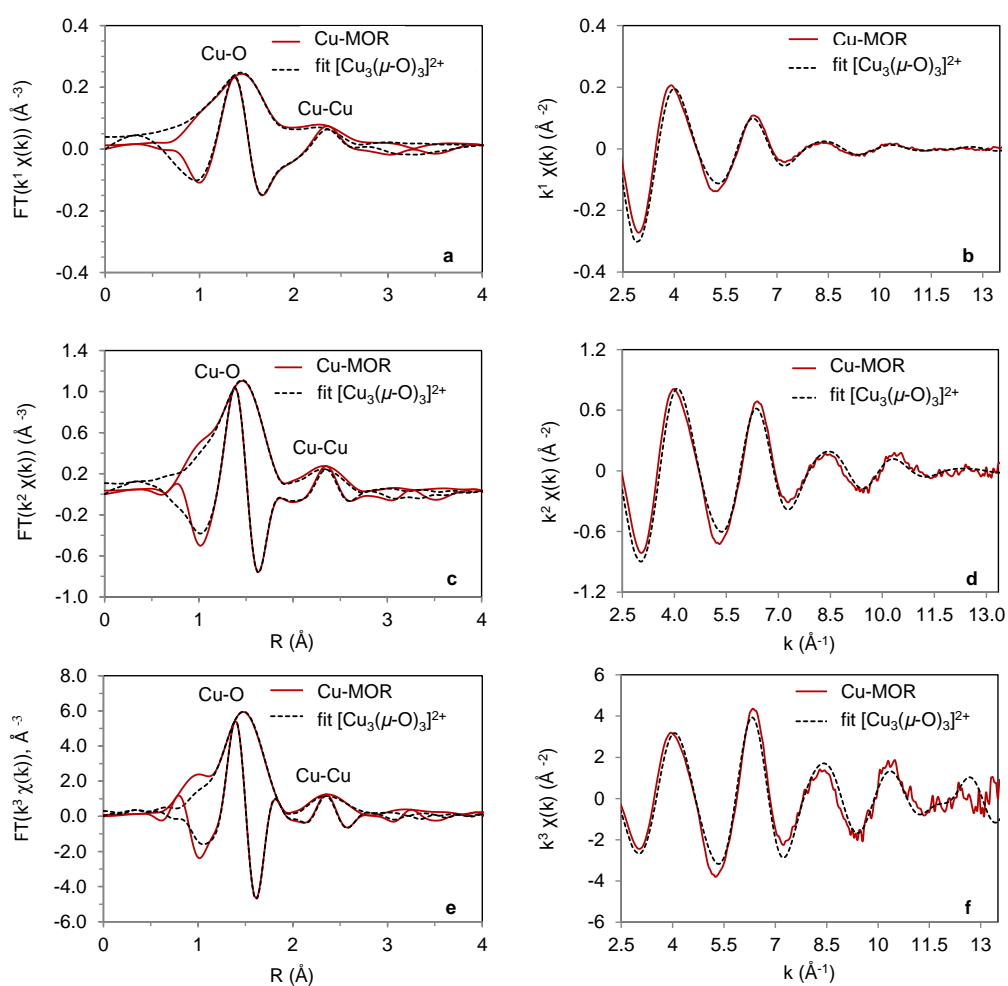


**Figure A 2.2:** Comparison of a,c,e) the  $k^1$ ,  $k^2$  and  $k^3$ -weighted Fourier transformed EXAFS at the Cu K-edge of the Cu-MOR zeolite activated in  $O_2$  at 723 K and EXAFS simulation of an intrazeolite trinuclear  $[Cu_3(\mu-O)_3]^{2+}$  complexes and b,d,f) the corresponding  $k^1$ ,  $k^2$  and  $k^3$ -weighted experimental EXAFS oscillations and their simulation using the DFT computed model. Color key: measured spectra (red lines), simulated spectra (black dotted lines).

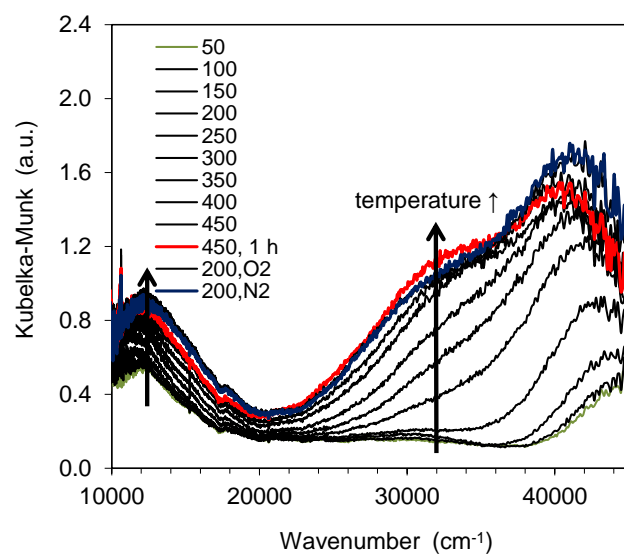


**Figure A 2.3:** UV-vis spectra of fresh Cu-MOR during activation in O<sub>2</sub> up to 450 °C. After treatment, temperature was decreased to 200 °C under O<sub>2</sub> and then flushed in N<sub>2</sub> for 1 hour at 200 °C (final spectra in blue).

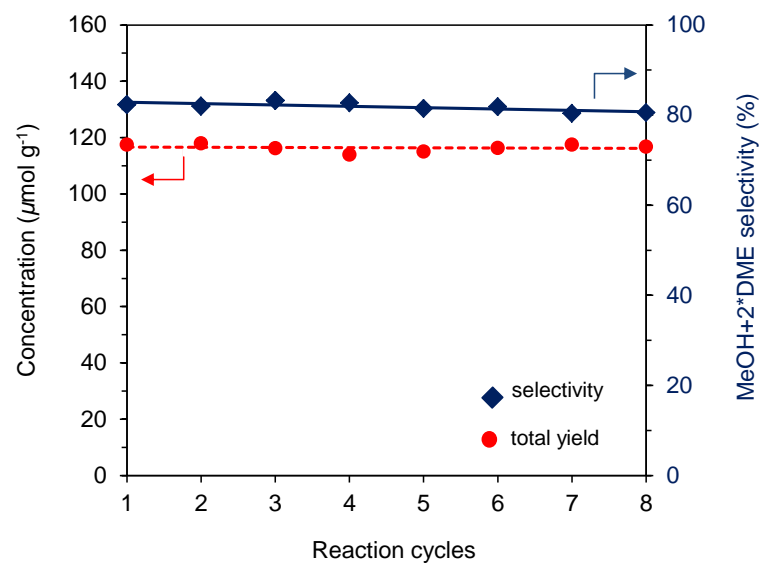


**Figure A 2.4:** Stability test of Cu-MOR for selective partial oxidation of methane to methanol. Recycling of the catalyst over 8 cycles with activation at 450 °C for 1h, methane loading at 200 °C for 30 min and steam treatment at 135 °C for 30 min in each cycle.

**Table A 2.1:** Co<sup>2+</sup> siting in MOR with Si/Al=11.<sup>7</sup>

Co conc. ( $\mu\text{mol/g}$ )	Paired Al sites <sup>a</sup>	Co <sup>2+</sup> siting <sup>b</sup>		
		$\alpha$ -type Co	$\beta$ -type Co	$\gamma$ -type Co
390	66%	25.7%	65.2%	9.1%

- a) Co<sup>2+</sup> ions should be coordinated only to framework oxygen atoms and balanced by two framework AlO<sub>4</sub><sup>-</sup> tetrahedral. Hydrolysis avoided by using cobalt nitrate solution.
- b) Quantification of the Co<sup>2+</sup> siting was performed by deconvolution of the UV-vis spectrum by fitting to the Gaussian curves with the following maxima:  $\alpha$ -type Co (14,800 cm<sup>-1</sup>),  $\beta$ -type Co (15,900; 17,500; 19,200; and 21,080 cm<sup>-1</sup>),  $\gamma$ -type Co (20,150 and 22,050 cm<sup>-1</sup>)<sup>[25]</sup>

<sup>7</sup> Measurement and analysis of UV-vis spectra of Cobalt exchanged mordenite was performed by Jiri Dědeček and Viktor Kreibich at the J. Heyrovský Institute of Physical Chemistry in Prague.

**Table A 2.2:** Comparison of Cu K-edge EXAFS fit results<sup>a</sup> for O<sub>2</sub>-activated Cu-MOR zeolite with DFT optimized geometric parameters of [Cu<sub>2</sub>( $\mu$ -O)]<sup>2+</sup>.

Backscatterer	Coordination number N <sup>b</sup>	Distance R <sup>DFT</sup> [Å]	Distance R <sup>EXAFS</sup> [Å]	Debye-Waller factor $\Delta\sigma^2$ [Å <sup>2</sup> ]
Cu-O <sub>EF</sub>	3	1.95	1.94 ( $\pm 0.04$ )	0.005 ( $\pm 0.001$ )
Cu-Cu	1	2.94	2.92 ( $\pm 0.07$ )	0.012 ( $\pm 0.004$ )
Cu-O <sub>F</sub>	1	3.56	3.52 ( $\pm 0.04$ )	0.011 ( $\pm 0.018$ )

<sup>a</sup>Combined  $k^1$ ,  $k^2$  and  $k^3$ -weighted fit,  $2.4 < k < 12.0$ ,  $1 < R < 3.6$ ,  $E_0 = -2$  (2), R factor = 0.009,  $S_0^2(\text{fixed}) = 0.9$ , statistical errors in brackets; <sup>b</sup>Coordination numbers were fixed during EXAFS fit to reduce the number of fitting parameters (values predicted by DFT calculations).

**Table A 2.3:** Comparison of Cu K-edge EXAFS fit results<sup>a</sup> for O<sub>2</sub>-activated Cu-MOR zeolite with DFT computed geometrical parameters of [Cu<sub>2</sub>(μ-O)<sub>2</sub>]<sup>2+</sup>.

Backscatterer	Coordination number N <sup>b</sup>	Distance R <sup>DFT</sup> [Å]	Distance R <sup>EXAFS</sup> [Å]	Debye-Waller factor Δσ <sup>2</sup> [Å <sup>2</sup> ]
Cu-O <sub>F/EF</sub>	4	1.95	1.94 (±0.05)	0.007 (±0.005)
Cu-Cu	1	2.94	2.91 (±0.07)	0.012 (±0.003)
Cu-O <sub>F</sub>	1	3.56	3.46 (±0.04)	0.008 (±0.012)

<sup>a</sup>Combined k<sup>1</sup>, k<sup>2</sup> and k<sup>3</sup>-weighted fit, 2.4<k<12.0, 1<R<3.6, E<sub>0</sub>= -2 (2), R factor= 0.008, S<sub>0</sub><sup>2</sup>(fixed)= 0.9, statistical errors in brackets; <sup>b</sup>Coordination numbers were fixed during EXAFS fit to reduce the number of fitting parameters (values predicted by DFT calculations).

**Table A 2.4:** DFT optimized geometric parameters of  $[\text{Cu}_3(\mu\text{-O})_3]^{2+}$  in Cu-MOR predicted by DFT calculation. All paths in a distance  $\leq 3.5$  Å were taken into account.

Scatterer	Backscatterer	Number of paths (DFT)	Distance [Å]
Cu1	O	1	1.79
	O	1	1.80
	O	1	1.96
	O	1	2.02
	Cu	1	3.04
	Cu	1	3.05
Cu2	O	1	1.77
	O	1	1.78
	O	1	2.04
	O	1	2.11
	Cu	1	2.74
	Cu	1	3.05
	O	1	3.23
	O	1	3.41
	O	1	3.44
Cu3	O	1	1.77
	O	1	1.82
	O	1	1.99
	O	1	2.63
	Cu	1	2.74
	Cu	1	3.04
	O	1	3.20
	O	1	3.44

## 2.8 References

- [1] Rosenzweig, A. C.; Frederick, C. A.; Lippard, S. J.; Nordlund, P. *Nature* **1993**, 366, 537.
- [2] Bordeaux, M.; Galarneau, A.; Drone, J. *Angew. Chem., Int. Ed.* **2012**, 51, 10712.
- [3] Chan, S. I.; Chen, K. H. C.; Yu, S. S. F.; Chen, C. L.; Kuo, S. S. J. *Biochemistry* **2004**, 43, 4421.
- [4] Himes, R. A.; Barnese, K.; Karlin, K. D. *Angew. Chem., Int. Ed.* **2010**, 49, 6714.
- [5] Lieberman, R. L.; Rosenzweig, A. C. *Nature* **2005**, 434, 177.
- [6] Balasubramanian, R.; Smith, S. M.; Rawat, S.; Yatsunyk, L. A.; Stemmler, T. L.; Rosenzweig, A. C. *Nature* **2010**, 465, 115.
- [7] Ng, K. Y.; Tu, L. C.; Wang, Y. S.; Chan, S. I.; Yu, S. S. F. *ChemBioChem* **2008**, 9, 1116.
- [8] Chan, S. I.; Wang, V. C. C.; Lai, J. C. H.; Yu, S. S. F.; Chen, P. P. Y.; Chen, K. H. C.; Chen, C. L.; Chan, M. K. *Angew. Chem., Int. Ed.* **2007**, 46, 1992.
- [9] Chan, S. I.; Lu, Y. J.; Nagababu, P.; Maji, S.; Hung, M. C.; Lee, M. M.; Hsu, I. J.; Minh, P. D.; Lai, J. C. H.; Ng, K. Y.; Ramalingam, S.; Yu, S. S. F.; Chan, M. K. *Angew. Chem., Int. Ed.* **2013**, 52, 3731.
- [10] Labinger, J. A.; Bercaw, J. E. *Nature* **2002**, 417, 507.
- [11] Periana, R. A.; Taube, D. J.; Evitt, E. R.; Loffler, D. G.; Wentrock, P. R.; Voss, G.; Masuda, T. *Science* **1993**, 259, 340.
- [12] Periana, R. A.; Taube, D. J.; Gamble, S.; Taube, H.; Satoh, T.; Fujii, H. *Science* **1998**, 280, 560.
- [13] Palkovits, R.; Antonietti, M.; Kuhn, P.; Thomas, A.; Schuth, F. *Angew. Chem., Int. Ed.* **2009**, 48, 6909.
- [14] Soorholtz, M.; White, R. J.; Zimmermann, T.; Titirici, M. M.; Antonietti, M.; Palkovits, R.; Schuth, F. *Chem. Commun.* **2013**, 49, 240.
- [15] Vanelderen, P.; Hadt, R. G.; Smeets, P. J.; Solomon, E. I.; Schoonheydt, R. A.; Sels, B. F. *J. Catal.* **2011**, 284, 157.
- [16] Vanelderen, P.; Vancauwenbergh, J.; Sels, B. F.; Schoonheydt, R. A. *Coord. Chem. Rev.* **2013**, 257, 483.
- [17] Groothaert, M. H.; Smeets, P. J.; Sels, B. F.; Jacobs, P. A.; Schoonheydt, R. A. *J. Am. Chem. Soc.* **2005**, 127, 1394.
- [18] Narsimhan, K.; Michaelis, V. K.; Mathies, G.; Gunther, W. R.; Griffin, R. G.; Roman-Leshkov, Y. *J. Am. Chem. Soc.* **2015**, 137, 1825.
- [19] Veefkind, V. A.; Smidt, M. L.; Lercher, J. A. *Appl. Catal., A* **2000**, 194, 319.

- [20] Eder, F.; Stockenhuber, M.; Lercher, J. A. *J. Phys. Chem. B* **1997**, *101*, 5414.
- [21] Kojima, M.; Rautenbach, M. W.; Oconnor, C. T. *J. Catal.* **1988**, *112*, 495.
- [22] Moreau, F.; Ayrault, P.; Gnep, N. S.; Lacombe, S.; Merlen, E.; Guisnet, M. *Microporous Mesoporous Mater.* **2002**, *51*, 211.
- [23] Dedecek, J.; Kaucky, D.; Wichterlova, B.; Gonsiorova, O. *Phys. Chem. Chem. Phys.* **2002**, *4*, 5406.
- [24] Dedecek, J.; Sobalik, Z.; Wichterlova, B. *Cat. Rev. - Sci. Eng.* **2012**, *54*, 135.
- [25] Dedecek, J.; Wichterlova, B. *J. Phys. Chem. B* **1999**, *103*, 1462.
- [26] Alayon, E. M. C.; Nachtegaal, M.; Kleymenov, E.; van Bokhoven, J. A. *Microporous Mesoporous Mater.* **2013**, *166*, 131.
- [27] Woertink, J. S.; Smeets, P. J.; Groothaert, M. H.; Vance, M. A.; Sels, B. F.; Schoonheydt, R. A.; Solomon, E. I. *Proc. Natl. Acad. Sci. U. S. A.* **2009**, *106*, 18908.
- [28] Tromp, M.; van Bokhoven, J. A.; Arink, A. M.; Bitter, J. H.; van Koten, G.; Koningsberger, D. C. *Chem. Eur. J.* **2002**, *8*, 5667.
- [29] Groothaert, M. H.; Lievens, K.; Leeman, H.; Weckhuysen, B. M.; Schoonheydt, R. A. *J. Catal.* **2003**, *220*, 500.
- [30] Neylon, M. K.; Marshall, C. L.; Kropf, A. J. *J. Am. Chem. Soc.* **2002**, *124*, 5457.
- [31] Alayon, E. M. C.; Nachtegaal, M.; Bodi, A.; van Bokhoven, J. A. *ACS Catal.* **2014**, *4*, 16.
- [32] Alayon, E. M.; Nachtegaal, M.; Ranocchiari, M.; van Bokhoven, J. A. *Chem. Commun.* **2012**, *48*, 404.
- [33] DuBois, J. L.; Mukherjee, P.; Stack, T. D. P.; Hedman, B.; Solomon, E. I.; Hodgson, K. O. *J. Am. Chem. Soc.* **2000**, *122*, 5775.
- [34] Maji, S.; Lee, J. C. M.; Lu, Y. J.; Chen, C. L.; Hung, M. C.; Chen, P. P. Y.; Yu, S. S. F.; Chan, S. I. *Chem. Eur. J.* **2012**, *18*, 3955.
- [35] Beznis, N. V.; Weckhuysen, B. M.; Bitter, J. H. *Catal. Lett.* **2010**, *136*, 52.
- [36] Beznis, N. V.; van Laak, A. N. C.; Weckhuysen, B. M.; Bitter, J. H. *Microporous and Mesoporous Mater.* **2011**, *138*, 176.
- [37] Kresse, G.; Hafner, J. *Phys. Rev. B* **1993**, *48*, 13115.
- [38] Perdew, J. P.; Burke, K.; Ernzerhof, M. *Phys. Rev. Lett.* **1996**, *77*, 3865.
- [39] Vankoningsveld, H.; Jansen, J. C.; Vanbekkum, H. *Zeolites* **1990**, *10*, 235.
- [40] Pidko, E. A.; van Santen, R. A.; Hensen, E. J. M. *Phys. Chem. Chem. Phys.* **2009**, *11*, 2893.
- [41] Pidko, E. A.; van Santen, R. A. *J. Phys. Chem. C* **2009**, *113*, 4246.
- [42] Mills, G.; Jonsson, H.; Schenter, G. K. *Surf. Sci.* **1995**, *324*, 305.

- [43] Momma, K.; Izumi, F. *J. Appl. Crystallogr.* **2011**, *44*, 1272.
- [44] Frisch, M. J.; Trucks, G. W.; Schlegel, H. B.; Frisch, M. J.; Trucks, G. W.; Schlegel, H. B.; Gaussian, Inc.: Wallingford, CT, 2009.
- [45] Stull, D. R.; Prophet, H. In *JANAF Thermochemical Tables*; 2 ed.; U.S. National Bureau of Standards, U.S. EPO: Washington, D.C., 1971.
- [46] Guhl, H.; Miller, W.; Reuter, K. *Phys. Rev. B* **2010**, *81*.
- [47] Reuter, K.; Scheffler, M. *Phys. Rev. B* **2003**, *68*.
- [48] Newville, M. *J. Synchrotron Rad.* **2001**, *8*, 322.
- [49] Ravel, B.; Newville, M. *J. Synchrotron Rad.* **2005**, *12*, 537.
- [50] Brown, G. M.; Chidamba, R. *Acta Crystallogr., Sect. B: Struct. Sci.* **1973**, *29*, 2393.
- [51] Oswald, H. R.; Reller, A.; Schmalle, H. W.; Dubler, E. *Acta Crystallogr., Sect. C: Cryst. Struct. Commun.* **1990**, *46*, 2279.

# 3 Synthesis of Single-Site Copper Catalysts for Methane Partial Oxidation

## 3.1 Abstract

Although copper exchanged zeolites are known for years as active materials for different catalytic processes, understanding of the formation of copper active species via ion exchange during dehydration and activation is fragmented and rudimentary. In this chapter,<sup>8</sup> it is demonstrated how specific synthesis protocols led to highly uniform copper species in mordenite and as a consequence a highly active single site catalyst for the selective oxidation of methane to methanol. The high partial methane oxidation activity of samples prepared from H-MOR is attributed to the absence of elements hindering the formation of the active copper oxo clusters. Formation of large clusters was avoided by limiting the pH below the point of zero charge of the zeolite surface silanol groups (pH < 6). The presence of Na<sup>+</sup> or other alkali and alkaline earth cations competing for the exchange positions preferred by Cu<sup>2+</sup> led to a heterogeneous speciation of Cu. The presence of co-cations competing for the 8-MR side pocket sites affects the Cu speciation.

---

<sup>8</sup> This chapter is based on the article of the same title as submitted to Chemical Communications:  
Grundner, S.; Luo, W.; Sanchez-Sanchez, M.; Lercher, J.A. *Chem. Commun.* **2016**

## 3.2 Introduction

Since the discovery of their high NO decomposition activity in 1986,<sup>[1]</sup> and their high selectivity for the partial oxidation of methane to methanol in 2005,<sup>[2]</sup> Cu exchanged zeolites have attracted broad attention. Numerous publications on the speciation of Cu in zeolites with different topologies exemplify the relevance of the structure of the Cu ions and/or Cu-O clusters for catalytic applications.<sup>[3-5]</sup> The hitherto limited control of the nature of the copper species via such synthesis approaches led to materials with a broad distribution of sites, many being only spectators. The formation of Cu spectators, often quantitatively more abundant than the active species, hampers the identification of active sites and impedes a rigorous comparison of activities among Cu-zeolite materials from different sources.

Commonly, the Na exchanged form of zeolites is for the preparation of transition metal exchanged zeolite catalysts because of the more straightforward control of the synthesis parameters.<sup>[6-8]</sup> However, mordenite (MOR) activities in methane oxidation were found to be significantly higher than previous reports when Cu was exchanged on H-MOR instead of on Na-MOR (see Chapter 2). It should be noted in passing that also other authors have reported remarkable differences in the activity of Cu-MOR in presence of Na<sup>+</sup> in the zeolite structure.<sup>[9]</sup> In the case of methane oxidation and consecutive carbonylation to acetic acid on Cu-MOR, significantly higher activity for both reaction steps was observed if H-MOR was used as parent material instead of Na-MOR. While in the case of the carbonylation step activity is related to adjacent protons that remained after Cu ion exchange,<sup>[10]</sup> there is no clear explanation for the higher overall amount of methane activated by the Cu sites when H-MOR is utilized instead of Na-MOR. It remains unclear if the observed differences in methane oxidation activity are due to a competition of co-cations with Cu for exchange sites, a hindered self-organization of the Cu-oxo cluster during thermal activation in the presence of co-cations or a shift in pH during Cu exchange.

In this chapter, the impact of gradual  $\text{Cu}^{2+}$  ion exchange on the formation of charged Cu oxide (Cu-oxo) complexes during thermal activation in Cu exchanged mordenite is explored. The effect of alkali and alkaline earth cations (co-cations) and the pH during ion exchange were also quantitatively explored in order to control the formation and nuclearity of Cu-oxo clusters active for methane partial oxidation at low temperatures.

## 3.3 Results and Discussion

### 3.3.1 Effect of Co-Cations on Activity for Methane Partial Oxidation

First, the effect of alkali and alkaline earth cations (co-cations) and the pH during ion exchange were quantitatively explored in order to control the formation and nuclearity of Cu-oxo clusters.

Cu-MOR samples with different Cu/Al ratios were prepared by ion exchange of H-MOR with  $\text{Cu}^{2+}$  in aqueous phase at ambient temperature. The zeolite was also exchanged with  $\text{Cu}^{2+}$  ions in presence of other cations ( $\text{Na}^+$ ,  $\text{K}^+$ ,  $\text{Mg}^{2+}$ ,  $\text{Ca}^{2+}$ ). The characterization of these materials is compiled in the Appendix (Table A 3.1). Since these cations exchanged protons associated with framework Al sites, Brønsted acidity was measured, in order to ensure that the exchange with co-cations was adequate (Figure 3.1). Only ca. 100  $\mu\text{mol}$  of Brønsted acid sites (BAS) remained after  $\text{Na}^+$  and  $\text{K}^+$  exchange, probably due to non-exchangeable BAS at the bottom of the MOR side pocket. Upon  $\text{Cu}^{2+}$  exchange at pH 5.7, only a negligible fraction of BAS was formed.

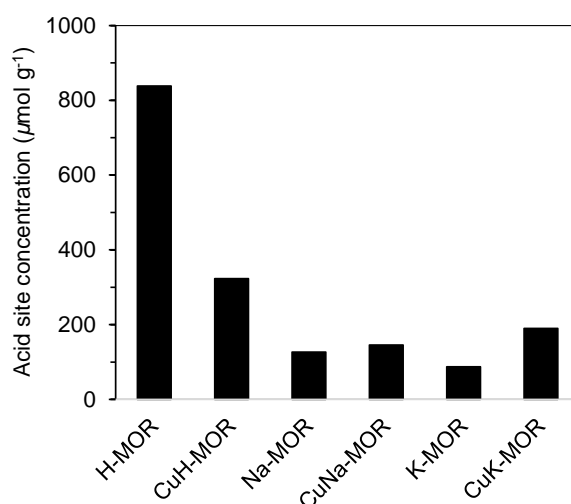


**Figure 3.1:** Impact of co-cations on Brønsted acidity. Brønsted acid site concentration of various MOR materials was quantified by the vibrational band of the pyridinium ion after adsorption of pyridine ( $1,545\text{ cm}^{-1}$ ). Cu exchange was performed at pH 5.7.

The comparable micro pore volume for a large series of Cu exchanged mordenites prepared from the protonic form and the Na form is indicative for the absence of large clusters and agglomerates within the zeolite pores of the activated materials (Table A 3.2). Independently of the counter anion of the Cu precursor in the exchange solution (nitrate or acetate), identical  $\text{Cu}^{2+}$  exchange degrees and methane oxidation activities were obtained as long as the solution was buffered to a pH of 5.7 during ion exchange.

The concentration of active sites in Cu zeolites can be quantified by the amount of products collected after a three-stage catalytic oxidation of methane (see Chapter 2). In this way, the specificity of ion exchange protocols for the sites responsible for oxidation of methane was evaluated. In Figure 3.2, it can be seen that  $\text{Cu}^{2+}$  ion exchange of H-MOR (CuH-MOR) yields the material with the highest Cu efficiency. The stoichiometry of three Cu atoms to one methane molecule converted points to a trinuclear Cu-oxo cluster as active site in MOR.<sup>[11]</sup> In contrast, the presence of alkaline cations (Na, K) or alkaline earth cations (Mg, Ca) drastically reduced this Cu efficiency to values of 4-5 Cu per oxidized methane. A constant selectivity of methane partial oxidation products (methanol and dimethyl ether) in the range of 75-80 % was observed for Cu-MOR over a broad range of Cu loading and methane contact times. The presence of co-cations did not affect the methanol selectivity.

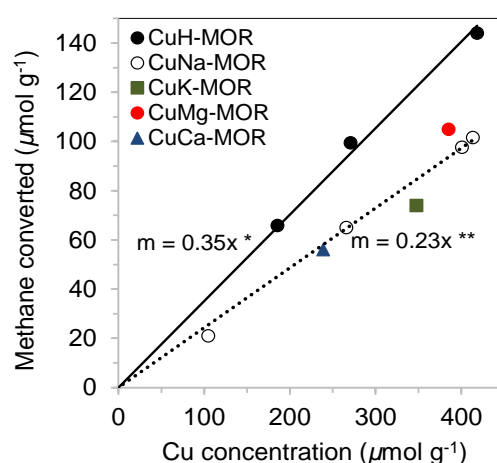


**Figure 3.2:** Methane converted versus  $\text{Cu}^{2+}$  concentration for Cu exchanged MOR with various co-cations. \* The slope of 0.35 indicates that ca. 3 Cu atoms are involved in the oxidation of one methane molecule. \*\*The slope of 0.23 indicates that in average more than 4 Cu atoms oxidize one methane molecule.

### 3.3.2 Impact of pH on Activity for Methane Partial Oxidation

The constant ratio of methane oxidized in relation to Cu present in the CuH-MOR series indicates that this synthetic approach leads to the formation of single-site trinuclear copper oxygen cationic cluster in MOR for oxidation of methane to methanol (see Chapter 2).<sup>[11]</sup> The presence of other cations causes a lower concentration of Cu in such sites (lower Cu efficiency), i.e., about 25% of Cu sites become inactive (Figure 3.2). In order to understand the role of other cations hindering the formation of the Cu active species, a series of CuH-MOR and CuNa-MOR materials were prepared by ion exchange at different pH, but with the same Cu concentrations (0.01 M).

While it has been experimentally established that the  $\text{Cu}^{2+}$  site active for partial methane oxidation is a multinuclear Cu site, oxide clusters containing more than three Cu cations show low selectivity towards methanol.<sup>[6,11-13]</sup> Thus, as a first boundary condition to form sites for methane partial oxidation selectively, the pH of ion exchange must be kept below 7 to avoid precipitation of  $\text{Cu}(\text{OH})_2$ .<sup>[14]</sup> Furthermore, the point of zero charge of the zeolite surface silanol groups is 6.0. Near and above this pH the deprotonation of Si-OH groups and consequently the exchange with  $\text{Cu}^{2+}$  will occur,<sup>[15]</sup> which also leads to the formation of nano-sized CuO particles during calcination. The formation of such undesirable CuO species was detected by transmission electron microscopy (Figure 3.3) for those samples prepared exceeding the upper pH limit of 6.0. On the other hand, to maximize the formation of copper active dimers and/or trimers, a high concentration of Brønsted acid sites (BAS) must be exchanged with  $\text{Cu}^{2+}$ . Therefore, also too low pH is not ideal, because it reduces the exchangeability of BAS.

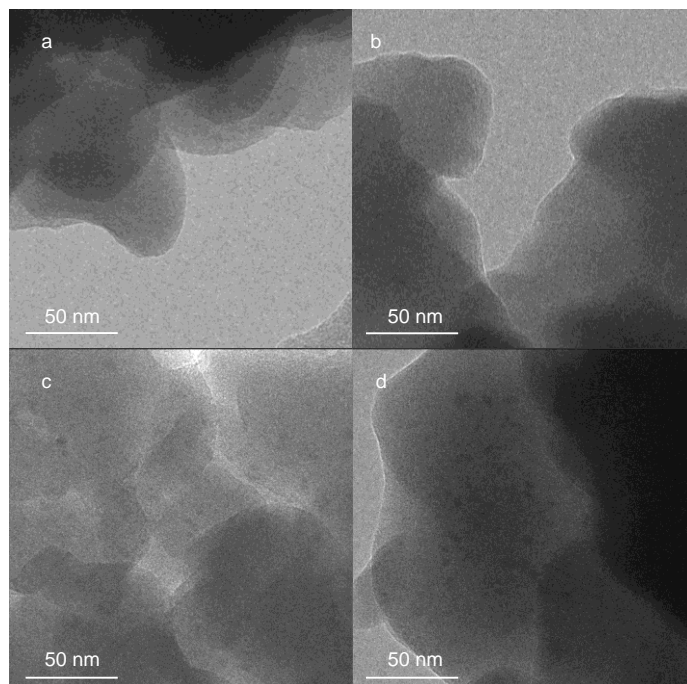


**Figure 3.3:** Transmission electron microscopy (TEM). Images of Cu exchanged mordenites. a) CuH-MOR exchanged at pH 5.7 (Cu/Al 0.3), b) CuNa-MOR exchanged at pH 5.7 (Cu/Al 0.3), c) CuH-MOR exchanged at pH 6.6 (Cu/Al 0.6) and d) CuNa-MOR exchanged at pH 6.5 (Cu/Al 0.6).

Considering these boundary conditions, ion exchange of BAS protons was maximized without formation of large copper oxide species by buffering the exchange solution to pH 5.7. Hydrolysis and back-exchange (with  $\text{NaNO}_3$ ) was used to probe quantitatively the nature of the Cu species. All Cu (irrespective whether it is a monomer, a dimer or a trimer) coordinated to framework Al tetrahedra is readily exchangeable with other mono- and divalent cations in water. In contrast, CuO or  $\text{Cu}(\text{OH})_2$  nanoparticles or clusters cannot be hydrolyzed and are not back-exchanged in consequence. This allows the quantitative differentiation of CuO or  $\text{Cu}(\text{OH})_2$  from the ion exchanged species in the micropores by chemical analysis of the material after back exchange. Since all  $\text{Cu}^{2+}$  was back-exchanged for  $\text{Na}^+$  in Cu-MOR samples prepared at  $\text{pH} < 6$  (see Appendix Table A 3.3) the presence of surface copper oxide aggregates was ruled out.

No significant changes in the selectivity to form these cationic clusters were observed for Cu exchanged H-MOR prepared in the pH range 2-6 (Figure 3.4 a), i.e., all Cu was present in the form of trinuclear Cu-oxide clusters. In contrast, the pH during  $\text{Cu}^{2+}$  exchange on Na-MOR had a significant impact on the activity for methane oxidation (Figure 3.4 b). Cu efficiency decreased substantially with increasing pH, pointing to the formation of more Cu cations not participating in methane oxidation. The loading of Cu (active and inactive) increased with increasing pH regardless of the co-cation. It is hypothesized that this increase is associated with the shift of the hydrolysis equilibrium from divalent  $[\text{Cu}(\text{H}_2\text{O})_6]^{2+}$  to monovalent  $[\text{Cu}(\text{H}_2\text{O})_5\text{OH}]^+$ .<sup>[16]</sup> This indicates that the latter species is predominant in aqueous ion exchange of zeolites at relatively high pH values,<sup>[17]</sup> and therefore a higher Cu exchange degree is obtained due the lower charge of this species which can be balanced by only one framework Al site.

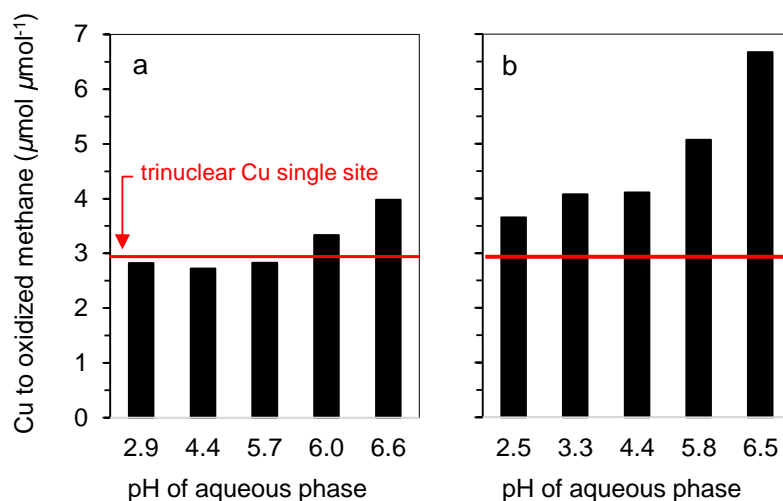


**Figure 3.4:** Impact of pH during Cu-exchange on methane oxidation activity of Cu-MOR. Cu to oxidized methane ratio of a) CuH-MOR and b) CuNa-MOR.

The lower fraction of active Cu in the presence of co-cations (Figure 3.2) indicates the formation of diverse Cu species, with only a part of them being active for methane oxidation. The high uniformity of Cu species formed in CuH-

MOR in a broad range of pH is in contrast to the significant variety of species, when co-cations are present. The self-organization of  $\text{Cu}^{2+}$  to a uniform oxygen containing cluster in H-MOR points to a high mobility of  $\text{Cu}^{2+}$  during thermally induced dehydration and oxidation. The hydrated  $\text{Cu}^{2+}$  cations predominant at low pH ( $[\text{Cu}(\text{H}_2\text{O})_6]^{2+}$ ), which balance the negative charge of two Al-O tetrahedra, are transformed by dissociation of one water molecule to  $[\text{Cu}(\text{H}_2\text{O})_5\text{OH}]^+$ , which balances the negative charge of only one Al-O tetrahedron.<sup>[18]</sup> The simultaneously formed  $\text{H}^+$  also balances the negative charge of one Al-O tetrahedron. Infrared spectra of adsorbed pyridine confirmed this hypothesis by quantitatively showing the formation of one BAS per incorporated  $\text{Cu}^{2+}$  for a series of CuNa-MOR exchanged at pH 4 (Figure 3.5).

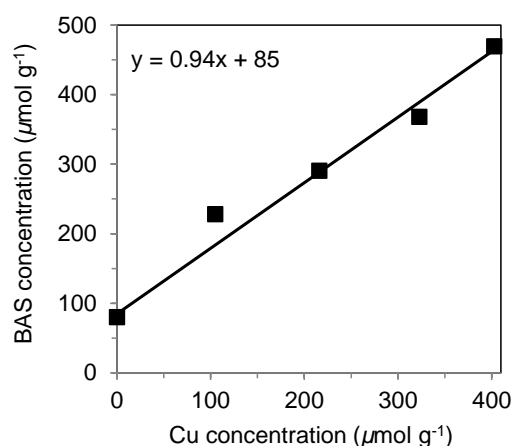


**Figure 3.5:** Brønsted acidity upon copper loading. Brønsted acid site concentration of CuNa-MOR quantified by the vibrational band of the pyridinium ion after adsorption of pyridine ( $1,545\text{ cm}^{-1}$ ) as a function of Cu loading. The series of CuNa-MOR was exchanged at pH 4.

Furthermore, the formation of acid sites upon Cu loading in a series of Na-MOR exchanged at pH 4 was studied by  $\text{NH}_3$ -TPD after adsorption and outgassing at  $150^\circ\text{C}$  and  $260^\circ\text{C}$  respectively. Two distinct desorption peaks at  $240$  and  $450^\circ\text{C}$  were observed after adsorption and outgassing at  $150^\circ\text{C}$  (Figure 3.6). Adsorption and outgassing at  $260^\circ\text{C}$  showed only one desorption peak. For both temperatures a linear correlation of Cu concentration and acid

site concentration was found. The slope of the correlation after adsorption at 150 °C was 2.03., whereas the slope after adsorption at 260 °C was 0.90. The desorption peak at low temperature is due to weaker NH<sub>3</sub> adsorption on the Lewis acid sites, whereas the adsorption peak at 450 °C corresponds to strong adsorption of NH<sub>3</sub> on BAS. The offset of 210  $\mu\text{mol}$  observed after adsorption and outgassing at 150 °C is due to NH<sub>3</sub> adsorbed on Lewis acidic extra-framework Al sites. Note that the slope of the correlation of BAS versus Cu concentration shows a value of 0.9 for both pyridine as well as NH<sub>3</sub> adsorption.

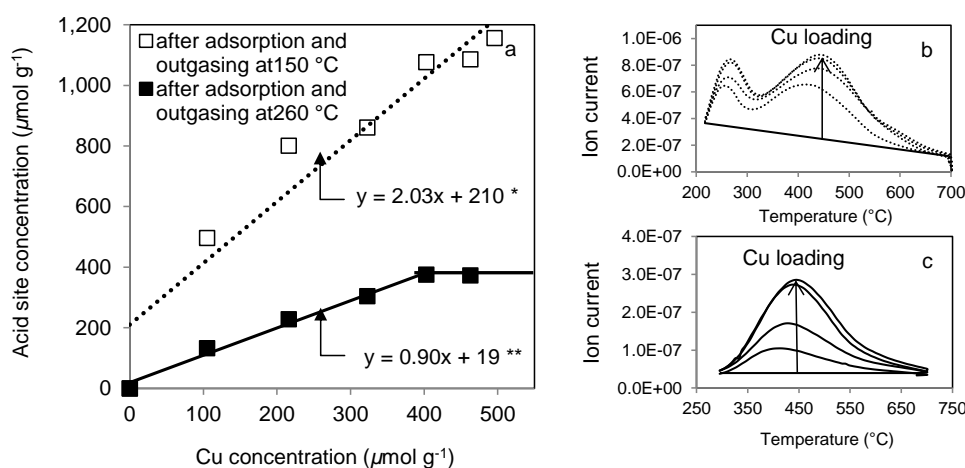


**Figure 3.6:** a) Acid site concentration of CuNa-MOR as a function of Cu loading determined by NH<sub>3</sub>-TPD, b) NH<sub>3</sub>-TPD after adsorption and outgassing at 150 °C and c) after adsorption and outgassing at 260 °C. \*The slope of 2.03 indicates formation of two acid sites per incorporated Cu. The offset of 210  $\mu\text{mol}$  is attributed to NH<sub>3</sub> adsorbed on Lewis acidic extra-framework Al sites. \*\*The slope of 0.90 indicates formation of one BAS per incorporated Cu.

Consequently, regardless of the hydrolysis equilibrium in aqueous phase, a population of monovalent  $[\text{Cu-OH}]^+$  species attached to framework Al sites are formed during thermal activation. Such species have the potential to transform to multinuclear Cu-oxo clusters via condensation with an adjacent  $[\text{Cu-OH}]^+$  forming a  $\mu$ -oxo bridge between  $\text{Cu}^{2+}$  cations.<sup>[19,20]</sup>

### 3.3.3 Siting of Sodium in Mordenite

In order to understand the lower concentrations of Cu species active for the selective oxidation of methane in CuNa-MOR compared to CuH-MOR and their consistently lower fraction as the pH increases, the location of  $\text{Na}^+$  in the parent Na-MOR and its exchange for  $\text{Cu}^{2+}$  was investigated in detail. The initial position of  $\text{Na}^+$  and the position of  $\text{Cu}^{2+}$  after ion exchange are related to the location of the exchangeable sites – that is, of framework Al - in mordenite. The concentration of these sites was determined by chemical analysis of  $\text{Na}^+$  content on a fully exchanged Na-MOR. This value is correlated to the total intensity of the OH band characteristic of BAS in a  $\text{Na}^+$  free H-MOR. For MOR, this infrared band is composed of two contributions, because the wavenumber of the O-H stretching band is slightly different for protons in the 12-MR main channels and for protons in the 8-MR pockets. Finally, the concentration of protons in each of these locations was quantified for H-MOR via adsorption of n-hexane and pyridine, which are probe molecules with different accessibility to the sites (see Chapter 2).<sup>[11,21]</sup>

Using the H-MOR proton distribution as a reference, the coordination sites occupied by  $\text{Cu}^{2+}$  and  $\text{Na}^+$  were deduced by determining the concentration and location of the bridging OH groups before (Figure 3.7 a) and after the ion-exchange with  $\text{Cu}^{2+}$  and  $\text{Na}^+$  leading to Cu-, Na- and CuNa-MOR. After exchange of H-MOR with  $\text{Cu}^{2+}$  and subsequent activation in  $\text{O}_2$ , only  $\text{H}^+$  located in the 8-MR pore mouth of the side pockets in MOR were consumed (see Chapter 2). In addition,  $\text{Na}^+$  was found to exchange preferentially at sites in the side pockets (Figure 3.7 b), in good agreement with previous reports.<sup>[22]</sup> Thus, it is concluded that independently of the location of the cations during ion exchange, in the final stage of dehydration and thermal activation  $\text{Na}^+$  is competing with  $\text{Cu}^{2+}$  for framework Al-O tetrahedra located in the side pockets. Therefore, the lower activity of CuNa-MOR compared to CuH-MOR is attributed to a competition of Na for T-sites required to host the active Cu-oxo cluster.

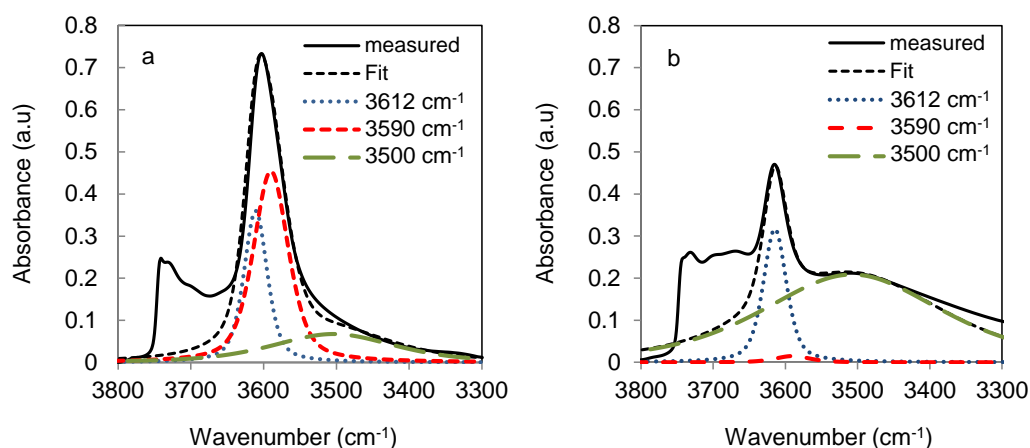


**Figure 3.7:** Deconvoluted infrared spectra of the O-H stretching vibrations of the BAS of a) H-MOR and b) Na-MOR with Na/Al 0.6 after activation at 450 °C. BAS are deconvoluted in bands attributed to main channel O-H (3,612  $\text{cm}^{-1}$ ), side pocket O-H stretching vibrations (3,590  $\text{cm}^{-1}$ ) and perturbed O-H stretching vibrations (3,500  $\text{cm}^{-1}$ ).

### 3.3.4 Copper Exchange Stoichiometry

When exchanging  $\text{Cu}^{2+}$  on Na-MOR the  $\text{Na}^+$  concentration in the zeolite decreased linearly with increasing  $\text{Cu}^{2+}$  loading, which demonstrates that all  $\text{Cu}^{2+}$  introduced into the samples gradually exchanged for  $\text{Na}^+$  at the preferred 8-MR sites (Figure 3.8). The slope of 2.2 for the series prepared by ion exchange at pH 4.4 indicates that one  $\text{Cu}^{2+}$  substituted two  $\text{Na}^+$  cations. This confirms the formation of  $[\text{Cu}(\text{H}_2\text{O})_6]^{2+}$  species balancing the negative charges of two Al-O tetrahedra. In contrast, Cu exchanged Na-MOR prepared at pH 5.7 showed a slope of 1.2 indicating that a monovalent  $[\text{Cu}(\text{H}_2\text{O})_5\text{OH}]^+$  species is replacing one  $\text{Na}^+$  at one framework Al-O tetrahedron. Therefore, the relatively higher catalytic efficiency of CuNa-MOR samples prepared at low pH is attributed to the exchange of two  $\text{Na}^+$  for divalent  $[\text{Cu}(\text{H}_2\text{O})_6]^{2+}$  allowing a more efficient elimination of competing  $\text{Na}^+$  cations.

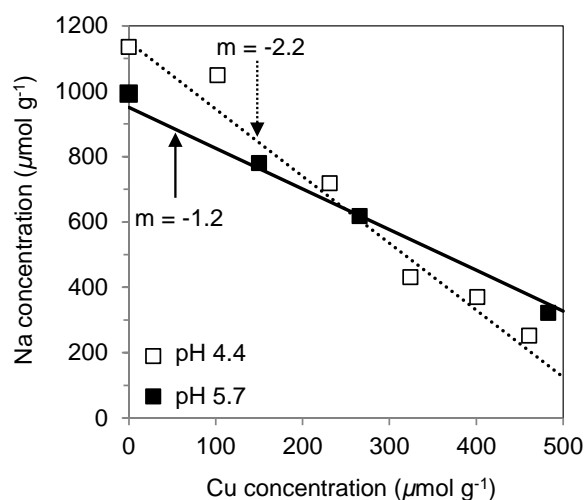


**Figure 3.8:** Na<sup>+</sup> concentrations in CuNa-MOR as a function of Cu loading. The slope of -2.2 indicates exchange of two Na<sup>+</sup> for each incorporated Cu for exchange at pH 4.4. The slope of -1.2 indicates an exchange stoichiometry of ca. one Na per incorporated Cu for CuNa-MOR exchanged at pH 5.7. A blank experiment showed the preparation procedure with copper acetate eliminates 150 μmol g<sup>-1</sup> Brønsted acid sites (BAS) by dealumination.

### 3.3.5 Impact of Sodium on Formation of Copper Oxo Clusters

Active Cu clusters currently proposed in literature consist of two or three Cu atoms interconnected by  $\mu$ -oxo bridges and attached to two framework Al in the 8-MR pore mouth of the side pockets.<sup>[11,23]</sup> It has been observed by infrared spectroscopy that the protons present in CuNa-MOR samples are mainly located in the 12-MR channel (see Appendix Table A 3.4). In Chapter 2, it was shown that Cu<sup>2+</sup> is exclusively exchanged in the side pockets. The formation of large CuO clusters was ruled out in these samples by back-exchange (see Appendix Table A 3.3). Na<sup>+</sup> concentration in the side pockets after Cu exchange of a fully exchanged Na-MOR was calculated by subtracting the Na<sup>+</sup> concentration in the main channel from the total Na<sup>+</sup> concentration. The Na<sup>+</sup> concentration in the main channel was determined by the difference from the amount of BAS in the main channel of the parent H-MOR (420 μmol g<sup>-1</sup>) and the determined concentration of main channel BAS remaining in each CuNa-MOR sample, derived from the O-H vibration at 3,612 cm<sup>-1</sup>. This calculation is

based on the fact that  $\text{Cu}^{2+}$  does not exchange in the main channel,<sup>[11]</sup> and therefore the decrease in intensity in the O-H vibration at  $3,612\text{ cm}^{-1}$  is solely attributed to  $\text{Na}^+$  exchange. Thus, the concentration of co-cations left in the zeolite after Cu exchange is inferred to occupy all exchanged sites in the 12-MR and those exchange positions in the side pockets that are not occupied by Cu species. This is illustrated in Figure 3.9 where the yield of the reaction is represented versus the concentration of  $\text{Cu}^{2+}$  and of  $\text{Na}^+$  in the side pockets.

While in Figure 3.2 it could be seen that samples containing same concentration of Cu (ca.  $400\text{ }\mu\text{mol g}^{-1}$ ) were significantly less active if a co-cation is present, in Figure 3.9 it is clear that such effect is related to the presence of different concentrations of  $\text{Na}^+$  in the side pockets. The competition of  $\text{Na}^+$  (or other co-cations) and  $\text{Cu}^{2+}$  for the thermodynamically most stable cationic positions in MOR reduces the statistical occupancy of vicinal  $\text{Cu}^{2+}$  in the side pockets and, therefore, the probability of  $[\text{CuOH}]^+$  exchanged species to form a multinuclear Cu-oxo-site. In other words, the decrease of the activity observed in CuX-MOR samples ( $X = \text{Na}, \text{K}, \text{Mg}$  and  $\text{Ca}$ ) is caused by the formation of inactive isolated  $\text{Cu}^{2+}$  in those side pockets that are partially occupied by  $\text{Na}^+$ . Thus, it is hypothesized that the formation of active Cu-oxo clusters requires the exchange of at least two Cu ions in two Al sites of the same 8-MR. For the formation of the highly efficient  $[\text{Cu}_3\text{O}_3]^{2+}$  cluster reported for CuH-MOR, a third Cu in the vicinity is required to react with the two  $\text{Cu}^{2+}$  located in the side pockets. Therefore, it is concluded that the presence of other cations significantly decreases the probability of self-assembly of di- and trinuclear copper oxo clusters active for methane oxidation.

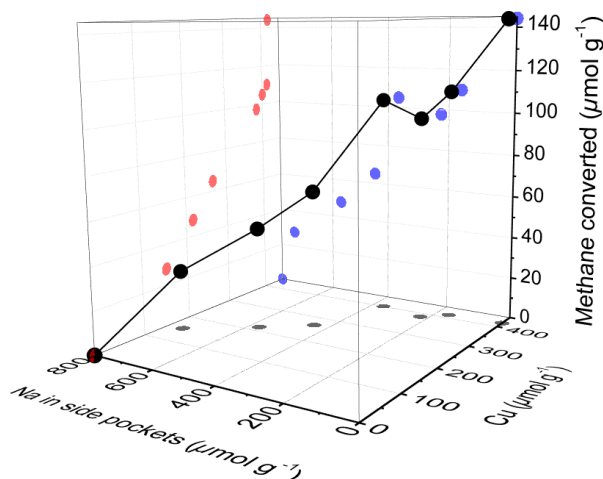


**Figure 3.9:** Methane converted as a function of Cu and Na concentration in the MOR side pockets.

Finally, it is known that the active Cu-oxo clusters are hydrolyzed during methanol extraction (see Chapter 2).<sup>[11]</sup> Thus, it is important to determine whether the active sites formed via controlled speciation in Cu-MOR can be regenerated after one catalytic cycle. Activity in partial oxidation of methane was measured, therefore, for several consecutive cycles with CuNa-MOR and CuH-MOR materials (Figure 3.10). Despite the hydrolysis of the active site and the expected mobility of  $\text{Cu}^{2+}$  and  $\text{Na}^+$  exchanged species upon contact with water, the catalytic activity and selectivity remained stable over 3 cycles for both CuH-MOR and CuNa-MOR materials. Thus, it is concluded that an identical concentration of active sites is formed in each subsequent thermal activation. This indicates that the final siting of  $\text{Na}^+$  and  $\text{Cu}^{2+}$  in dehydrated MOR is thermodynamically determined and only depends on the concentration of both cations in the exchanged material. The concentration of Cu and co-cations is controlled, on the other hand, by the composition of the parent zeolite and by ion exchange pH, as stated in section 3.3.2.

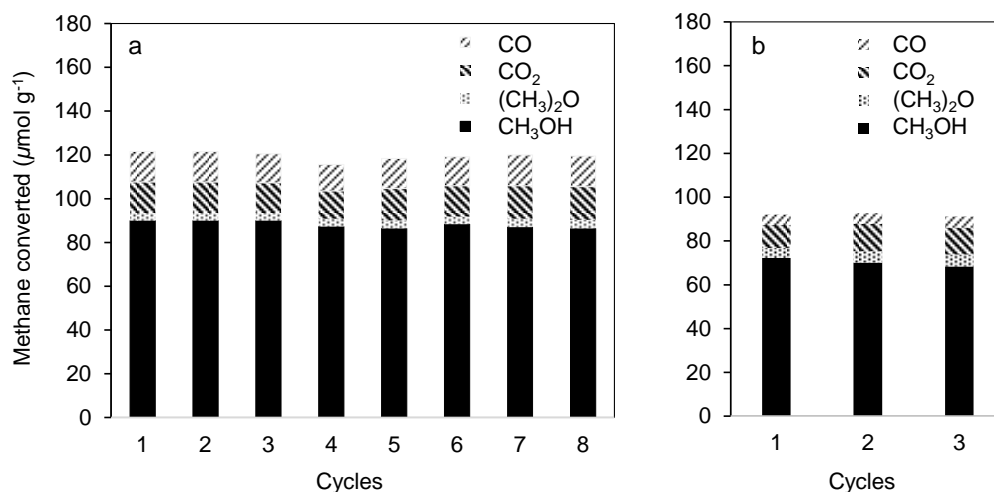


**Figure 3.10:** Catalytic stability of a) CuH-MOR and b) CuNa-MOR for selective partial oxidation of methane to methanol. Recycling of the catalyst over 8 cycles with activation at 450 °C for 1h, methane loading at 200 °C for 30 min and steam treatment at 135 °C for 30 min in each cycle.

### 3.3.6 *In Situ* UV-vis Spectroscopy

In order to study the differences in Cu speciation caused by the presence of Na, *in situ* UV-vis spectroscopy was performed during thermal treatment. In Chapter 2, the single-site trinuclear copper oxo cluster in activated CuH-MOR was characterized by a broad band at ca. 31,000  $\text{cm}^{-1}$  in the UV-vis spectrum.<sup>[11]</sup> The presence of copper species other than the trinuclear copper oxo cluster should result in the appearance of new UV-vis bands. Figure 3.11 a shows the He activated spectrum of CuNa-MOR. A broad band at 31,000  $\text{cm}^{-1}$  evolved during activation in He at 450 °C. Additional bands at 15,600, 18,300 and 21,200  $\text{cm}^{-1}$  evolved after cooling in He to 50 °C. Note, that none of these bands was detected in the spectrum of the He activated CuH-MOR single-site catalyst. Thermal treatment at temperatures above 350 °C in inert atmosphere results in autoreduction of  $\text{Cu}^{2+}$  to  $\text{Cu}^+$ . Upon oxidation of this autoreduced sample, the bands in the range of 15,000-20,000  $\text{cm}^{-1}$  disappeared (Figure 3.11 b). However, the intensity of the broad feature at 31,000  $\text{cm}^{-1}$  increased after  $\text{O}_2$  activation. Furthermore, a new shoulder at 21,900  $\text{cm}^{-1}$  arose. In recent literature, this feature was assigned to a dinuclear  $[\text{Cu}_2(\mu\text{-O})]^{2+}$  site in samples prepared from Na-MOR,<sup>[23]</sup> similar to the band at 22,700  $\text{cm}^{-1}$  attributed to Cu

active species for methane oxidation on CuZSM-5.<sup>[2]</sup> This is a further indication that the presence of co-cations shifts the speciation towards monomers and dimers.

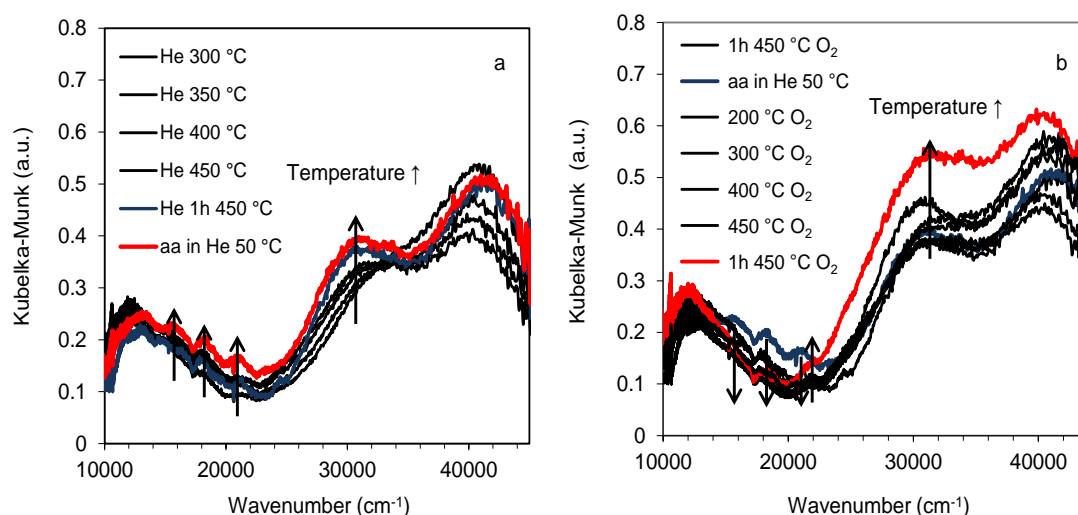


**Figure 3.11:** UV-vis spectra of a) fresh CuNa-MOR during activation in He up to 450 °C. After treatment, temperature was decreased to 50 °C under He (final spectra in red) and b) subsequent heating in O<sub>2</sub> to 450 °C (final spectra in red).

Upon contact with CH<sub>4</sub> at 200 °C, the shoulder at 21,900 cm<sup>-1</sup> in sample CuNa-MOR disappeared rapidly while the feature at 31,000 cm<sup>-1</sup> disappeared with a much slower rate in CH<sub>4</sub> flow (Figure 3.12). Hence, changes in both features indicate that, after activation in oxygen, two different Cu species able to interact with methane coexist in CuNa-MOR samples.

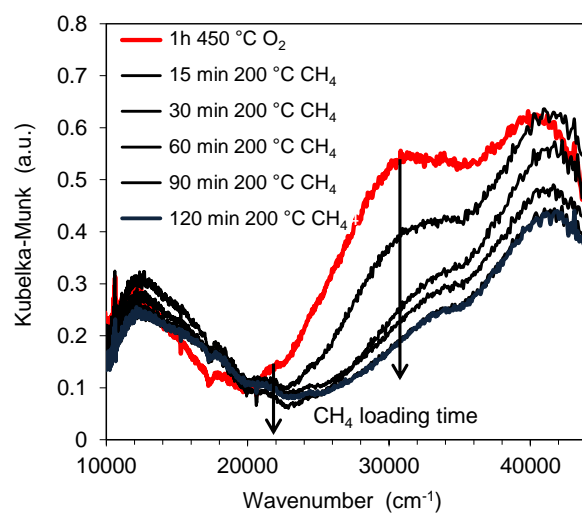


**Figure 3.12:** *In situ* UV-vis spectra of CuNa-MOR after activation in O<sub>2</sub> at 450 °C and subsequent methane loading at 200 °C.

### 3.4 Conclusions

From the results presented here, the remarkably higher selectivity to form cationic trinuclear Cu-oxo clusters and the constant methanol yield for samples prepared from H-MOR is attributed to the absence of elements hindering the formation of the active clusters. Formation of unselective CuO large clusters was avoided by limiting the pH below the point of zero charge of the zeolite surface silanol groups ( $\text{pH} < 6$ ). The presence of  $\text{Na}^+$  or other alkali and alkaline earth cations competing for the exchange positions preferred by  $\text{Cu}^{2+}$  led to a heterogeneous speciation of Cu. Depending on the abundance of the co-cations in the side pockets, tri-, di or mononuclear Cu-oxo sites will be formed. Cu monomers are inactive in methane oxidation, while both  $\mu$ -oxo  $\text{Cu}_2\text{O}$  and  $\text{Cu}_3\text{O}_3$  clusters have been identified as active sites.<sup>[11,12]</sup> In fact, the presence of co-cations competing for the 8-MR side pocket sites would statistically shift the speciation of Cu towards dimers and inactive monomers. This model explains on the one hand the lower Cu efficiency of catalysts typically prepared with Na-MOR as starting material and, on the other hand, that *in situ* spectroscopy studies on such catalysts detected only a majority of  $\text{Cu}_2\text{O}$  sites.<sup>[13,23,24]</sup>

### 3.5 Experimental Section

#### Preparation and basic characterization of copper exchanged mordenites

The Brønsted acidic form of MOR, H-MOR, was obtained by calcination of a commercial zeolite NH<sub>4</sub>-MOR (Clariant, Si/Al = 11) in synthetic air at 500 °C for 8 h. The same batch of the parent material as in our previous work was used. Na-MOR was prepared by exchange of H-MOR with 0.5 M NaNO<sub>3</sub> at 60 °C for 24h. K-MOR, Ca-MOR and Mg-MOR were prepared analogously by ion exchange with the corresponding nitrates. Cu-MOR samples with different Cu/Al ratios were prepared by ion exchange of H-MOR and Na-MOR with Cu<sup>2+</sup> in aqueous phase at ambient temperature. Cu(CH<sub>3</sub>COO)<sub>2</sub> · H<sub>2</sub>O, Cu(NO<sub>3</sub>)<sub>2</sub> · H<sub>2</sub>O as well as CuCl<sub>2</sub> were used as Cu precursors. The molarity of these solutions (100 ml/g zeolite) was varied between 0.01 and 0.001 M. The pH value was adjusted by dropwise addition of HNO<sub>3</sub> (0.01 M) or NH<sub>4</sub>OH (10 wt.% in H<sub>2</sub>O) respectively. Identical Cu loadings and methane oxidation activities were obtained, if [N(C<sub>4</sub>H<sub>9</sub>)<sub>4</sub>]OH (40% in H<sub>2</sub>O) was used for pH adjustment. After the last exchange step, the samples were rinsed four times with deionized water (50 ml per g MOR each time) with an intermittent centrifugation between each rinse and finally dried at 110 °C for 24 h. For back-exchange, Cu-MOR samples were first calcined for 2h at 500 °C under O<sub>2</sub> flow. The calcined samples were then exchanged in 0.5 M NaNO<sub>3</sub> solution for 24h at 60 °C, and finally rinsed and dried as described above.

Elemental composition was measured by atomic absorption spectroscopy (AAS) on a UNICAM 939 AA-Spectrometer. BET specific surface area and pore volume were determined by nitrogen adsorption-desorption isotherms measured on a PMI Sorptomatic 1990 instrument at 77 K. The sample was activated in vacuum at 250 °C for 2 h prior to the measurement. Transmission electron microscopy (TEM) images were taken by a JEM-2010 Jeol transmission microscope operating at 120 kV. Prior to the measurement, the

sample was suspended in ethanol, deposited on a carbonated copper grid and outgased in vacuum.

## Testing of activity for selective oxidation of methane to methanol

Cu-MOR samples (100 mg) were tested for their activity towards methane oxidation in an atmospheric pressure stainless steel plug flow reactor with 4 mm inner diameter. The reaction included three consecutive steps: (i) activation in O<sub>2</sub> at 450 °C for 1 h, (ii) CH<sub>4</sub> loading at 200 °C for 4 h and (iii) steam-assisted CH<sub>3</sub>OH desorption at 135 °C for 30 min, with an intermediate He purge between each step. The reaction products were identified and quantified by online mass spectroscopy ( $m/z$  28, 31, 44 and 46 for CO, CH<sub>3</sub>OH, CO<sub>2</sub> and (CH<sub>3</sub>)<sub>2</sub>O, respectively). (CH<sub>3</sub>)<sub>2</sub>O formed via condensation of two partially oxidized CH<sub>4</sub> molecules corresponds to two CH<sub>3</sub>OH equivalents. The sum of all detected products is referred to as total yield.

## Infrared spectroscopy

The samples for IR spectroscopy were prepared as self-supporting wafers (10 mg·cm<sup>-3</sup>) and first activated in vacuum ( $1.0 \cdot 10^{-7}$  mbar) at 450 °C for 1 h. Infrared spectra of adsorbed n-hexane were recorded at 30 °C on a Vertex 70 spectrometer from Bruker Optics at a resolution of 4 cm<sup>-1</sup>. Infrared spectra of adsorbed pyridine were measured on a Thermo Nicolet 5700 FT-IR spectrometer with a resolution of 4 cm<sup>-1</sup>. After activation, subsequent adsorption and evacuation of 0.1 mbar pyridine, the total concentration of Brønsted acid sites (BAS) was determined at 150 °C by integration of the IR band at 1540 cm<sup>-1</sup>.

## Temperature-programmed desorption of ammonia

Acid sites were further characterized by temperature-programmed desorption of NH<sub>3</sub>. After activation at 450 °C 1 mbar NH<sub>3</sub> was adsorbed on the pelletized sample. After equilibration for 1 h and outgassing for 2 h, the sample was heated under dynamic vacuum while the NH<sub>3</sub> desorption was monitored by mass spectrometry ( $m/z$  16).

## 3.6 Acknowledgements

The research was partly supported by the U.S. Department of Energy, Office of Basic Energy Sciences, Division of Chemical Sciences under Award DE-SC0012702. It was also supported by the EU NEXT-GTL (Innovative Catalytic Technologies & Materials for Next Gas to Liquid Processes) project. Wanqiu Luo is acknowledged for her experimental work. Gary L. Haller is acknowledged for fruitful discussions.

## 3.7 Appendix

### Determination of the $\text{Na}^+$ concentration in side pockets

In a first step, the acid site concentration in the side pockets was determined by  $\text{Na}^+$  exchange. Different concentrations of  $\text{Na}^+$  were incorporated in the zeolite micropores via aqueous  $\text{Na}^+$ -exchange, as described above. Infrared spectra of the so prepared Na-MOR materials with various  $\text{Na}^+$  concentrations were compared to the spectra of pure H-MOR. Adsorption of n-hexane allowed selective perturbation of the main channel O-H-vibration ( $3,612\text{ cm}^{-1}$ ). Consequently, the O-H vibrations due to BAS in the side pockets were selectively examined by this technique. It was observed, that the band at  $3,590\text{ cm}^{-1}$  decreased with increasing  $\text{Na}^+$  loading and finally, the band disappeared when  $750\text{ }\mu\text{mol Na}^+$  ( $\text{Na}/\text{Al}_\text{F} = 0.65$ ) were exchanged into the zeolite. Comparison of the infrared spectra before n-hexane adsorption revealed that the band attributed to main channel O-H vibrations remained unchanged up to a  $\text{Na}^+$  concentration of  $750\text{ }\mu\text{mol g}^{-1}$ . For higher  $\text{Na}^+$  concentration also the main channel O-H-vibration decreased and finally disappeared when  $1160\text{ }\mu\text{mol g}^{-1}\text{ Na}^+$  was exchanged into the zeolite. These experiments demonstrate the highly selective exchange of  $\text{Na}^+$  into the 8-MR side pockets of MOR and at the same time allowed to quantify the BAS concentration in the side pockets.

**Table A 3.1:** Elemental analysis of Cu-MOR with various co-cations.

Sample	Cu loading [wt.%]	Co-cation loading [wt.%]	Cu/Al [mol mol <sup>-1</sup> ]	Co-cation/Al [mol mol <sup>-1</sup> ]
H-MOR	0.00	0.00	0.00	0.00
Cu-MOR	2.66	0.00	0.31	0.00
Na-MOR	0.00	2.45	0.00	0.85
CuNa-MOR	3.07	0.75	0.39	0.26
K-MOR	0.00	4.02	0.00	0.76
CuK-MOR	2.21	2.29	0.27	0.46
Mg-MOR	0.00	1.23	0.00	0.40
CuMg-MOR	2.45	0.63	0.29	0.19
Ca-MOR	0.0	2.14	0.00	0.41
CuCa-MOR	1.52	1.74	0.19	0.34

**Table A 3.2:** BET analysis of Cu-MOR.

Sample	Cu loading [wt.%]	Cu/Al [mol mol <sup>-1</sup> ]	BET surface area [m <sup>2</sup> g <sup>-1</sup> ]	V <sub>micropore</sub> [cm <sup>3</sup> g <sup>-1</sup> ]
H-MOR	0.0	0.00	534	0.20
Cu-MOR	1.0	0.12	499	0.18
Cu-MOR	2.9	0.34	501	0.19
Cu-MOR	5.2	0.62	422	0.16
Na-MOR	0.0	0.00	484	0.23
CuNa-MOR	3.1	0.39	430	0.21
CuNa-MOR	3.8	0.49	409	0.20
CuNa-MOR	5.0	0.61	371	0.17

**Table A 3.3:** Comparison of copper loading and activity of Cu-MORs prepared at various pH before and after back-exchange.

sample	Initial preparation			Back-exchange <sup>a</sup>	
	pH during exchange	Cu/Al [mol mol <sup>-1</sup> ]	Methane converted [μmol g <sup>-1</sup> ]	Cu conc. [μmol g <sup>-1</sup> ]	Methane converted [μmol g <sup>-1</sup> ]
CuH-MOR	4.4	0.21	99	0.02	2
CuNa-MOR	5.0	0.36	99	0.03	2
CuH-MOR	5.7	0.31	151	0.04	6
CuNa-MOR	6.5	0.61	115	0.27	5

<sup>a</sup>Samples were calcined under O<sub>2</sub> flow at 500 °C for 2 h and back-exchanged with 0.5 M NaNO<sub>3</sub> solution at 65 °C for 24 h.

**Table A 3.4:** Elemental analysis and acid site distribution in Cu exchanged mordenites.

Na	Cu	BAS <sub>total</sub>	BAS <sub>main channel</sub> <sup>a</sup>	BAS <sub>side pockets</sub> <sup>b</sup>
[ $\mu\text{mol g}^{-1}$ ]	[ $\mu\text{mol g}^{-1}$ ]	[ $\mu\text{mol g}^{-1}$ ]	[ $\mu\text{mol g}^{-1}$ ]	[ $\mu\text{mol g}^{-1}$ ]
0	419	800	420	380
307	384	385	358	27
319	414	303	282	21
948	102	240	240	0
421	401	469	384	85
718	216	291	291	0
618	266	268	268	0

a) Obtained by quantification of the band at  $3,612\text{ cm}^{-1}$  (after deconvolution of the band at  $3,610\text{ cm}^{-1}$  into  $3,612$ ,  $3,590$  and  $3,500\text{ cm}^{-1}$ ).

b) Obtained by quantification of the band at  $3,590\text{ cm}^{-1}$  (after deconvolution of the band at  $3,610\text{ cm}^{-1}$  into  $3,612$ ,  $3,590$  and  $3,500\text{ cm}^{-1}$ ).

## 3.8 References

- [1] Iwamoto, M.; Furukawa, H.; Mine, Y.; Uemura, F.; Mikuriya, S. I.; Kagawa, S. *J. Chem. Soc., Chem. Commun.* **1986**, 1272.
- [2] Groothaert, M. H.; Smeets, P. J.; Sels, B. F.; Jacobs, P. A.; Schoonheydt, R. A. *J. Am. Chem. Soc.* **2005**, 127, 1394.
- [3] Kwak, J. H.; Varga, T.; Peden, C. H. F.; Gao, F.; Hanson, J. C.; Szanyi, J. *J. Catal.* **2014**, 314, 83.
- [4] Groothaert, M. H.; van Bokhoven, J. A.; Battiston, A. A.; Weckhuysen, B. M.; Schoonheydt, R. A. *J. Am. Chem. Soc.* **2003**, 125, 7629.
- [5] Dedeczek, J.; Sobalik, Z.; Tvaruzkova, Z.; Kaucky, D.; Wichterlova, B. *J. Phys. Chem.* **1995**, 99, 16327.
- [6] Smeets, P. J.; Groothaert, M. H.; Schoonheydt, R. A. *Catal. Today* **2005**, 110, 303.
- [7] Alayon, E. M.; Nachtegaal, M.; Ranocchiari, M.; van Bokhoven, J. A. *Chem. Commun.* **2012**, 48, 404.
- [8] Alayon, E. M. C.; Nachtegaal, M.; Bodi, A.; van Bokhoven, J. A. *ACS Catal.* **2014**, 4, 16.
- [9] Narsimhan, K.; Michaelis, V. K.; Mathies, G.; Gunther, W. R.; Griffin, R. G.; Román-Leshkov, Y. *J. Am. Chem. Soc.* **2015**, 137, 1825.
- [10] Bhan, A.; Allian, A. D.; Sunley, G. J.; Law, D. J.; Iglesia, E. *J. Am. Chem. Soc.* **2007**, 129, 4919.
- [11] Grundner, S.; Markovits, M. A. C.; Li, G.; Tromp, M.; Pidko, E. A.; Hensen, E. J. M.; Jentys, A.; Sanchez-Sanchez, M.; Lercher, J. A. *Nat. Commun.* **2015**, 6, 7546.
- [12] Woertink, J. S.; Smeets, P. J.; Groothaert, M. H.; Vance, M. A.; Sels, B. F.; Schoonheydt, R. A.; Solomon, E. I. *Proc. Natl. Acad. Sci. U. S. A.* **2009**, 106, 18908.
- [13] Alayon, E. M. C.; Nachtegaal, M.; Kleymenov, E.; van Bokhoven, J. A. *Microporous Mesoporous Mater.* **2013**, 166, 131.
- [14] Hidmi, L.; Edwards, M. *Environ. Sci. Technol.* **1999**, 33, 2607.
- [15] Schreier, M.; Teren, S.; Belcher, L.; Regalbuto, J. R.; Miller, J. T. *Nanotechnology* **2005**, 16, 582.
- [16] Lo Jacono, M.; Fierro, G.; Dragone, R.; Feng, X.; d'Itri, J.; Hall, W. K. *J. Phys. Chem. B* **1997**, 101, 1979.
- [17] Iwamoto, M.; Yahiro, H.; Tanda, K.; Mizuno, N.; Mine, Y.; Kagawa, S. *J. Phys.*

*Chem.* **1991**, *95*, 3727.

- [18] Hirschler, A. E. *J. Catal.* **1963**, *2*, 428.
- [19] Larsen, S. C.; Aylor, A.; Bell, A. T.; Reimer, J. A. *J. Phy. Chem.* **1994**, *98*, 11533.
- [20] Valyon, J.; Hall, W. K. *J. Phys. Chem.* **1993**, *97*, 7054.
- [21] Eder, F.; Stockenhuber, M.; Lercher, J. A. *J. Phys. Chem. B* **1997**, *101*, 5414.
- [22] Veefkind, V. A.; Smidt, M. L.; Lercher, J. A. *Appl. Catal., A* **2000**, *194*, 319.
- [23] Vanelderen, P.; Snyder, B. E. R.; Tsai, M.-L.; Hadt, R. G.; Vancauwenbergh, J.; Coussens, O.; Schoonheydt, R. A.; Sels, B. F.; Solomon, E. I. *J. Am. Chem. Soc.* **2015**, *137*, 6383.
- [24] Groothaert, M. H.; Smeets, P. J.; Sels, B. F.; Jacobs, P. A.; Schoonheydt, R. A. *J. Am. Chem. Soc.* **2005**, *127*, 1394.

## 4 Elementary Steps of the Selective Oxidation of Methane to Methanol over Copper Exchanged Mordenite

### 4.1 Abstract

Copper exchanged zeolites have the potential to selectively oxidize methane to methanol in a three step process consisting of thermal activation, methane reaction and steam assisted product extraction. The kinetics and the mechanism of the three steps have been investigated separately. Thermal activation is the step with the highest barrier. The activation process consists of several elementary steps including dehydration,  $\mu$ -oxo-bridging, autoreduction and re-oxidation of copper. In this study, it was demonstrated that autoreduction is the crucial step of activation which requires temperatures of 450 °C, whereas dehydration of copper ions is largely complete at 350 °C. The generation of mobile monovalent copper during thermal treatment in inert (autoreduction) facilitates the redistribution of copper and therefore enhances the formation of multinuclear copper clusters. The re-oxidation of the autoreduced copper cluster precursor is a fast process which is zero order in O<sub>2</sub> and occurs at temperatures below 50 °C. The optimum methane reaction temperature was determined to be 200 °C. At this temperature an initial methane oxidation rate of 5  $\mu\text{mol min}^{-1}$  was determined. At higher methane loading temperatures, a consecutive reaction mechanism leads to total oxidation of methane during steam treatment. The reaction order of 0.6 with respect to methane is consistent with methane activation via homolytic C-H bond cleavage followed by a direct radical rebound reaction mechanism.

## 4.2 Introduction

Thermal oxygen activation of Cu exchanged zeolites is a complex process that consist of several elementary steps which are commonly described by the following mechanism. Initially, thermal treatment results in the removal of water from the zeolite pores. A broad number of studies demonstrated that dehydration of the zeolite pores is largely complete at 350 °C.<sup>[1-4]</sup> Thus, water ligands coordinated to Cu<sup>2+</sup> ions located in the zeolite cavities are removed during activation, resulting in the movement of Cu<sup>2+</sup> towards their final exchange positions.<sup>[5-7]</sup> The generation of monovalent [Cu-OH]<sup>+</sup> species attached to framework Al sites was proposed in this step.<sup>[8]</sup> Such species have the potential to transform to multinuclear Cu-oxo clusters via condensation with adjacent [Cu-OH]<sup>+</sup> forming a  $\mu$ -oxo bridge between Cu<sup>2+</sup> cations and a H<sub>2</sub>O molecule.<sup>[9-11]</sup> Furthermore, when thermal treatment is performed at temperatures above 350 °C in inert atmosphere, it results in autoreduction of Cu<sup>2+</sup> to Cu<sup>+</sup>.<sup>[9,12,13]</sup> This process is thought to occur via recombination and desorption of the bridging O of  $\mu$ -oxo bridged Cu species as O<sub>2</sub>.<sup>[11,14]</sup> In the presence of O<sub>2</sub>, Cu<sup>+</sup> is re-oxidized quantitatively to Cu<sup>2+</sup> at temperatures below 350 °C.<sup>[12]</sup>

Since the high activity of Cu-zeolites for the direct catalytic decomposition of NO was attributed to Cu<sup>+</sup> species, this mechanism seems straightforward to rationalize the necessity of activation and reaction temperatures of 450 °C for the DeNO<sub>x</sub> reaction.<sup>[9,15,16]</sup> However, it is still not understood why in oxidation catalysis over Cu-zeolites –where presumably the active species is a Cu<sup>2+</sup>- activation at least at 450 °C is required. The role of autoreduction and oxidation of Cu as well as the interplay of these processes at various temperatures leading to the formation of copper oxo clusters has not been elucidated yet. Furthermore, there is a lack of understanding of the dynamics of Cu mobility during Cu dehydration. The processes involved in hydration-dehydration of Cu species and the speciation of exchanged Cu in zeolites have only been studied comprehensively by *in situ* spectroscopy for Cu on chabazite (CHA) under SCR

conditions in the presence of H<sub>2</sub>O, NH<sub>3</sub> and NO in the feed. These conditions are, however, very different to those applied in oxidation catalysis.<sup>[5]</sup>

To date, the mechanism of the C-H activation in selective partial oxidation of methane to methanol over Cu-zeolites has not been elucidated experimentally. While the three step process for selective partial oxidation of methane to methanol over Cu-MOR was studied by ultraviolet-visible and Cu K-edge X-ray absorption spectroscopy, the mechanism of active site formation and methane C-H activation have not been elucidated.<sup>[17-20]</sup> Previous mechanistic studies are mainly based on DFT calculations.<sup>[19,21]</sup> EPR studies give only limited insight in the mechanism of methane oxidation since the majority of the sites found in calcined Cu-ZSM-5 and Cu-MOR are EPR silent.<sup>[22,23]</sup>

In this chapter the role of dehydration, oxidation, autoreduction and the role of Cu ion movement in MOR during thermal activation are investigated in detail by kinetics and *in-situ* spectroscopic studies. The activation energy, the rate of methane oxidation as well as the reaction order with respect to methane were elucidated in order to get a better insight on the mechanism of methane oxidation to methanol. Furthermore, the kinetics of the steam assisted desorption of products are investigated briefly.

## 4.3 Results and Discussion

### 4.3.1 Processes Involved in the Thermal Activation

#### 4.3.1.1 Titration of active sites for selective methane oxidation

The study was performed on the same Cu-MOR sample studied in Chapter 2, with a Cu loading of  $420 \mu\text{mol g}^{-1}$  corresponding to a Cu/Al ratio of 0.31. The active site of this sample was elucidated as single-site trinuclear copper oxo cluster  $[\text{Cu}_3(\mu\text{-O})_3]^{2+}$  (see Chapter 2).<sup>[19]</sup> In a typical experiment, the sample was calcined in  $\text{O}_2$  flow at  $450^\circ\text{C}$  for 1 h and subsequently cooled in  $\text{O}_2$ . As demonstrated in Chapter 2, passing a flow of 90% methane over the sample at  $200^\circ\text{C}$  for 4 h allows titration of all sites active for methane activation. The steam assisted desorption allowed quantification of the methane oxidation products and consequently of the active site concentration in Cu-MOR. Dimethyl ether was accounted as secondary product resulting from acid catalyzed condensation of two methanol molecules (see Appendix Figure A 4.1). Therefore dimethyl ether concentration was also taken into account for the determination of the selectivity of partial oxidation.

For each series of experiments only one parameter of the activation step was varied, while the conditions of the methane loading step and the steam treatment step were kept constant. In a first step, the impact of activation temperature on methane oxidation activity was studied, in order to get a basic understanding of the activation process. The freshly prepared sample was activated in pure  $\text{O}_2$  for 1 h at different temperatures and subsequently cooled to  $200^\circ\text{C}$  in  $\text{O}_2$  before it was contacted with methane. An exponential increase in activity with increasing temperature of activation was observed in the range of  $200\text{--}450^\circ\text{C}$ . Activity leveled off at  $500^\circ\text{C}$  (Figure 4.1). It is remarkable that even at activation temperatures as low as  $200^\circ\text{C}$ , a significant amount of methane was oxidized, ca. 30% of the maximum activity reached at catalyst activation at  $500^\circ\text{C}$ . The constant selectivity over the whole temperature range is indicative for the formation of only one type of active copper species over the

whole temperature range. As a first conclusion, these experiments demonstrate the necessity of high temperatures for an efficient activation process.

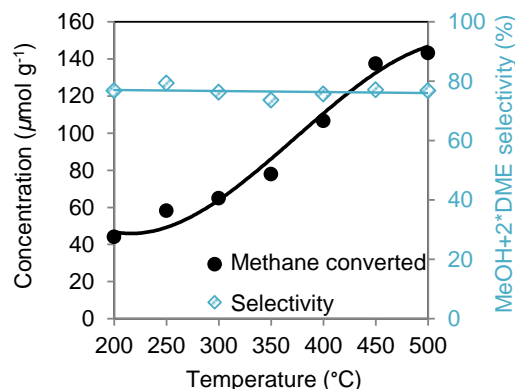


**Figure 4.1:** Activity and selectivity of Cu-MOR with a Cu loading of  $420 \mu\text{mol g}^{-1}$  after activation in pure  $\text{O}_2$  at various temperatures. Methane loading was performed at  $200^\circ\text{C}$  in 90%  $\text{CH}_4$  for 4h.

The previous series of experiments has not clarified if a thermodynamic equilibrium has been established after 1h activation time at each temperature or the activation is still governed by kinetics. Thus, the activation time was extended for various temperatures (Figure A 4.2). In the temperature range of  $250\text{--}450^\circ\text{C}$ , activity was doubled for a temperature increase of  $100^\circ\text{C}$ . However, an extension of the activation time from 1 to 3 h resulted only in a small increase of activity. This indicates that the activation process can be considered as thermodynamically equilibrated after 1h of thermal treatment at temperatures in the range of  $350\text{--}450^\circ\text{C}$ .

In order to study the mechanism of oxygen activation on Cu-MOR, the rate of oxidation was studied as a function of  $\text{O}_2$  partial pressure. Variation of the  $\text{O}_2$  partial pressure in the range of 50-1000 mbar did not show any impact on activity (see Appendix Figure A 4.3). Thus, a reaction order of 0 with respect to  $\text{O}_2$  is obtained. In this case, a reaction order 0 can be interpreted as facile incorporation of O in the cluster precursor during the oxidation process. Moreover, activation at various temperatures was compared under different type of oxidants:  $\text{O}_2$  and  $\text{N}_2\text{O}$ . While  $\text{O}_2$  is a two O donor,  $\text{N}_2\text{O}$  can only provide

one O atom to a Cu site. Methane oxidation is a process involving the transfer of one O from the Cu-oxo cluster to a methane molecule.<sup>[19]</sup> Moreover, previous studies suggested that oxidation of  $\text{Cu}^+$  to  $\text{Cu}^{2+}$  occurs via insertion of one O atom between two vicinal  $\text{Cu}^+$  species that were formed during autoreduction.<sup>[13]</sup> Therefore a one O oxidation process of Cu species with  $\text{O}_2$  would require O-O cleavage, migration of the other O atom on the zeolite surface and its subsequent recombination to  $\text{O}_2$  or alternatively its reaction with another Cu site. Therefore, differences in oxidation kinetics are expected for these two oxidants  $\text{O}_2$  and  $\text{N}_2\text{O}$ . Surprisingly, Figure 4.2 shows that for both oxidants identical yields and selectivities were achieved after activation at the same temperature. The lack of any difference in  $\text{O}_2$  and  $\text{N}_2\text{O}$  activation indicates that oxidation is likely not the limiting step of thermal activation.

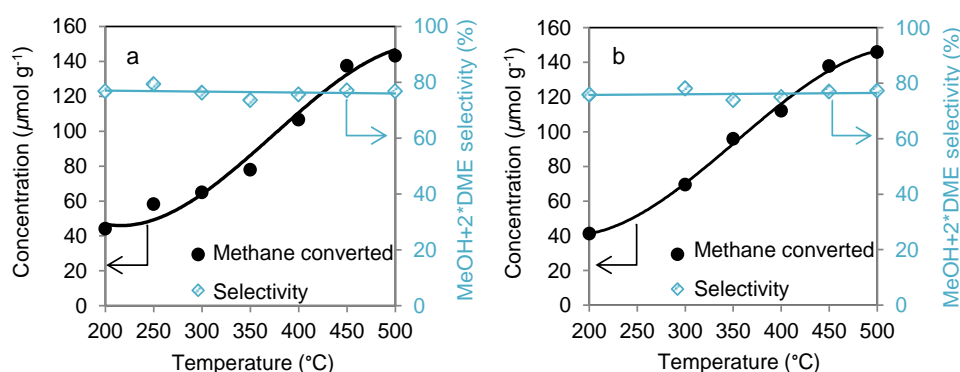


**Figure 4.2:** Comparison of activity and selectivity of Cu-MOR with a Cu loading of 420  $\mu\text{mol g}^{-1}$  after activation in a) pure  $\text{O}_2$  and b)  $\text{N}_2\text{O}$  at various temperatures. Methane loading was performed at 200 °C in 90%  $\text{CH}_4$  for 4h.

To obtain deeper insight in the oxidation step itself, the oxidation process needs to be decoupled from dehydration of the zeolite during thermal activation. It was demonstrated that thermal activation requires temperatures of 450 °C (Figure 4.1), while oxidation was determined to be zero order with respect to  $\text{O}_2$  (Figure A 4.3). Based on these results, Cu-MOR was first activated in a He flow at 500 °C for 1h, cooled down in He flow and finally contacted with  $\text{O}_2$  at lower temperature (50-200 °C). Figure 4.3 shows that after oxidation at 50 °C for 10 min the maximum concentration of active sites

corresponding to a stoichiometry of one converted methane molecule per three Cu atoms is already generated. Comparable results were obtained for thermal activation in He and subsequent low temperature oxidation in a flow of 16 ml min<sup>-1</sup> with a N<sub>2</sub>O partial pressure of 50 mbar in He (Figure 4.3 b). Even at 50 °C no significant difference of O<sub>2</sub> and N<sub>2</sub>O reactivity was obtained, suggesting that the Cu cluster precursor is a very reactive species towards oxidation. Consequently, the temperature dependence of thermal activation observed in Figure 4.2 is not related to the insertion of oxygen. Thus, the necessity of high activation temperatures is proposed to be related to the formation of the active site precursor, which is revealed as the rate determining step of the activation process.

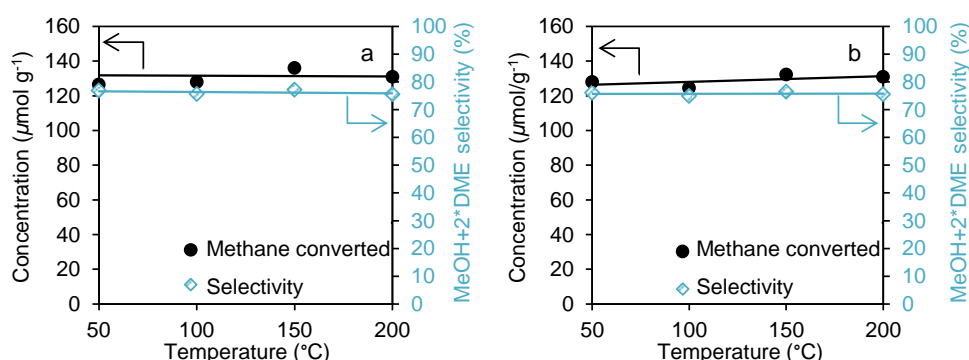


**Figure 4.3:** Activity and selectivity of Cu-MOR with a Cu loading of 420 μmol g<sup>-1</sup> after activation in He for 1h at 500 °C and subsequent oxidation in a) 5% O<sub>2</sub> and b) 5% N<sub>2</sub>O in He at various temperatures for 10 min (16 ml min<sup>-1</sup>). Methane loading was performed at 200 °C in 90% CH<sub>4</sub> for 4h.

It was already proposed by some authors that an intermediate step of autoreduction of Cu<sup>2+</sup> to Cu<sup>+</sup> occurs during thermal treatment in O<sub>2</sub> at temperatures > 350 °C.<sup>[9,24]</sup> In order to study the impact on active site formation of the intermediate step of reduction of Cu<sup>2+</sup> to Cu<sup>+</sup> and its subsequent re-oxidation to Cu<sup>2+</sup> at lower temperature, the reduction step was enhanced by the introduction of a reducing agent. The sample was exposed first to a flow of H<sub>2</sub> at 250 °C and subsequently to a flow of O<sub>2</sub> at 250 °C for 1 h respectively, prior to contacting with methane.<sup>[25]</sup> Note, that in literature, H<sub>2</sub> reduction of Cu<sup>2+</sup> in zeolites to Cu<sup>+</sup> is reported to occur at temperatures below 300 °C.<sup>[24-26]</sup>

However, no effect on methane oxidation activity was obtained by this redox treatment at 250 °C compared to activation in O<sub>2</sub> at 250 °C for 2 h (Figure A 4.2). This result can be interpreted in two ways. On the one hand, the lack of any impact of H<sub>2</sub> reduction could indicate that Cu<sup>+</sup> is not a relevant intermediate for the formation of the trinuclear copper oxo cluster. This hypothesis will be evaluated in the next section by means of *in situ* spectroscopy. On the other hand, migration of Cu<sup>+</sup> at high temperature might be crucial for the formation of the active site. Dedecek *et al.* stated that migration of Cu ions during reduction is minimized by reduction in H<sub>2</sub> at low temperatures (<350 °C) compared to the migration accompanying the autoreduction at higher temperatures (>350 °C).<sup>[25]</sup> Thus, the lack of any effect of H<sub>2</sub> reduction at 250 °C prior to re-oxidation on active site formation is a first hint that redistribution of Cu sites in form of Cu<sup>+</sup> is essential for the formation of the multinuclear copper oxo cluster. The higher mobility of Cu<sup>+</sup> compared to Cu<sup>2+</sup> in the electrostatic field of the zeolite pores of CuSSZ-13 is proposed to be due to the weaker ionic interactions of monovalent Cu<sup>+</sup> with the negatively charged zeolite framework.<sup>[5]</sup> In line with this conclusion, Hall *et al.* speculated that the reduction of Cu<sup>2+</sup> to Cu<sup>+</sup> facilitated redistribution of Cu and therefore enhanced the formation of active sites in Cu-ZSM-5.<sup>[13]</sup>

#### 4.3.1.2 *In situ* spectroscopy

For a fundamental understanding of the redox chemistry of Cu embedded in zeolites during thermal oxygen activation, a time-resolved study of the changes of Cu oxidation state was carried out. *In situ* X-ray absorption spectroscopy (XAS) is an excellent tool for this matter, because very characteristic features for Cu<sup>+</sup> and Cu<sup>2+</sup> in different coordination can be observed in the X-ray absorption near edge structure (XANES). In the ultraviolet-visible (UV-vis) spectrum of Cu-MOR a broad band centered at ca. 31,000 cm<sup>-1</sup> was previously assigned to a trinuclear copper oxo cluster (see Chapter 2).<sup>[19]</sup> In this chapter, *in situ* UV-vis spectroscopy is performed in order to observe evolution of the band associated to active sites during thermal activation and reaction under various conditions.

*In situ* XAS was performed under the standard activation conditions as evaluated in the previous section (4.3.1.1). Figure 4.4 shows the Cu K-edge XANES spectra during heating of as prepared Cu-MOR in pure O<sub>2</sub> up to 450 °C. The presence of a weak pre-edge feature at 8978 eV due to 1s → 3d transition of Cu<sup>2+</sup> demonstrates the dominant Cu<sup>2+</sup> character of all spectra taken along the activation process. The loss in intensity of the maximum adsorption feature at 8997 eV with increasing temperature is indicative for the removal of water ligands.<sup>[18]</sup> No significant change of the whiteline intensity at 8997 eV is observed above 350 °C, indicating that dehydration of the Cu<sup>2+</sup> centers is already complete at this temperature. The rising edge feature at 8987 eV attributed to a 1s → 4p transition of Cu<sup>2+</sup> indicates a change from octahedral to tetrahedral coordinated Cu<sup>2+</sup> during thermal treatment (Figure 4.4 b).<sup>[17]</sup> This can be rationalized as the dehydration of the octahedral Cu<sup>2+</sup> complexes in the pores to framework coordinated tetrahedral Cu<sup>2+</sup> species. Comparison of the XANES spectra recorded during activation at 350 °C with the spectra after activation at 450 °C for 1h revealed a slight decrease of the rising edge feature at 8987 eV attributed to a 1s → 4p transition of Cu<sup>2+</sup>, indicating a decrease in Cu<sup>2+</sup> population. At the same time, a feature at 8983 eV attributed to a 1s → 4p transition of Cu<sup>+</sup> is generated in the temperature range between 350-450 °C (Figure 4.4 c). Hence, even in the presence of O<sub>2</sub>, autoreduction of Cu<sup>2+</sup> to Cu<sup>+</sup> occurs in some extent when temperature is above 350 °C.

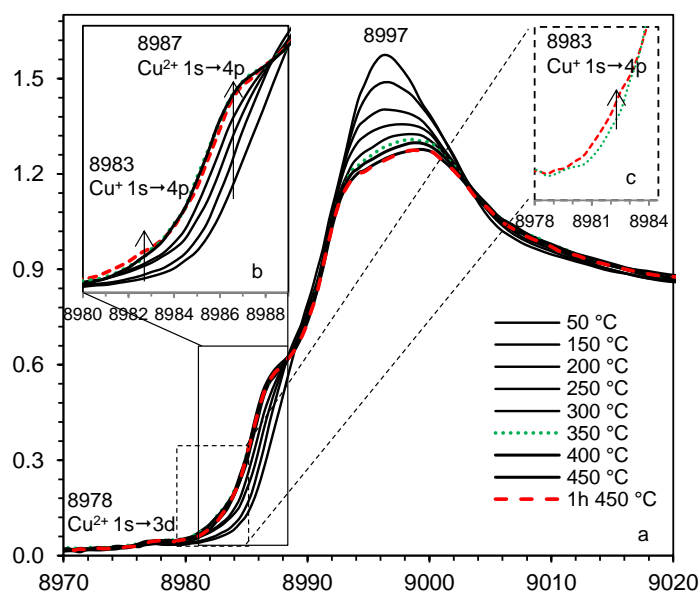


**Figure 4.4:** a) Cu K-edge XANES spectra of Cu-MOR during thermal activation in O<sub>2</sub>, b) rising edge feature and c) comparison of Cu(I) feature at 8983-8984 eV after activation at 350 °C and 1h at 450 °C.

In the presence of O<sub>2</sub>, autoreduction is superimposed with oxidation and therefore, cannot be studied unambiguously. In order to get a deeper insight in the process of autoreduction with regard to its temperature dependence, thermal activation in an inert atmosphere was studied by XANES spectroscopy. Figure 4.5 shows the XANES spectra recorded during heating of a fresh sample in He to 450 °C. Analogously to activation in O<sub>2</sub>, the intensity of the maximum adsorption feature at 8997 eV is decreasing with increasing temperature and reaches a constant intensity at 350 °C, indicating that dehydration of Cu<sup>2+</sup> is largely complete at 350 °C.<sup>[18]</sup> The intensity of the rising edge feature at 8987 eV, characteristic for tetrahedral Cu<sup>2+</sup> coordination, is reaching a maximum at 300 °C. However, the most characteristic change during activation in He is the emergence of a pronounced feature between 8983 and 8984 eV which is attributed to a 1s → 4p transition of Cu<sup>+</sup>.<sup>[27]</sup> A drastic increase of the intensity of this feature was observed in the range of 350-450 °C, showing that autoreduction is the dominant reaction above 350 °C in inert atmosphere. After He treatment at 450 °C for 2 h, two distinct features at 8983 and 8984 eV evolved (Figure 4.5 b), suggesting the formation of two

distinct  $\text{Cu}^+$  species with different coordination. The position of the feature at 8983 eV together with the shape of the rising edge is indicative of linearly coordinated  $\text{Cu}^+$ . The feature at 8984 eV can be attributed to  $\text{Cu}^+$  with a higher coordination number, most likely 4-fold coordination.<sup>[28]</sup> The low coordination of species at 8983 eV is attributed to mobile  $\text{Cu}^+$  that is not coordinated at a cationic site because Cu at those sites has a coordination number of four.<sup>[25]</sup> After cooling the sample to 200 °C, only one broad feature in the  $\text{Cu}^+$  region is visible. Therefore *in situ* XANES has shown the reversible formation of linearly coordinated  $\text{Cu}^+$  at high temperatures demonstrating the dynamics of  $\text{Cu}^+$  motion during activation at temperatures above 350 °C.

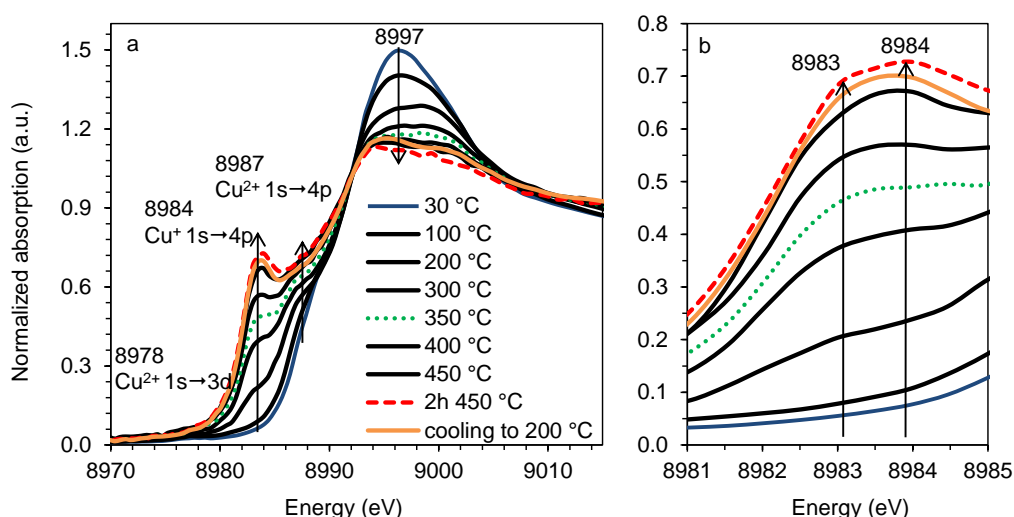


**Figure 4.5:** a) Over view of the Cu K-edge XANES spectra of Cu-MOR during thermal activation in He b) XANES region attributed  $\text{Cu}^+$   $1s \rightarrow 4p$  transition.

Autoreduction is proposed to occur via spontaneous desorption of O from  $\mu$ -oxo bridged  $\text{Cu}^{2+}$ .<sup>[8,10,11]</sup> To date, however, there is still no experimental prove for this hypothesis. Extended X-ray absorption fine structure (EXAFS) allows an analysis of the coordination shell of Cu during activation under oxygen. Cu-O distance and coordination number as well as Cu-Cu distance in the second coordination shell can be identified by EXAFS (see Chapter 2). Therefore, the hypothesis of autoreduction via formation of  $\mu$ -oxo-bridged  $\text{Cu}^{2+}$  and subsequent desorption of the bridging O was evaluated by this technique.

Figure 4.6 shows the EXAFS spectra of Cu-MOR during thermal activation in O<sub>2</sub> flow. The most prominent peak in all spectra can be observed below 2 Å in *R*-space and is associated with backscattering from O to which Cu is directly bonded. The features above 2.0 Å in *R*-space arise from Cu-Cu and second shell Cu-O single-scattering paths (see Chapter 2). With increasing temperature a distinct peak at large interatomic distances (*R* ~ 2.5 Å - not phase corrected), corresponding to the second coordination shell of Cu is arising at temperatures above 200 °C, which is attributed to a Cu-Cu path.<sup>[19,29]</sup> The intensity of the first shell feature is decreasing with increasing temperature indicating a decrement of O coordinated to Cu<sup>2+</sup>. Below 350 °C this decrease is due to dehydration resulting in the transformation of octahedral Cu<sup>2+</sup> to tetrahedral Cu<sup>2+</sup>. However, *in situ* XANES spectra have shown that dehydration is largely complete at 350 °C (Figure 4.4). Therefore, the further decrease in O coordination in the range of 350-450 °C is attributed to autoreduction and formation of mobile Cu<sup>+</sup> with low coordination. The presence of a Cu-Cu path already below 200 °C, together with the significant decrease of the Cu-O path above 350 °C are indications of a reduction mechanism involving the desorption of O from  $\mu$ -oxo bridges to form Cu<sup>+</sup> species.

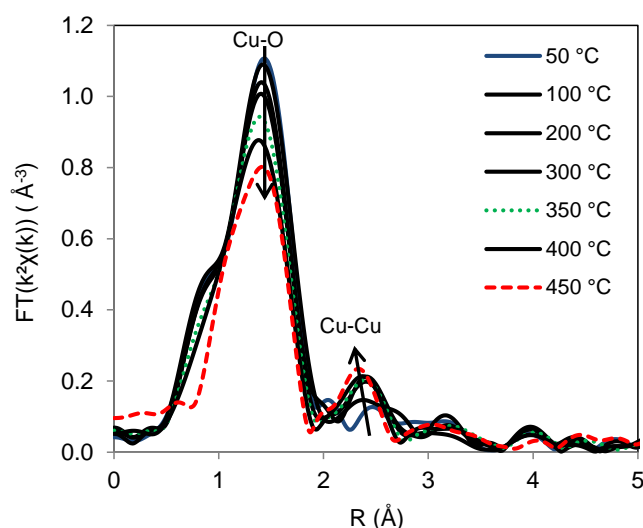


**Figure 4.6:** Cu K-edge FT EXAFS of Cu-MOR sample during thermal activation in O<sub>2</sub> flow with a heating rate of 10 °C min<sup>-1</sup>.

Based on the results obtained so far, it is hypothesized that active site formation occurs via dehydration of  $\text{Cu}^{2+}$  species, followed by autoreduction to  $\text{Cu}^+$ , subsequent organization of  $\text{Cu}^+$  species to form a reduced cluster precursor at high temperature and, finally the facile oxidation of the oxo-cluster precursor. To obtain spectroscopic evidence, the XANES spectra of Cu-MOR activated in  $\text{O}_2$  will be compared with spectra of Cu-MOR activated in He at 450 °C followed by oxidation at 200 °C.

Figure 4.7 shows XANES spectra of Cu-MOR along the catalytic cycle followed by a consecutive thermal regeneration of the active species in inert atmosphere and subsequent low temperature oxidation, using the conditions as applied in section 4.3.1.1. The characteristic feature for tetrahedral  $\text{Cu}^{2+}$  at 8987 eV arose upon initial activation in  $\text{O}_2$  at 450 °C. After reaction of the activated sample with methane for 4h, a significant fraction of 4-fold coordinated  $\text{Cu}^+$  was generated, as can be seen by the generation of the feature at 8984 eV. Steam treatment for 2 h resulted in a drastic increase of the white line intensity at 8997 eV and the disappearance of the rising edge feature at 8987 eV which indicates complete hydration and re-oxidation of all Cu sites to hydrated octahedral  $\text{Cu}^{2+}$ .<sup>[17]</sup> Consecutive regeneration of the active species was performed at high temperature activation in inert atmosphere and subsequent low temperature oxidation. The catalyst was first activated in He at 450°C for 1 h and subsequently oxidized in  $\text{O}_2$  at 200 °C for 15 min. The  $\text{Cu}^+$  feature at 8984 eV emerged after activation in He due to autoreduction. The  $\text{Cu}^+$  feature disappeared completely after exposure to  $\text{O}_2$  at 200 °C for 15 min and an identical XANES spectrum compared to the initial activation in  $\text{O}_2$  was obtained. This indicates that the autoreduced precursor of the trinuclear copper oxo cluster is completely re-oxidized to its active form independently of the oxidation temperature applied (within the temperature range of 50-200 °C), in good agreement with the results from activity tests (Figure 4.3) .

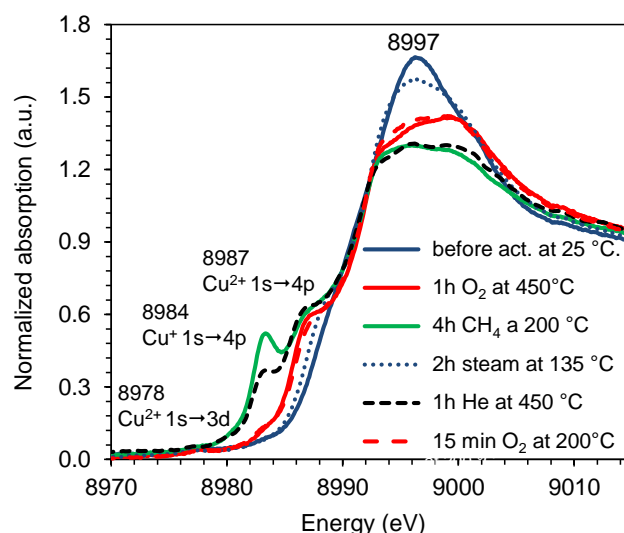


**Figure 4.7:** *In situ* Cu K-edge XANES spectra of Cu-MOR during a full cycle of selective partial oxidation of methane to methanol and subsequent second thermal activation in He followed by low temperature oxidation.

The time and temperature dependent generation of the trinuclear copper oxo cluster from its pre-reduced precursor upon O<sub>2</sub> addition was monitored by UV-vis spectroscopy. In Chapter 2, the trinuclear copper oxo cluster in activated Cu-MOR was associated with a contribution to a broad band at ca. 31,000 cm<sup>-1</sup> in the UV-vis spectrum, because this feature was observed to decrease upon reaction with methane.<sup>[19]</sup> In this chapter, it was observed that the characteristic band at 31,000 cm<sup>-1</sup> present in a He activated Cu-MOR sample dramatically increased after contact with O<sub>2</sub> at temperatures as low as 30 °C (see Appendix Figure A 4.4). This, together with the lack of dependence of the activity with temperature or nature of the oxidation (Figure 4.3), indicates a facile formation of the trinuclear copper oxo cluster upon contact with an oxidant. Subsequent heating of the sample in O<sub>2</sub> to 300 °C had no effect on the intensity of the UV-vis absorption band. The constant intensity of the band at 31,000 cm<sup>-1</sup> during heating in O<sub>2</sub> from 50 °C to 300 °C demonstrates that oxidation is already complete at 50 °C (Figure 4.8). However, for temperatures above 300 °C under O<sub>2</sub> the intensity of this band decreased. Further heating in O<sub>2</sub> up to 450 °C led to a decrease of this band to its initial intensity, indicating partial disintegration of the structure of the trinuclear copper oxo cluster. This result is in good agreement with the observations in EXAFS where it was proposed that

auto-reduction even occurs in some extent during thermal treatment in O<sub>2</sub> in the temperature range of 300-450 °C. However, XANES revealed that the majority of Cu occurs in form of tetrahedral Cu<sup>2+</sup>, even after equilibration at 450 °C in O<sub>2</sub> atmosphere.

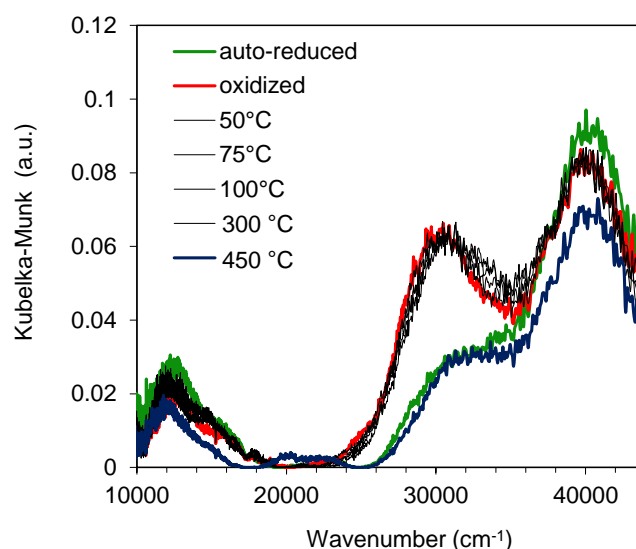


**Figure 4.8:** *In situ* UV-vis spectra of Cu-MOR after activation in He at 450 °C, cooling to 50 °C and subsequent heating in O<sub>2</sub>.

#### 4.3.1.3 Discussion of the elementary steps of activation

Temperatures of 450 °C during oxygen activation are known to be essential for the generation of the active copper oxo cluster (Figure 4.1). However, kinetic studies and *in situ* spectroscopy revealed that oxygen insertion in the Cu active cluster occurs at low temperatures and therefore it is not the rate determining step of the activation process (Figure 4.3, 4.7 and 4.8). Therefore, the necessity of high temperature treatment must be related to other elementary steps prior to oxidation. Since *in situ* XAS spectroscopy demonstrated that the transformation of the octahedral Cu<sup>2+</sup> complexes in the zeolite pores into framework Al bonded tetrahedral Cu<sup>2+</sup> was largely complete at 350 °C, dehydration is ruled out as rate limiting step (Figure 4.4). Above 350 °C auto-reduction occurs, even in the presence of O<sub>2</sub>, resulting in the generation of mobile linear coordinated Cu<sup>+</sup> (Figure 4.5). The mechanism of auto-reduction of

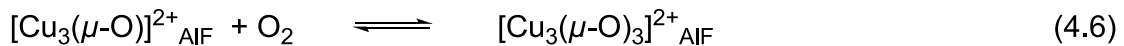
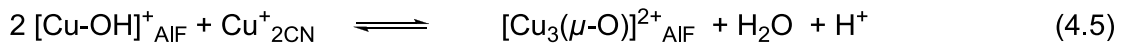
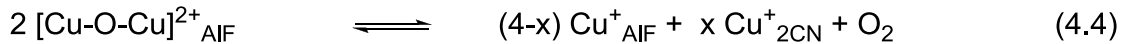
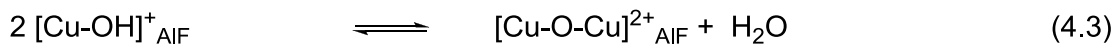
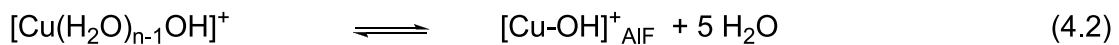
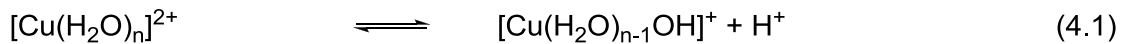
Cu zeolites is discussed controversially in literature.<sup>[9,13]</sup> EXAFS spectroscopy confirmed the hypothesis of a reduction via O desorption from  $\mu$ -oxo bridges between  $\text{Cu}^{2+}$  (Figure 4.6). In presence of  $\text{O}_2$ , there is a O desorption-adsorption equilibrium which is shifted to the adsorption side, and consequently only a small fraction of  $\text{Cu}^+$  can be observed in the XANES spectra in  $\text{O}_2$  atmosphere. However, the drastic decrease of the characteristic UV-vis band at  $31,000\text{ cm}^{-1}$  during heating in  $\text{O}_2$  to  $450\text{ }^\circ\text{C}$  indicates that O desorption from the trinuclear copper oxo cluster results in the loss of integrity of this structure.

Finally, it is necessary to understand in which way the autoreduction phenomenon enables the formation of the trinuclear copper oxo cluster. One explanation might be an increased reactivity of  $\text{Cu}^+$  towards O capture from molecular  $\text{O}_2$ . Another one is that the increased mobility of linear  $\text{Cu}^+$  species existing at high temperatures facilitates  $\text{Cu}^+$  migration which is necessary for assembling the Cu-oxo cluster. The latter hypothesis is supported by the reduction of  $\text{Cu}^{2+}$  to  $\text{Cu}^+$  at  $250\text{ }^\circ\text{C}$  under  $\text{H}_2$  prior to re-oxidation at  $250\text{ }^\circ\text{C}$ . Such treatment did not promote the formation of active copper oxo clusters, indicating that  $\text{Cu}^+$  mobility –which is minimized at the low temperature of  $\text{H}_2$  reduction<sup>[25]</sup>– plays an important role in the activation (Figure A 4.2). In line with this conclusion, Hall et al. speculated that autoreduction of  $\text{Cu}^{2+}$  to  $\text{Cu}^+$  facilitated redistribution of Cu and therefore enhanced the formation of active sites in Cu-ZSM-5.<sup>[13]</sup>

After activation in  $\text{O}_2$  for 1h at  $450\text{ }^\circ\text{C}$ , the system is equilibrated (Figure A 4.2). A dynamic desorption-adsorption equilibrium of O at Cu sites is established. Hence, even for low steady state concentrations of  $\text{Cu}^+$ , the mobility of the species is enabled. In a standard thermal activation at  $450\text{ }^\circ\text{C}$  in  $\text{O}_2$ , the complete re-oxidation of the generated  $\text{Cu}^+$  precursor probably occurs during the cooling down in  $\text{O}_2$  to methane activation temperatures ( $150\text{--}200^\circ\text{C}$ ). Below  $300\text{ }^\circ\text{C}$  the rate of spontaneous desorption of O from the Cu sites is negligible compared to the rate of oxidation and in consequence a fully oxidized cluster is obtained.

Based on the results of this study, a mechanism for the formation the trinuclear copper oxo cluster  $[\text{Cu}_3(\mu\text{-O})_3]^{2+}$  is postulated: This mechanism is not strictly consecutive since a simultaneous occurrence of the steps (iii), (iv) and (v) is assumed. The presence of trace water formed by (iii) and (v) might be beneficial for the mobility of species formed during (iv).

- (i) Generation of a monovalent  $\text{Cu}^{2+}$  species via partial hydrolysis in solution or via a Hirschler-Plank-Mechanism in the zeolite pores (equation 4.1).<sup>[1,30]</sup>
- (ii) Dehydration of octahedral  $\text{Cu}^{2+}$  to tetrahedral  $\text{Cu}^{2+}$  species that are coordinated to framework Al sites (equation 4.2)
- (iii)  $\mu$ -oxo-bridging (equation 4.3) of framework Al attached tetrahedral  $\text{Cu}^{2+}$
- (iv) Autoreduction of  $\text{Cu}^{2+}$  to  $\text{Cu}^+$  by desorption of bridging framework O (equation 4.4).
- (v) Migration of the mobile linear coordinated (CN2)  $\text{Cu}^+$  species ( $\text{Cu}^+_{\text{CN2}}$ ) to two framework Al coordinated Cu species and formation of the active site precursor. A proton is generated in order to occupy the vacant framework Al site. (equation 4.5)
- (vi) Oxidation of the precursor to the active copper oxo cluster (equation 4.6)



## 4.3.2 Methane Oxidation

### 4.3.2.1 Energy of activation of methane oxidation

The study was performed on the same Cu-MOR sample studied in section 4.3.1 of this Chapter and in Chapter 2. The Cu loading was  $420 \mu\text{mol g}^{-1}$  corresponds to a Cu/Al ratio of 0.31. The active site of this sample was elucidated as single-site trinuclear copper oxo cluster  $[\text{Cu}_3(\mu\text{-O})_3]^{2+}$  (see Chapter 2).<sup>[19]</sup> For each series of experiments only one parameter during methane reaction was varied, while the conditions of the sample activation step and the steam treatment step were kept constant. In a typical experiment, the sample was calcined in  $\text{O}_2$  flow at  $450^\circ\text{C}$  for 1h and subsequently cooled in  $\text{O}_2$ . The steam assisted desorption allowed quantification of the methane oxidation products.

First the impact of the methane reaction temperature on methanol yield and selectivity was investigated. The  $\text{O}_2$  activated catalyst was contacted with a flow of 5% methane for 30 min. Under such reaction conditions, less than 50% of the maximum possible methane conversion has been reached (see Chapter 2), implying that methane oxidation is kinetically governed. Reaction of Cu-MOR with methane above  $200^\circ\text{C}$  resulted in a decreasing methanol and dimethyl ether selectivity. The yield of  $\text{CO}_2$  and particularly of CO is increasing above  $200^\circ\text{C}$ . This observation indicates that the mechanism follows a consecutive transformation of the Cu coordinated methanol molecule to a secondary intermediate such as a surface formate species which will evolve to CO and  $\text{CO}_2$  upon steam treatment. Figure 4.9 a shows the temperature dependency of methane oxidation on Cu-MOR. In the range of  $130\text{-}200^\circ\text{C}$ , a constant selectivity in the range of 75-80% is observed. The Arrhenius plot revealed an apparent activation energy of  $48 \text{ kJ mol}^{-1}$  (Figure 4.9 b). This value is in the range although somewhat lower than the activation energy of  $65 \text{ kJ mol}^{-1}$  obtained by means of UV-vis spectroscopy by Woertink *et al.*<sup>[21]</sup>

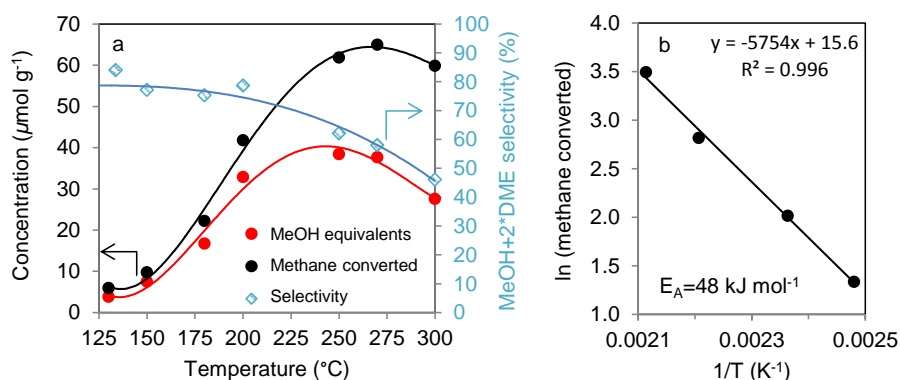


**Figure 4.9:** a) Methane converted and selectivity of methane oxidation as a function of methane reaction temperature after 30min in a flow of 50 mbar CH<sub>4</sub> over Cu-MOR with a Cu loading of 420 μmol g<sup>-1</sup> and b) corresponding Arrhenius-Plot for the temperature range of 130-200 °C revealing an apparent activation energy of 48 kJ mol<sup>-1</sup>.

#### 4.3.2.2 Deduction of reaction rates and reaction order of methane oxidation

The previous experiments revealed that 200 °C is the optimum temperature for selective partial oxidation of methane to methanol over Cu-MOR. At this temperature the maximum methane conversion and methanol selectivity are obtained. Under those conditions, the initial rate of methane oxidation can be determined by variation of the contact time (Figure 4.10 a). An initial rate of 5 μmol min<sup>-1</sup> for a flow of 16 ml min<sup>-1</sup> with a methane partial pressure of 50 mbar was determined (Figure 4.10 b), corresponding to a TOF of 2·10<sup>-4</sup> s<sup>-1</sup> or 0.01 min<sup>-1</sup>.

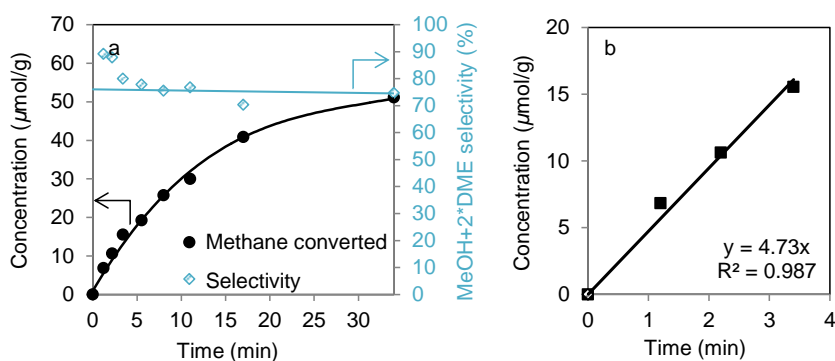


**Figure 4.10:** a) Methane converted and selectivity as a function of methane reaction time over Cu-MOR with a Cu loading of 420 μmol g<sup>-1</sup> and b) the linear regime of this function for determination of the initial reaction rate.

The mechanism of methane activation over Cu exchanged zeolites is still a matter of discussion. Homolytic C-H bond cleavage via hydrogen abstraction is assumed to be the rate determining step of methane activation.<sup>[31]</sup> DFT calculations of methane oxidation over Cu zeolites support a radical rebound mechanism via coupling of a copper hydroxyl radical with a methyl radical.<sup>[19,21]</sup> To date, some experimental evidence for this mechanism has been found by UV-vis spectroscopy,<sup>[21]</sup> but, to the best of the author's knowledge, kinetic studies of methane oxidation on Cu zeolites have not been performed.

The reaction order with respect to methane was determined by the measurement of initial reaction rates at 150 °C, over a broad range of methane partial pressures (Figure 4.11 a-e). In spite of the highest activity of methane oxidation at 200 °C, a temperature of 150 °C was selected in order to determine rates in a clearly defined kinetic regime. Note, that the constant selectivity and the linearity of the Arrhenius plot in the range of 130-200 °C indicate the same mechanism and sites being active within this temperature range (Figure 4.9). A reaction order of 0.6 with respect to methane was determined by the slope of the double logarithmic plot of the initial rates versus the corresponding methane partial pressures (Figure 4.11 f). A fractional reaction order is often indicative of a complex reaction mechanism, which is consistent with the proposed mechanism of methane activation over Cu-zeolites via homolytic C-H bond cleavage followed by a direct radical rebound on the cluster oxygen leading to formation of methanol.<sup>[19,21]</sup>

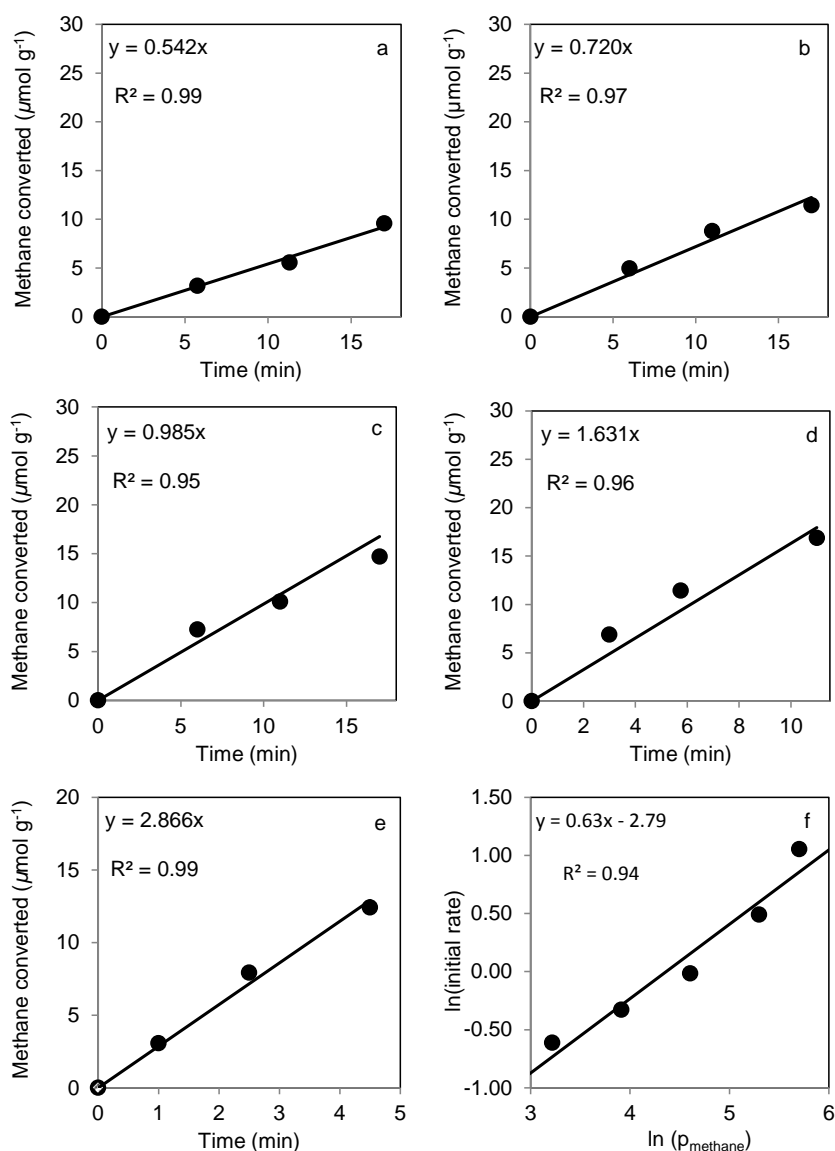


**Figure 4.11:** Linear regimes of the plots of methane converted as a function of time for various methane partial pressures of a) 25 mbar, b) 50 mbar, c) 100 mbar, d) 200 mbar, e) 300 mbar over Cu-MOR with a Cu loading of  $420 \mu\text{mol g}^{-1}$  and f) the corresponding double logarithmic plot of the initial reaction rate as a function of methane partial pressure.

#### 4.3.2.3 Discussion of methane activation kinetics

A temperature of 200 °C was established as optimum operation temperature for maximizing methane oxidation on Cu-MOR. It should be noted that products were quantified during steam assisted desorption and therefore consecutive reactions of the desorbed product must be taken into account. Below 200 °C, methane oxidation occurs with high selectivity towards methanol (75-80%).

However, CO<sub>2</sub> (20%) was also detected during steam assisted desorption. CO<sub>2</sub> adsorption on Cu-zeolites is reported to be very weak, even at room temperature.<sup>[32]</sup> Hence, CO<sub>2</sub> desorbed during steam treatment must be formed as secondary product during steam assisted desorption by over-oxidation of methanol. Thus, strong coordination of the methoxide intermediate to the Cu-zeolite catalyst is a key feature for prevention of total oxidation.<sup>[19,33]</sup>

At higher temperatures, the consecutive transformation of the surface methoxide forms presumably surface formate species which subsequently decomposes to CO<sub>x</sub> during steam treatment. At 300 °C, the total conversion of methane registered after steam treatment decreased. This is attributed to the catalytic total oxidation of methane with formation of CO<sub>x</sub> and its desorption into the gas phase during the methane loading step. Therefore, total oxidation products released during methane activation step are not quantified during steam treatment. Active oxygen species from the catalyst are depleted at these high temperatures due to formation of CO<sub>x</sub> and therefore less are available for the formation of strongly adsorbed products. Consequently, a decrease in the concentration of oxidation products quantified during steam assisted desorption is observed above 275 °C.

Reaction of methane with the trinuclear copper oxo cluster produces a methanol molecule that is strongly adsorbed on the catalyst. However, determining the initial turn over frequency (TOF) allows a comparison of the activity with other promising systems for selective methane oxidation to methanol. The initial rate of 5 μmol min<sup>-1</sup> at 200 °C for the best catalyst with a Cu-loading of 420 μmol g<sup>-1</sup> corresponds to a TOF of 0.01 min<sup>-1</sup> (methanol selectivity 75-80%). Comparable TOF were obtained for selective methane oxidation to methanol with H<sub>2</sub>O<sub>2</sub> over supported PdAu nanoparticles at 70°C and 30 bar methane (0.005 min<sup>-1</sup>, methanol selectivity > 70%).<sup>[34]</sup> The initial TOF of methane oxidation over platinum bipyrimidine complexes in concentrated sulfuric acid at 180 °C is also in the same order of magnitude (0.06 min<sup>-1</sup>, methanol selectivity > 90%).<sup>[33]</sup> The reaction order of methane of 0.6 is consistent with the proposed mechanism of methane oxidation over Cu-zeolites via homolytic C-H bond cleavage followed by a direct radical rebound reaction mechanism.<sup>[19,21]</sup>

### 4.3.3 Effect of Steam Treatment in Methanol Production

Due to the formation of a strongly chemisorbed intermediate, a steam treatment is required in order to desorb the reaction products.<sup>[3,35,36]</sup> Typically, 135-150 °C are chosen as steam treatment temperature. As mentioned in 4.3.2., formation of CO and CO<sub>2</sub> during this step is presumably due to reaction of the desorbed methanol molecule with remaining copper oxo species during steam treatment. Based on this observation, we hypothesize that total oxidation products may be suppressed if the hydrolysis of the copper oxo clusters occurs at a faster rate than the consecutive oxidation of desorbed methanol. Therefore, it is necessary to determine if variations of temperature in the steam treatment affect the selectivity of the overall process.

Figure 4.12 shows that steam treatment temperature does not have an impact on methane conversion or methanol equivalents selectivity in the temperature range of 100-200 °C. This enables closing the temperature gap between methane loading and steam treatment step, which is advantageous from an engineering point of view. Hence, it was concluded that steam assisted desorption does not affect the yield and selectivity to products of the reaction within the range of reaction conditions explored. However, it is expected that increased steam partial pressure and steaming temperature affect the catalyst lifetime by dealumination.<sup>[37]</sup>

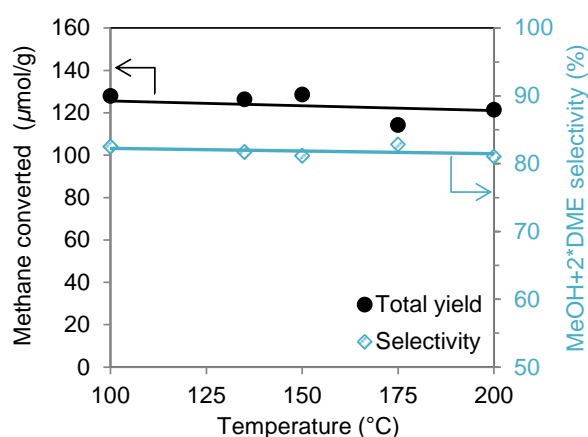


**Figure 4.12:** Methane conversion and methanol equivalent selectivity over Cu-MOR with a Cu loading of 420  $\mu\text{mol g}^{-1}$  as a function of the steam treatment temperature.

## 4.4 Conclusions

The evolution of ion exchanged  $\text{Cu}^{2+}$  species in the zeolite pores was monitored *in situ* during thermal activation and the mechanism for the formation of the active trinuclear copper oxo cluster was elucidated. XAS spectroscopy demonstrated that dehydration of the octahedral  $\text{Cu}^{2+}$  complexes in the zeolite pores leads to framework Al bonded tetrahedral  $\text{Cu}^{2+}$  in the temperature range of 200-350 °C and to the formation of  $\text{Cu}^+$  due to autoredox at temperatures above 300 °C. The high mobility of the linearly coordinated  $\text{Cu}^+$  species generated at high temperatures (450 °C) enables the reorganization of Cu in the framework and the formation of the precursor of the active cluster. The last step of activation is the oxidation of this precursor to form the active trinuclear copper oxo cluster, which takes place already at low temperatures (in the range of 30-200 °C).

A temperature of 200 °C was established as optimum operation temperature for maximizing methane oxidation on Cu-MOR. Below 200 °C, methane oxidation occurs with high selectivity towards methanol (75-80%). In this regime, an apparent activation energy of 48 kJ mol<sup>-1</sup> was determined for methane oxidation over Cu-MOR. CO<sub>2</sub> was formed as secondary product during steam assisted desorption by over-oxidation of methanol. At higher temperatures (200-300 °C), a decrease of methanol selectivity was observed, due to further oxidation of surface methanol. At 300 °C, total oxidation of methane with formation of CO<sub>x</sub> and its desorption into the gas phase occurs during the methane loading step. The TOF calculated at 200 °C from initial rates is comparable to other promising systems for methane oxidation to methanol.<sup>[34]</sup> The reaction order of methane of 0.6 is consistent with the proposed mechanism of homolytic C-H bond cleavage followed by a direct radical rebound reaction mechanism.<sup>[19,21]</sup> The temperature of steam assisted desorption did not affect methanol selectivity.

## 4.5 Experimental Section

### Preparation of Cu exchanged mordenite

H-MOR was obtained by calcination of commercial zeolite NH<sub>4</sub>-MOR (Clariant, Si/Al 11) in synthetic air at 500 °C for 8 h. Cu-MOR with Cu/Al 0.31 was prepared by aqueous ion exchange of HMOR with Cu<sup>2+</sup>. The Cu<sup>2+</sup> exchange was carried out at ambient temperature by contacting 5 g zeolite with 300 ml of an 0.01 M aqueous Cu(CH<sub>3</sub>COO)<sub>2</sub> (Sigma Aldrich, 99.99%) solution. Cu-MOR with Cu/Al 0.07 was prepared by aqueous ion exchange of HMOR with Cu<sup>2+</sup>. The Cu<sup>2+</sup> exchange was carried out at ambient temperature by contacting 5 g zeolite with 300 ml of an 0.0025 M aqueous Cu(CH<sub>3</sub>COO)<sub>2</sub>. The pH of the solution was 5..7 during exchange. A typical exchange time was 20 h. After exchange, the sample was rinsed four times with doubly de-ionized water (50 ml per g MOR each time) with an intervening centrifugation step between each rinse. These rinse cycles were performed to ensure that the pores did not contain further non-exchanged Cu ions, which would form large CuO clusters during activation. The sample was then dried in static ambient air at 110 °C for 24 h. The Si, Al and Cu contents were measured by atomic absorption spectroscopy (AAS) on a UNICAM 939 AA spectrometer after dissolution in boiling hydrofluoric acid. BET surface area was measured on a PMI automated Sorptomatic 1990 after activation at 350 °C.

### Testing of activity for selective oxidation of methane to methanol

Cu-MOR samples were tested for their activity towards methane oxidation in an atmospheric pressure stainless steel plug flow reactor with 4 mm inner diameter. The reaction included three consecutive steps: (i) activation, (ii) CH<sub>4</sub> loading and (iii) steam-assisted CH<sub>3</sub>OH desorption. In a typical experiment, 0.1 g of Cu-MOR (250 - 400 µm) was calcined in an O<sub>2</sub> flow (16 ml/min) at 450 °C for 1 h. The activated catalyst was cooled to 200 °C in O<sub>2</sub> and flushed in He. In the subsequent CH<sub>4</sub> loading step, 90% CH<sub>4</sub> in He (16 ml/min) was passed over the sample for 4 h. The temperature was then decreased in He to

135 °C. A steam-assisted CH<sub>3</sub>OH desorption step was carried out by passing an equimolar mixture of H<sub>2</sub>O steam and He (20 ml/min) through the reactor bed for 30 min. The reaction products were identified and quantified by online mass spectroscopy by monitoring the time dependent evolution of signals at m/e 28, 31, 44 and 46 characteristic for CO, CH<sub>3</sub>OH, CO<sub>2</sub> and (CH<sub>3</sub>)<sub>2</sub>O, respectively. The He signal (m/e = 4) was used as an internal standard. Productivity was calculated as the product of the effluent flow rate and the integral of the product concentrations as a function of time. The product (CH<sub>3</sub>)<sub>2</sub>O was assumed to be formed via condensation of two partially oxidized CH<sub>4</sub> molecules corresponding to two CH<sub>3</sub>OH equivalents. The sum of all detected products is referred to as total yield or methane converted.

### X-ray absorption spectroscopy

The XAS measurements were carried out with the support of European Synchrotron Radiation Facility (ESRF) in Grenoble on Beamline BM26 DUBBLE. The electron energy was 3 GeV with a beam current of 300 mA. The beam size at the sample was 200  $\mu$ m x 250  $\mu$ m. Samples were prepared as self-supporting wafers (60-80 mg) and placed into an *in situ* XAS cell. The X-ray absorption spectra were collected *in situ* at the Cu K edge (8979 eV) during activation in oxygen at 450 °C, during exposure of the sample to CH<sub>4</sub> and after steam treatment. To avoid condensation, all lines of the setup were thermostated at 110 °C. The samples were activated in an O<sub>2</sub> flow of 30 ml/min at 450 °C for 1 h (heating ramp 10 °C/min) and afterwards cooled to 200 °C. After a short flush with He, CH<sub>4</sub> was loaded for 4 h at 220 °C (flow 30 ml/min). The temperature was then decreased under He flow to 135 °C and an equal molar mixture of water steam/He (50 ml/min) was passed for 2 h through the cell. The Cu K-edge XANES data processing and EXAFS analysis were performed using IFEFFIT version 1.2.11d with the Horae package (Athena and Artemis)<sup>[38,39]</sup>.

## UV-vis spectroscopy

UV-vis measurements of the Cu-exchanged H-MOR samples were performed with an Avantes Avaspec 2048 spectrometer in the diffuse reflectance (DR) mode. The samples were measured as powders and placed in a quartz flow reactor (6 mm inner diameter) with square optical-grade quartz windows. The reactor was placed horizontally in a lab-made heating chamber with an 8-mm diameter hole on top, through which a high-temperature optical fiber (Avantes FCR- 7UV400–2ME-HTX UV-vis reflection probe) could be vertically directed to the reactor. The temperature was measured by a thermocouple located on the bottom of the quartz reactor. In a typical experiment, the UV/vis spectra were collected during treatment in oxygen, nitrogen or methane. The intensity of the DR UV/vis spectra is presented in the form of the Kubelka-Munk function, defined as  $F(R) = (1-R)^2/(2 \cdot R)$  with  $R = R_s/R_r$ , with  $R_s$  -the reflectance of the sample and  $R_r$  -the reflectance of the H-MOR parent material used as a reference. The samples were first treated at 450 °C for 1 h in He (flow 16 ml/min), heating with a rate of 10°C/min. Subsequently, the sample was cooled to ambient temperature, He was replaced with O<sub>2</sub> and the sample was heated to 450 °C in O<sub>2</sub> flow (flow 16 ml/min). After cooling of the activated sample to 200 °C, the sample was contacted with a CH<sub>4</sub> (flow 16 ml/min).

## 4.6 Acknowledgements

The research was partly supported by the U.S. Department of Energy, Office of Basic Energy Sciences, Division of Chemical Sciences under Award DE-SC0012702. It was also supported by the EU NEXT-GTL (Innovative Catalytic Technologies & Materials for Next Gas to Liquid Processes) project. The XAS measurements were carried out with the support of European Synchrotron Radiation Facility (ESRF) in Grenoble on Beamline BM26 DUBBLE.

## 4.7 Appendix

### Dimethyl ether formation

In this work, beside the main product methanol and the total oxidation products CO and CO<sub>2</sub>, formation of dimethyl ether was observed. This is consistent with the studies of selective conversion of methane to methanol over Cu-CHA.<sup>[40]</sup> In order to elucidate if dimethyl ether is formed by an alternative parallel reaction or if it is a secondary product, resulting from condensation of two methanol molecules, the formation of dimethyl ether was investigated over Cu-MOR with varying Cu loadings. Since the methanol yield is proportional to the active site concentration, variation of the Cu loading allows investigation of the impact of methanol concentration on dimethyl ether formation under the same reaction conditions. The dimethyl ether concentration is increasing with methanol formation in a second order correlation. Dimethyl ether is formed as secondary product from condensation of two methanol molecules over BAS during steam assisted desorption. For the best catalyst showing a relatively high methanol yield, 10% of the methanol molecules undergo this reaction, whereas for low Cu loadings and therefore low methanol yields, less than 5% of methanol is transformed to dimethyl ether.

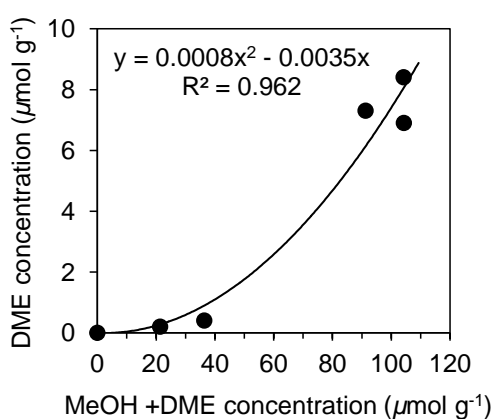


**Figure A 4.1:** Dimethyl ether yield as a function of the concentration of the partial oxidation products methanol and dimethyl ether and the corresponding curve fit indicating a second order correlation.

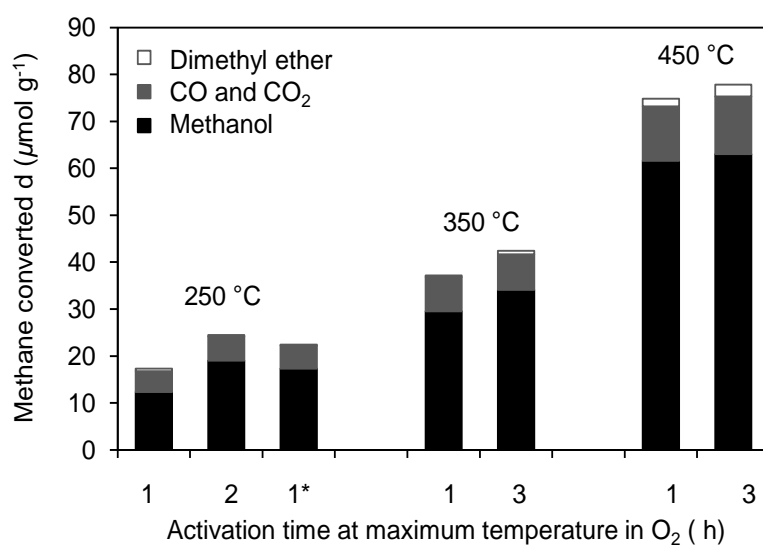


**Figure A 4.2:** Impact of activation temperature and time at maximum temperature on methane conversion. \*Activation at 250 °C for 1h in  $\text{H}_2$  and 1h in  $\text{O}_2$ .

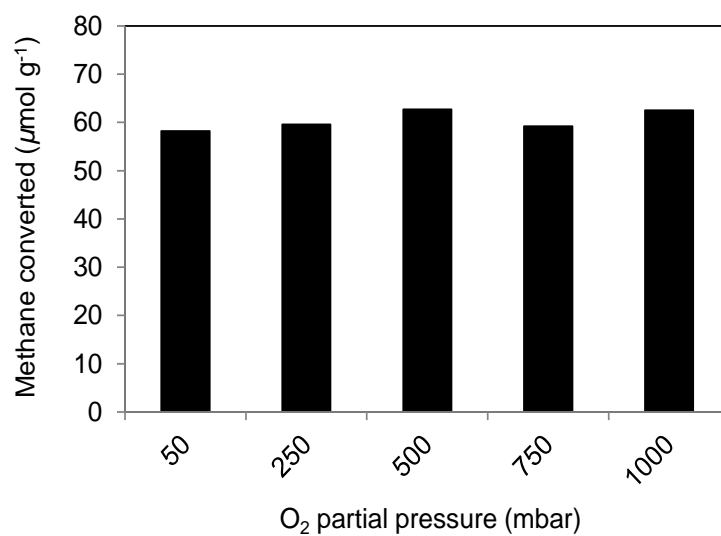


**Figure A 4.3:** Impact of O<sub>2</sub> partial pressure during activation at 450 °C and subsequent cool down in O<sub>2</sub> on methane conversion after 30 min methane loading.

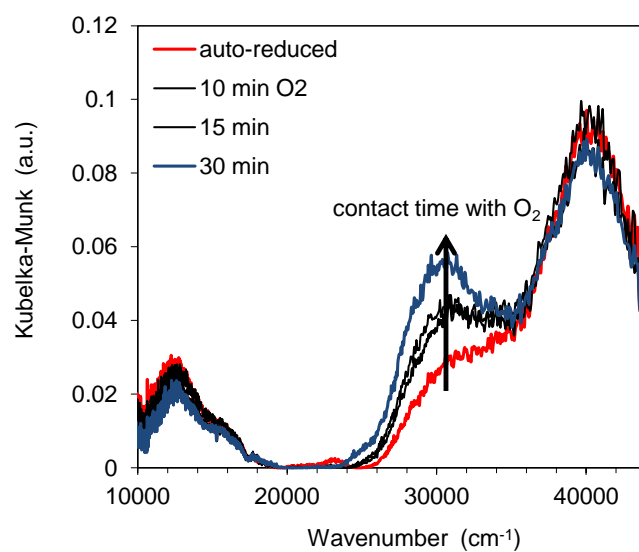


**Figure A 4.4:** *In situ* UV-vis spectra of Cu-MOR after activation in He at 450 °C and subsequent reaction with O<sub>2</sub> at 30 °C.

## 4.8 References

- [1] Lo Jacono, M.; Fierro, G.; Dragone, R.; Feng, X.; d'Itr, J.; Hall, W. K. *J. Phys. Chem. B* **1997**, *101*, 1979.
- [2] Milligan, W. O.; Weiser, H. B. *J. Phys. Chem.* **1937**, *41*, 1029.
- [3] Nash, M. J.; Shough, A. M.; Fickel, D. W.; Doren, D. J.; Lobo, R. F. *J. Am. Chem. Soc.* **2008**, *130*, 2460.
- [4] Bugaev, L. A.; van Bokhoven, J. A.; Sokolenko, A. P.; Latokha, Y. V.; Avakyan, L. A. *J. Phys. Chem. B* **2005**, *109*, 10771.
- [5] Kwak, J. H.; Varga, T.; Peden, C. H. F.; Gao, F.; Hanson, J. C.; Szanyi, J. J. *Catal.* **2014**, *314*, 83.
- [6] Dedecek, J.; Wichterlova, B. *J. Phys. Chem. B* **1997**, *101*, 10233.
- [7] Attfield, M. P.; Weigel, S. J.; Cheetham, A. K. *J. Catal.* **1997**, *170*, 227.
- [8] Iwamoto, M.; Yahiro, H.; Tanda, K.; Mizuno, N.; Mine, Y.; Kagawa, S. *J. Phys. Chem.* **1991**, *95*, 3727.
- [9] Larsen, S. C.; Aylor, A.; Bell, A. T.; Reimer, J. A. *J. Phys. Chem.* **1994**, *98*, 11533.
- [10] Valyon, J.; Hall, W. K. *J. Phys. Chem.* **1993**, *97*, 7054.
- [11] Sarkany, J.; Ditri, J. L.; Sachtler, W. M. H. *Catal. Lett.* **1992**, *16*, 241.
- [12] Jacobs, P. A.; Wilde, W. D.; Schoonheydt, R. A.; Uytterhoeven, J. B.; Beyer, H. *J. Chem. Soc., Faraday Trans.* **1976**, *72*, 1221.
- [13] Li, Y. J.; Hall, W. K. *J. Catal.* **1991**, *129*, 202.
- [14] Lei, G. D.; Adelman, B. J.; Sarkany, J.; Sachtler, W. M. H. *Appl. Catal., B* **1995**, *5*, 245.
- [15] Beutel, T.; Sarkany, J.; Lei, G. D.; Yan, J. Y.; Sachtler, W. M. H. *J. Phys. Chem.* **1996**, *100*, 845.
- [16] Smeets, P. J.; Groothaert, M. H.; van Teeffelen, R. M.; Leeman, H.; Hensen, E. J. M.; Schoonheydt, R. A. *J. Catal.* **2007**, *245*, 358.
- [17] Alayon, E. M. C.; Nachtegaal, M.; Kleymenov, E.; van Bokhoven, J. A. *Microporous Mesoporous Mater.* **2013**, *166*, 131.
- [18] Alayon, E. M. C.; Nachtegaal, M.; Bodi, A.; van Bokhoven, J. A. *ACS Catal.* **2014**, *4*, 16.
- [19] Grundner, S.; Markovits, M. A. C.; Li, G.; Tromp, M.; Pidko, E. A.; Hensen, E. J. M.; Jentys, A.; Sanchez-Sanchez, M.; Lercher, J. A. *Nat. Commun.* **2015**, *6*, 7546.
- [20] Smeets, P. J.; Groothaert, M. H.; Schoonheydt, R. A. *Catal. Today* **2005**, *110*,

303.

- [21] Woertink, J. S.; Smeets, P. J.; Groothaert, M. H.; Vance, M. A.; Sels, B. F.; Schoonheydt, R. A.; Solomon, E. I. *Proc. Natl. Acad. Sci. U. S. A.* **2009**, *106*, 18908.
- [22] Groothaert, M. H.; Pierloot, K.; Delabie, A.; Schoonheydt, R. A. *Phys. Chem. Chem. Phys.* **2003**, *5*, 2135.
- [23] Vanelderen, P.; Vancauwenbergh, J.; Tsai, M. L.; Hadt, R. G.; Solomon, E. I.; Schoonheydt, R. A.; Sels, B. F. *ChemPhysChem* **2014**, *15*, 91.
- [24] Gao, F.; Washton, N. M.; Wang, Y.; Kollár, M.; Szanyi, J.; Peden, C. H. F. *J. Catal.* **2015**, *331*, 25.
- [25] Dedecek, J.; Sobalik, Z.; Tvaruzkova, Z.; Kaucky, D.; Wichterlova, B. *J. Phys. Chem.* **1995**, *99*, 16327.
- [26] Da Costa, P.; Moden, B.; Meitzner, G. D.; Lee, D. K.; Iglesia, E. *Phys. Chem. Chem. Phys.* **2002**, *4*, 4590.
- [27] Alayon, E. M.; Nachtegaal, M.; Ranocchiari, M.; van Bokhoven, J. A. *Chem. Commun.* **2012**, *48*, 404.
- [28] Kau, L. S.; Spirasolomon, D. J.; Pennerhahn, J. E.; Hodgson, K. O.; Solomon, E. I. *J. Am. Chem. Soc.* **1987**, *109*, 6433.
- [29] Groothaert, M. H.; van Bokhoven, J. A.; Battiston, A. A.; Weckhuysen, B. M.; Schoonheydt, R. A. *J. Am. Chem. Soc.* **2003**, *125*, 7629.
- [30] Hirschler, A. E. *J. Catal.* **1963**, *2*, 428.
- [31] Dietl, N.; Schlangen, M.; Schwarz, H. *Angew. Chem., Int. Ed.* **2012**, *51*, 5544.
- [32] Zhang, W. X.; Yahiro, H.; Mizuno, N.; Izumi, J.; Iwamoto, M. *Langmuir* **1993**, *9*, 2337.
- [33] Periana, R. A.; Taube, D. J.; Gamble, S.; Taube, H.; Satoh, T.; Fujii, H. *Science* **1998**, *280*, 560.
- [34] Ab Rahim, M. H.; Forde, M. M.; Jenkins, R. L.; Hammond, C.; He, Q.; Dimitratos, N.; Lopez-Sanchez, J. A.; Carley, A. F.; Taylor, S. H.; Willock, D. J.; Murphy, D. M.; Kiely, C. J.; Hutchings, G. J. *Angew. Chem., Int. Ed.* **2013**, *52*, 1280.
- [35] Sheppard, T.; Hamill, C. D.; Goguet, A.; Rooney, D. W.; Thompson, J. M. *Chem. Commun.* **2014**, *50*, 11053.
- [36] Narsimhan, K.; Michaelis, V. K.; Mathies, G.; Gunther, W. R.; Griffin, R. G.; Roman-Leshkov, Y. *J. Am. Chem. Soc.* **2015**, *137*, 1825.
- [37] Lutz, W.; Toufar, H.; Kurzhals, R.; Suckow, M. *Adsorption* **2005**, *11*, 405.
- [38] Newville, M. *J. Synchrotron Rad.* **2001**, *8*, 322.

- [39] Ravel, B.; Newville, M. *J. Synchrotron Rad.* **2005**, *12*, 537.
- [40] Wulfers, M. J.; Teketel, S.; Ipek, B.; Lobo, R. F. *Chem. Commun.* **2015**, 51, 4447.

## 5 Summary and Conclusions

The aim of this thesis was the preparation and characterization of single-site copper oxygen cluster in zeolite mordenite for the selective conversion of methane to methanol. The choice of a mordenite sample with high concentration of Al in the side pockets, together with an optimized synthetic approach for Cu exchange allowed preparation of Cu-MOR materials with a significantly higher activity in methane activation than those reported in the literature for analogous systems. A linear dependence of the activity on the Cu concentration on a large series of samples with different Cu loading was observed. The stoichiometry of one converted methane molecule per three Cu atoms for these Cu-MOR materials with various Si/Al ratios demonstrated that it is possible to develop a Cu zeolite with only one type of active site. *In situ* XAS spectroscopy showed that the single-sites in activated Cu-MOR are trinuclear copper oxo clusters, namely  $[\text{Cu}_3(\mu\text{-O})_3]^{2+}$ , anchored to two framework Al atoms located at the pore mouth of the 8-MR side pockets. The cluster model obtained from EXAFS analysis was in excellent agreement with the results obtained by infrared spectroscopy, where it was observed that three Cu ions would exchange two protons. This active  $[\text{Cu}_3(\mu\text{-O})_3]^{2+}$  species was found to be highly stable under dry conditions, in agreement with *ab initio* thermodynamic analysis. Even though steam treatment led to the hydrolysis of the trimeric clusters, it was possible to regenerate the active species without loss of activity.

The impact of catalyst preparation on the concentration and uniformity of the Cu sites was investigated in detail. Specific synthesis protocols were found to lead to the formation of highly uniform copper species in mordenite and, as a consequence, a highly active single-site catalyst for the selective oxidation of methane to methanol. The high selectivity to form cationic trinuclear copper oxo clusters for samples prepared from H-mordenite was attributed to the absence of elements hindering the formation of the active clusters. The high uniformity of Cu species formed in CuH-MOR in a broad range of pH is in contrast to the significant variety of species that are presumably formed when co-cations are present. The presence of alkali and alkaline earth cations competing for the

exchange positions preferred by  $\text{Cu}^{2+}$  led to a heterogeneous speciation with a shift of the speciation from trimers to monomeric and dimeric Cu species.

The evolution of ion exchanged  $\text{Cu}^{2+}$  species in the zeolite pores was monitored *in situ* during thermal activation and the mechanism for the formation of the active trinuclear copper oxo cluster was elucidated. Dehydration of the  $\text{Cu}^{2+}$  aquo complexes in the zeolite with octahedral coordination to form framework Al bonded 4-fold  $\text{Cu}^{2+}$  was nearly complete at 350 °C. The high mobility of the linearly coordinated  $\text{Cu}^+$  species generated at high temperatures via autoreduction (450 °C) enables the reorganization of Cu in the framework and the formation of a trinuclear copper cluster precursor. The last step of activation is the oxidation of this precursor to the active trinuclear copper oxo cluster, which takes place already at low temperatures (in the range of 30-200 °C).

A temperature of 200 °C was established as optimum operation temperature for maximizing methane oxidation on Cu-MOR. At temperatures equal or below 200 °C, methane oxidation occurred with high selectivity towards methanol (75-80%). In this regime, an apparent activation energy of 48 kJ mol<sup>-1</sup> was determined for methane oxidation over Cu-MOR. CO<sub>2</sub> was formed as secondary product during steam assisted desorption by over-oxidation of methanol. At higher temperatures (200-300 °C), methanol selectivity decreases, indicating that total combustion is getting more dominant at those temperatures. The initial rates of reaction at 200 °C enabled to calculate a TOF for these catalysts, which was comparable to other promising systems for methane oxidation to methanol. The reaction order of methane of 0.6 is consistent with the proposed mechanism of homolytic C-H bond cleavage followed by a direct radical rebound reaction mechanism. The temperature of steam assisted desorption did not affect methanol selectivity.

## 6 Zusammenfassung

Das Ziel dieser Arbeit war die Synthese und Charakterisierung von Single-Site-Kupferoxidclustern in Mordenit, die selektiv Methan zu Methanol oxidieren. Die Wahl eines Mordeniten mit hoher Aluminiumkonzentration in den Seitentaschen der Mordenitstruktur sowie die Optimierung des Kupferaustausches ermöglichten die Herstellung von Kupfer-Mordenit-Materialien, die die literaturbekannte Aktivität vergleichbarer Systeme für die Methanoxidation deutlich übertrafen. Es wurde eine lineare Abhängigkeit der Aktivität von der Kupferkonzentration für eine Vielzahl von Proben mit unterschiedlicher Kupferbeladung beobachtet. Die Stöchiometrie von umgesetzten Methan zu Kupfer von 1:3 zeigte, dass es gelungen ist einen Kupfer-Zeolithen mit einheitlichen Zentren herzustellen. *In-situ*-Spektroskopie zeigte, dass die einheitlichen Zentren in aktivierten Kupfer-Mordenit trinukleare Kupferoxidcluster sind, die an zwei Gitteraluminiumzentren im Porenmund der Seitentaschen gebunden sind. Somit stimmt die EXAFS-Analyse mit dem Befund der Infrarotspektroskopie überein. Die aktive Spezies wurde in Übereinstimmungen mit DFT-Berechnungen als unter trockenen Bedingungen sehr stabil charakterisiert. Trotz Hydrolyse der aktiven Zentren in Gegenwart von Wasserdampf können die Zentren unter vollständiger Wiederherstellung der ursprünglichen Aktivität regeneriert werden.

Der Einfluss der Katalysatorpräparation auf die Konzentration und Einheitlichkeit der Kupferzentren wurde ausführlich untersucht. Es wurde gezeigt, dass durch eine spezifische Synthesevorschrift einheitliche Kupferspezies in Mordenit erzeugt werden konnten, wodurch eine hohe Aktivität für die selektive Methanoxidation zu Methanol erreicht wurde. Die hohe Selektivität der Bildung der trinuklearen Kupferoxidcluster in H-Mordeniten folgt aus der Abwesenheit von Elementen, die die Bildung der aktiven Zentren behindern könnten. Die Einheitlichkeit der Kupferzentren in H-Mordenit steht in starkem Gegensatz zur Diversität der Kupferspezies in Zeolithen in Gegenwart anderer Kationen. Alkali- und Erdalkalikationen konkurrieren mit Kupferkation um die Austauschplätze in den Seitentaschen

der Mordenitstruktur, was zu einer Verschiebung der Kupferspezifikation zu dimeren und monomeren Kupferzentren führt.

Mittels *In-situ*-Spektroskopie wurde die Veränderung der ionengetauschten  $\text{Cu}^{2+}$ -Spezies in den Zeolithporen während der thermischen Aktivierung beobachtet und der Mechanismus der Kupferoxidclusterbildung aufgeklärt. Die durch Entwässerung in den Zeolithporen herbeigeführte Umwandlung von oktaedrisch koordinierten Kupferkomplexen zu an Gitteraluminiumzentren gebundenen vierfach koordinierten Kupferkomplexen ist bei 350 °C nahezu abgeschlossen. Die hohe Mobilität von linear koordinierten Kupfer(I)spezies, die bei hohen Temperaturen gebildet werden, ermöglicht eine Umstrukturierung von Kupferionen zu einer Vorstufe des trinuklearen Kupferoxidclusters. Im letzten Schritt der Aktivierung wird diese Vorstufe bei niedrigen Temperaturen zum aktiven trinuklearen Kupferoxidcluster oxidiert.

200 °C wurde als optimale Methanbeladungstemperatur zur Maximierung des Methanumsatzes ermittelt. Unterhalb von 200 °C erfolgt die Methanoxidation selektiv zu Methanol. In diesem Temperaturbereich wurde für die Methanoxidation über Cu-MOR eine apparente Aktivierungsenergie von 48 kJ mol<sup>-1</sup> ermittelt. Während der Wasserdampfbehandlung wurde CO<sub>2</sub> durch Totaloxidation des desorbierten Methanols als Sekundärprodukt gebildet. Der zunehmende Rückgang der Methanolselektivität bei hohen Temperaturen deutet auf die Totaloxidation von Methan zu CO<sub>2</sub> hin. Die Wechselzahl bei 200 °C ist mit anderen vielversprechenden Systemen zur selektiven Oxidation von Methan zu Methanol vergleichbar. Die Reaktionsordnung von 0,6 ist mit dem postulierten Mechanismus der Methanoxidation über Kupfer-Zeolithen mittels homolytischen C-H-Bindungsbruch und darauffolgendem radikalischen Rebound-Reaktionsmechanismus vereinbar. Die Temperatur während der Wasserdampfbehandlung beeinflusste die Methanolselektivität nicht.

# Curriculum Vitae

## Sebastian Grundner

born on 12/24/1985 in Bad Reichenhall

11/2011 – 12/2015	PhD student at Chair of Chemical Technology II at Technischen Universität München with Prof. Dr. Johannes A. Lercher  Topic: Selective Methane Oxidation on Zeolite Stabilized Copper Oxide Clusters
09/2009 - 10/2011	Master of Science (M.Sc.), Chemistry, at Technischen Universität München
03/2011 - 10/2011	Master's Thesis at University of California Santa Barbara Structure and Reactivity of Surface Organometallic Chromium Complexes as Model Systems for the Phillips catalyst
10/2006 - 08/2009	Bachelor of Science (B.Sc.), Chemistry, at Technischen Universität München  Bachelor's Thesis: „SILP Hydrogenation Catalyst“
08/2005 - 04/2006	Civil service at Pidinger Werkstätten der Lebenshilfe BGL
09/1996 - 06/2005	High-school diploma at Karlsgymnasium Bad Reichenhall

# List of Publications

The author of this thesis is first author of the listed publications and posters. He did the main contributions in experimental design, performing of experiments, data analysis and manuscript preparation. Although Chapter 2 and 3 are based on the listed publications, the content and structure of Chapter 2 and 3 are significantly different from these publications.

## Journals

Sebastian Grundner, Monica A. Markovits, Gunna Li, Moniek Tromp, Evgeny A. Pidko, Emil J. M. Hensen, Andreas Jentys, Maricruz Sanchez-Sanchez and Johannes A. Lercher „*Single-site trinuclear copper oxygen clusters in mordenite for selective conversion of methane to methanol*”. *Nat. Commun.* **2015**, 6, 7546. doi: 10.1038/ncomms8546 (2015).

Sebastian Grundner, Wanqiu Luo, Maricruz Sanchez-Sanchez and Johannes Lercher “*Synthesis of Single-Site Copper Catalysts for Methane Partial Oxidation*” *Chem. Commun.* submitted.

## Poster Presentations

Sebastian Grundner, André C. van Veen and Johannes A. Lercher „*Selective Partial Oxidation of Methane over Cu-MOR – Study of the impact of the zeolite matrix*”, 26. *Deutsche Zeolith-Tagung*, Paderborn, 02/2014

Sebastian Grundner, André C. van Veen and Johannes A. Lercher „*Selective Partial Oxidation of Methane over Cu-MOR*”, 46. *Jahrestreffen Deutscher Katalytiker*, Weimar, 03/2013